AN ABSTRACT OF THE DISSERTATION OF

Kayla B. Clements for the degree of Doctor of Philosophy in Nuclear Engineering presented on December 10, 2024.

Title: Uncertainty Quantification and Global Sensitivity Analysis Methods for Monte Carlo Radiation Transport Solvers

Abstract approved: _____

Todd S. Palmer

Uncertainty quantification (UQ) and global sensitivity analysis (GSA) aim to quantify and characterize how input variability affects the variability of the output of a computational model. Accurate and efficient UQ and GSA methods have been widely researched for deterministic simulators, in which multiple evaluations of the same input will produce identical outputs. Stochastic simulators, however, have an intrinsic randomness and produce different outputs for multiple evaluations of the same input, introducing additional variability to model output and complicating existing UQ and GSA methods. A standard approach to evaluate the effect of input uncertainty is to increase the resolution of the stochastic solver such that the total observed output variance converges to the parametric variance; the high computational expense of this approach can be prohibitive when coupled with sampling-based UQ and GSA methods.

We present variance deconvolution, a novel approach for sampling-based UQ and GSA coupled with stochastic computational models in which the variance due to the stochastic solver is explicitly computed and removed from the total observed variance. The variance deconvolution estimator is developed from a robust theoretical analysis of the impact of solver stochasticity on output variance. The statistical properties of the new variance estimator are rigorously derived and its performance is compared to that of the standard

method for both UQ and GSA. The proposed method is verified with the analytic Ishigami function and an attenuation-only one-dimensional radiation transport problem. To test the method's applicability for large-scale Monte Carlo radiation transport problems, variance deconvolution was used to perform UQ and GSA on the 3-D C5G7-TD benchmark in its initial unrodded configuration.

We show analytically and corroborate numerically that the variance deconvolution estimators for UQ and GSA are unbiased, unlike the standard approach. For UQ, we show that the variance deconvolution approach is more accurate and precise than the standard estimator for the same computational budget. For GSA, results confirm the convergence of the approach and highlight the approach's utility particularly when the sensitivity indices are not near-zero and when there is a large amount of solver noise. For the 3-D C5G7 problem, variance deconvolution allowed for a 50X reduction in computational cost compared to the standard approach.

©Copyright by Kayla B. Clements
December 10, 2024
All Rights Reserved

Uncertainty Quantification and Global Sensitivity Analysis Methods for Monte Carlo Radiation Transport Solvers

by

Kayla B. Clements

A DISSERTATION

submitted to

Oregon State University

in partial fulfillment of
the requirements for the
degree of

Doctor of Philosophy

Presented December 10, 2024
Commencement June 2025

Doctor of Philosophy dissertation of Kayla B. Clements presented on December 10, 2024.

APPROVED:

Major Professor, representing Nuclear Engineering

Head of the School of Nuclear Science and Engineering

Dean of the Graduate School

I understand that my dissertation will become part of the permanent collection of Oregon State University libraries. My signature below authorizes release of my dissertation to any reader upon request.

Kayla B. Clements, Author

ACKNOWLEDGEMENTS

To my parents, Hilary and Steve – this is as much yours as it is mine. Thank you.

Thank you to my sister, my friends, my family, and my partner for your endless support over the past five years.

Thank you to Dr. Todd Palmer for your continuous support and advisement.

Sandia National Laboratories is a multimission laboratory managed and operated by National Technology & Engineering Solutions of Sandia, LLC, a wholly owned subsidiary of Honeywell International Inc., for the U.S. Department of Energy's National Nuclear Security Administration under contract DE-NA0003525. This paper describes objective technical results and analysis. Any subjective views or opinions that might be expressed in the paper do not necessarily represent the views of the U.S. Department of Energy or the United States Government. This work was supported by the Center for Exascale Monte-Carlo Neutron Transport (CEMeNT) a PSAAP-III project funded by the Department of Energy, grant number DE-NA003967.

CONTRIBUTION OF AUTHORS

The research objectives of this dissertation are explored in three presented manuscripts. The following outlines the contributions to the included manuscripts of co-authors other than the major professor.

Dr. Gianluca Geraci and Dr. Aaron J. Olson assisted with the mathematics and writing of Chapters 2, 3, and 5. Dr. Ilham Variansyah developed the Monte Carlo / Dynamic Code model of the C5G7 nuclear reactor benchmark for the work in Chapter 5.

TABLE OF CONTENTS

TABLE OF CONTENTS (Continued)

Page

TABLE OF CONTENTS (Continued)

LIST OF FIGURES

Figure Page

LIST OF TABLES

LIST OF ALGORITHMS

Chapter 1: Introduction

1.1 Motivation

Computational models are computer programs developed with mathematics, physics, and computer science in order to simulate and study complex systems. Computational models are used in a wide range of fields – common examples include weather forecasting, flight simulators, infectious disease tracking, and earthquake simulations. In scientific disciplines, laboratory experiments are frequently designed and tested by first performing thousands of computational model simulations. In the field of nuclear engineering, computational models are used for everything from small-scale experiment design to large-scale nuclear reactor design.

The mathematical methods used in computational models can be classified as either *deterministic* or *stochastic*. Deterministic methods are used to directly solve an equation or system of equations, while stochastic methods are used to model random processes that can be well-described by probability distributions. In computer codes, stochastic solvers simulate randomness using (pseudo-)random number generators, where the initial seed could be chosen by the analyst but subsequent stream of numbers is random [79]. If repeatedly executed with the same input parameters, deterministic solvers will always produce an identical output; by design, if repeatedly executed with the same input parameters but different initial seeds, stochastic solvers will not. Both classes of methods have their uses and drawbacks. Deterministic methods can be very computationally efficient but require discretizing each of the underlying function's independent variables, which can become prohibitively memory intensive as the problem's phase space increases or as increased resolution is desired. Stochastic methods do not require discretization and can be used for systems that are difficult or impossible to model deterministically, but the output from a stochastic solver will have some associated uncertainty that must be resolved (referred to from here as *solver variance*). Solver variance can be reduced by averaging the results of repeated solver executions and will tend towards zero at the limit of infinite solver

executions, but this process can also lead to significantly increased computational expense.

In the field of nuclear engineering, computational models for radiation transport (RT) use deterministic and stochastic methods, both separately and in combination. Deterministic RT models typically solve some form of the Boltzmann transport equation, an integro-differential function of (at-most) seven (7) independent variables: three (3) in space, two (2) in direction, and time and energy. Stochastic models use Monte Carlo (MC) RT methods, in which particle behavior is simulated by sampling probability distributions that describe the various ways particles may interact with the system. MC RT methods are valuable for their ability to model physical data continuously as a function of particle energy and direction, and are well-suited to handling time-dependent problems with complex geometries because they do not require discretization of the phase space [62, 58]. In addition to radiation transport, stochastic solvers are used in a wide variety of disciplines such as compute networks [20, 32], turbulent flows [61], financial modeling [88], and disease prediction [112].

Whether computational models are used for research, industry, or safety and regulation, it is consistently important that predictions from computational models are reported with their associated uncertainties. This requirement can be met using uncertainty quantification (UQ, also called uncertainty analysis) and sensitivity analysis (SA), both of which are important steps in rigorous code validation and model verification [42]. The goal of *uncertainty quantification* is to provide some quantitative measure of the uncertainty of a model's output. *Inverse UQ* is used to calibrate or correct the model itself by comparing model output to experimental results. This work is focused on *forward UQ*, in which input parameter uncertainty is propagated through the model to determine the effect on model output, typically by evaluating low-order moments of the output like mean and variance or by determining the complete probability distribution of the output. The goal of *sensitivity analysis* is to determine how output uncertainty can be apportioned, or divided and allocated, to different sources of input uncertainty. Local SA characterizes a system's response to small perturbations around a parameter's nominal value by computing partial derivatives of the model response at that value [47, 8]. On the other hand, *global* sensitivity analysis (GSA) aims to rank parameters in order of importance to model response across the entire input parameter space by computing sensitivity indices. Though the aims and

techniques of UQ and SA differ, they go hand-in-hand and are often performed in tandem to fully characterize the effects of input uncertainty.

There are many classes of methods for UQ and SA. In *sampling-based methods* for UQ and GSA, uncertain parameters are repeatedly sampled from their probability distributions and used as model input, then UQ and GSA statistics are directly computed from the many model outputs. Sampling-based methods are useful and powerful for their wide applicability, as they do not make any assumptions about the linearity, smoothness, or regularity of the underlying computational model. Their primary drawback is the high computational cost associated with the multiple code evaluations needed to compute well-resolved statistics; efficient sampling schemes and numerical algorithms for sampling-based UQ and GSA are areas of ongoing research [86]. While UQ and GSA methods that are surrogate- or expansion-based typically require fewer code evaluations, they can be susceptible to any lack of smoothness or regularity of the underlying function [97, 19].

UQ and SA methodologies generally assume that the computational model itself is deterministic, i.e., that all of the output variability is induced by input parameter variability (subsequently referred to as *parametric variance*). When the inputs to a stochastic model have some associated uncertainty, the total observed output variance is a combination of the solver variance and the parametric variance [94, 16], which complicates UQ and SA. A standard approach to approximate the parametric variance using a stochastic solver is to increase the number of solver realizations, knowing that the total variance will approach the parametric variance in the limit of an infinite number of solver samples [90]. However, doing this for each of the multiple code evaluations needed for sampling-based UQ and GSA exacerbates the already-high computational cost. UQ and GSA for are too important to forego even with the additional complexity from stochastic solvers. This dissertation develops,and assesses the performance of, methods for sampling-based UQ and GSA when the underlying computational model is stochastic. While these methods are developed with nuclear engineering applications in mind, the work and its results are applicable to a wide range of disciplines that use stochastic modeling.

1.2 Uncertainty quantification and global sensitivity analysis

There are many branches of UQ that consider the impact of uncertainty from a variety of sources, such as parameters of the model itself or numerical error from approximation. In forward UQ, input parameter uncertainty is propagated through the computational model to compute key statistics of the output – low-order moments, probability distribution functions and cumulative density functions of system responses, and/or envelopes of possible system responses.

Mathematically written, we consider a generic model output $Q = Q(\boldsymbol{\xi}), \boldsymbol{\xi} = (\xi_1, \ldots, \xi_k) \in \Xi \subset \mathbb{R}^k$, where the model has k input parameters $\xi_1, \ldots, \xi_k$ that are independent random variables with arbitrary joint distribution function $p(\boldsymbol{\xi})$. To characterize the effect of input uncertainty on Q, we are interested in statistics of Q, like its mean and variance

$$\mathbb{E}_{\xi}[Q] = \int_{\Xi} Q(\boldsymbol{\xi})\, p(\boldsymbol{\xi}) d\boldsymbol{\xi} \qquad \text{and} \qquad \mathbb{V}ar_{\xi}[Q] = \int_{\Xi} \Big(Q(\boldsymbol{\xi}) - \mathbb{E}_{\xi}[Q] \Big)^2 p(\boldsymbol{\xi}) d\boldsymbol{\xi}, \quad (1.1)$$

where we have used a subscript to indicate that ξ is the variable of integration.

UQ and GSA often go hand-in-hand, with UQ typically preceding GSA in current practice: once the uncertainty of the output has been quantified, GSA is used to rank parameters in order of importance to model response across the entire input parameter space. There are many statistics that can be used as measures of importance for parameter ranking; the chosen statistic depends on what question the practitioner hopes to answer, defined in [97] as the GSA setting.

There are a few key settings that fall under the umbrella of variance-based GSA [101]:

- Factor Prioritization – Used to identify the input or group of inputs whose variability accounts for most of the output variability. Once identified, focus can be shifted towards reducing the variability of these parameters.

- Factor Fixing – Used to identify the input or group of inputs whose variability makes little to no contribution to the output variability. Once identified, these parameters can essentially be set at some arbitrary value within their probability distribution, because varying them does not largely affect the output.

- Variance Cutting – Used to identify the smallest set of factors one could act upon in order to reduce the output variance below a given threshold. This ensures the most effective optimization for a given output uncertainty goal.

Variance-based GSA determines how impactful a factor or set of factors is to the output variance by computing a *sensitivity index* (SI), the ratio of the factor's conditional variance to the unconditional parametric variance. The *first-order SI* of parameter ξ_i represents the main effect contribution of ξ_i, i.e., the sole effect of parameter ξ_i on Q.

$$\mathbb{S}_i = \frac{\mathbb{V}ar_{\xi_i}\left[\mathbb{E}_{\xi_{\sim i}}\left[Q \mid \xi_i\right]\right]}{\mathbb{V}ar_{\xi}\left[Q\right]}, \tag{1.2}$$

There are k first-order SIs, one for each input parameter. All first-order SIs are between 0 and 1 and $\sum_{i=1}^{k} \mathbb{S}_i \leq 1$. Additionally, higher-order SIs represent the contribution of the interactions between factors, e.g., a second-order SI represents the interaction between two parameters. In addition to its first-order SI, a parameter can be described by its total-order SI $\mathbb{T}_I$, which accounts for its total contribution to the output variance by combining its first-order effect and all of its higher-order interaction effects. The total-order SI of ξ_i can be expressed as the sum of $\mathbb{S}_i$ and all of the higher-order terms that include ξ_i. For example, in a model with three parameters, the total effect of ξ_1 would include the first-order effect of ξ_1 plus its interactions with ξ_2 and ξ_3: $\mathbb{T}_1 = \mathbb{S}_1 + \mathbb{S}_{12} + \mathbb{S}_{13} + \mathbb{S}_{123}$. Alternatively, the total-order SI of ξ_i can also be expressed [43, 95] by conditioning on the set $\boldsymbol{\xi}_{\sim i}$, which contains all factors except ξ_i, as

$$\mathbb{T}_i = \frac{\mathbb{E}_{\xi_{\sim i}}\left[\mathbb{V}ar_{\xi_i}\left[Q \mid \boldsymbol{\xi}_{\sim i}\right]\right]}{\mathbb{V}ar_{\xi}\left[Q\right]} = 1 - \frac{\mathbb{V}ar_{\xi_{\sim i}}\left[\mathbb{E}_{\xi_i}\left[Q \mid \boldsymbol{\xi}_{\sim i}\right]\right]}{\mathbb{V}ar_{\xi}\left[Q\right]}. \tag{1.3}$$

Since $\mathbb{V}ar_{\xi_i}\left[\mathbb{E}_{\xi_{\sim i}}\left[Q \mid \boldsymbol{\xi}_{\sim i}\right]\right]$ can be understood as the main effect of everything that is not ξ_i, the remaining $\mathbb{E}_{\xi_{\sim i}}\left[\mathbb{V}ar_{\xi_i}\left[Q \mid \boldsymbol{\xi}_{\sim i}\right]\right] = \mathbb{V}ar\left[Q\right] - \mathbb{V}ar_{\xi_{\sim i}}\left[\mathbb{E}_{\xi_i}\left[Q \mid \boldsymbol{\xi}_{\sim i}\right]\right] \overset{\text{def}}{=} \mathbb{E}_{\sim i}$ is the effect of any terms that do contain ξ_i. Rather than compute all higher-order terms, it is customary to compute the set of first- and total-order indices for a good description of the importance of parameters and their interactions at a reasonable cost [97].

1.3 Sampling-based methods

Methods for UQ and GSA can be classified as either intrusive or non-intrusive. *Intrusive* UQ is often relatively more numerically efficient, but requires some modification to the underlying computational model. Sampling-based methods for UQ and GSA are *non-intrusive*, as they involve evaluations of an existing computational model with minimal or no modifications. The Saltelli method [101] for computing sensitivity indices using Monte-Carlo based sampling is described below for a model with k uncertain inputs:

1. Generate two (N, k) matrices of random numbers, A and B. The base sample N is a number of independent re-samplings of input parameters that can range from a few hundreds to a few thousands.

2. Form the matrix C_i by replacing the i^{th} column of B with the i^{th} column of A.

3. Compute the model output as a function of input matrices A, B, and C_i to obtain $N \times 1$ vectors of model output $y_A = f(A)$, $y_B = f(B)$, and $y_{Ci} = f(C_i)$.

4. For all k columns of A, construct C_i and compute y_{Ci}.

First-order sensitivity indices can be estimated:

$$S_i = \frac{V[E(Y|X_i)]}{V(Y)} = \frac{y_a \cdot y_c - f_0^2}{y_a \cdot y_a - f_0^2} \tag{1.4}$$

where $\cdot$ indicates the dot product and

$$f_0^2 = \left(\frac{1}{N}\sum_j = 1^N y_A^{(j)}\right)^2 \; y_A \cdot y_A. \tag{1.5}$$

The total-effect index can be estimated:

$$S_{Ti} = 1 - \frac{V[E(Y|X_{\sim i})]}{V(Y)} = 1 - \frac{y_B \cdot y_C - f_0^2}{y_A \cdot y_A - f_0^2}. \tag{1.6}$$

Since the publication of Satelli's approach for computing first- and total-order effects, several algorithmic modifications have been introduced to improve the efficiency and accuracy and the main and total order effects [100, 9].

1.4 Monte Carlo radiation transport

The theoretical analysis in Chapters 2 and 4 is presented assuming a generic stochastic computational model. Both Chapters present numerical results using a Monte Carlo radiation transport solver as the stochastic computational model, and Chapter 5 is entirely based on a MC RT benchmark.

MC RT simulations for treat the physical system of interest as a statistical process, using nuclear data to construct probability distributions that describe the various ways particles can behave in the system. A particle is provided an initial state including position, direction of motion, and energy level. Then, (pseudo-)random numbers and the relevant probability distributions are used compute how far the particle will travel before having some interaction with the system and what that interaction will be (e.g., absorption, scatter, fission). The particle continues moving from interaction to interaction until it exits the system, either via absorption or by traveling beyond the system's geometric boundaries. The user-defined quantity (or quantities) of interest (flux, current, k-eigenvalue, etc.) determines what particle interactions are tallied and where.

A *particle history* describes the record of a single particle's transport through the system from initiation to termination and all of the tallies it contributed to. The output of a single MC RT simulation is the average of many particle histories, all of which used different and independent random number streams. From the Central Limit Theorem [60], as the number of particle histories tends to infinity, the output of the MC RT simulation will converge to the 'true' value of the quantity of interest and the variance of that output will decrease to zero at a rate of ${N_\eta}^{-1/2}$, where N_η is the number of simulated particle histories.

Both MC and deterministic RT methods are widely used, and which are more useful depends on the information desired by the user, the problem space, the complexity of the system, and the available computational tools and resources. For example, deterministic solutions require an accurate discretization scheme and numerical method for what is often

a complex phase-space and set of differential equations [58]. Because MC RT methods are event based rather than phase-space based, they are more amenable to the simulation of time-dependent problems with complicated geometries that may be difficult to discretize. In *analog* MC RT, the probability distributions that govern the simulation are constructed directly from physical data, such that the simulated physics is directly analogous to the physical behavior of the particle in a real system [64]. To reduce computation time, improve scaling with problem size, and/or reduce output variance, *non-analog* methods have been introduced that forego exact physics but conserve accurate results. For example, if the tally of interest is geometrically located where few particles end up traveling, analog methods can require a large number of particle histories to obtain a statistically significant result [64]. Charged-particle transport often implements non-analog methods because their the physics is characterized by very small mean free paths between interaction and very small angle and energy changes when scattering. Whether non-analog MC RT methods are used or not, the inherent stochasticity of the computational model still contributes some variance to the output.

Expressed mathematically, we introduce a random variable η to represent the inherent variability of the stochastic solver, and define our previous quantity of interest Q as the expectation over η of a function $f(\boldsymbol{\xi}, \eta)$, $Q(\boldsymbol{\xi}) = \mathbb{E}\left[f(\boldsymbol{\xi}, \eta) \mid \boldsymbol{\xi}\right] \stackrel{\text{def}}{=} \mathbb{E}_\eta\left[f(\boldsymbol{\xi}, \eta)\right]$. The function $f(\boldsymbol{\xi}, \eta)$ can be directly evaluated as the output from the stochastic solver with input $\boldsymbol{\xi}$, but the expectation $\mathbb{E}_\eta\left[f(\boldsymbol{\xi}, \eta)\right]$ and variance $\mathbb{V}ar_\eta\left[f(\boldsymbol{\xi}, \eta)\right] \stackrel{\text{def}}{=} \sigma_\eta^2(\boldsymbol{\xi})$ are not directly available. Instead, we approximate $Q(\boldsymbol{\xi})$ as the sample mean of N_η independent evaluations of f, $Q\left(\boldsymbol{\xi}\right) \approx \frac{1}{N_\eta}\sum_{j=1}^{N_\eta} f(\boldsymbol{\xi}, \eta^{(j)}) \stackrel{\text{def}}{=} \tilde{Q}_{N_\eta}(\boldsymbol{\xi})$. In the context of MC RT, $\eta^{(j)}$ corresponds to the internal stream of random numbers throughout a single particle history, $f(\boldsymbol{\xi}, \eta^{(j)})$ corresponds to the result (e.g., tally) of that single particle history, and $\tilde{Q}_{N_\eta}(\boldsymbol{\xi})$ corresponds to the output of a MC RT simulation that used a total of N_η particle histories.

As the systems modeled with MC RT become more complex, a single simulation of the model becomes more computationally expensive. Sampling-based UQ and GSA require numerous model evaluations to compute well-resolved statistics of interest. Problems with real-world complexity require a large number of particle histories to not just converge, but converge to the point that the solver variance can be assumed to have a negligible contribution to the statistics defined in Section 1.2. In the following, we propose and

analyze a *variance deconvolution* estimator to make UQ and GSA with stochastic solvers more tractable by removing the need to over-resolve the solver variance.

1.5 Dissertation Objectives and Overview

Having established the motivation and background for uncertainty quantification, global sensitivity analysis, and Monte Carlo radiation transport solvers, the research objectives of this dissertation are presented.

1. Develop robust theory for an accurate, efficient, and broadly applicable variance deconvolution estimator for uncertainty quantification with stochastic solvers.

2. Assess the effect of stochastic solvers on GSA sensitivity indices. Extend variance deconvolution to develop robust theory for a variance deconvolution estimator for sampling-based sensitivity indices.

3. Demonstrate applicability of the variance deconvolution UQ and GSA estimators to large-scale radiation transport problems, particularly problems relevant to the Center for Exascale Monte Carlo Neutron Transport's challenge problem.

The next four sections of this dissertation present four works that explore these research objectives: one published academic journal article, one academic journal article under review, and one journal-ready draft.

Chapter 2 presents a manuscript published in the *Journal for Quantitative Spectroscopy and Radiative Transfer* that developed a theoretical framework and sampling-based estimator for forward uncertainty propagation that accounts for the additional variability introduced by a stochastic solver. The accuracy of the estimator was verified with an 1-dimensional mono-energetic attenuation-only radiation transport problem, and performance of the estimator was additionally explored by introducing scattering physics to the radiation transport problem.

Chapter 3 presents a full peer-reviewed conference paper presented at *The International Conference on Mathematics and Computational Methods Applied to Nuclear Science and Engineering* that takes first steps in exploring the impact of stochastic solvers on ANOVA-based sensitivity indices. That work serves as a precursor to the work in Chapter 4,

which presents a draft manuscript for submission to the *Journal of Computational Physics* that extends the variance deconvolution theoretical framework. A variance deconvolution estimator was introduced to the widely-used Saltelli method for computing sensitivity indices and the accuracy of the estimator was evaluated with asymptotic limit analysis. The accuracy of the estimator was shown numerically with the Ishigami function, a common test case for sensitivity index estimators. The performance of the estimator was evaluated using an example radiation transport problem that is one-dimensional in space and multi-group in energy.

Chapter 5 presents a full conference paper accepted for presentation at *The International Conference on Mathematics and Computational Methods Applied to Nuclear Science and Engineering* that tests the applicability of the developed methods for a large-scale Monte Carlo radiation transport problem. A k-eigenvalue simulation of the initial condition of the 3-D C5G7-TD benchmark, a miniature LWR with eight uranium oxide fuel assemblies and eight mixed oxide fuel assemblies surrounded by a water reflector. Manufacturing uncertainties of fuel pin radius and fuel pin density were sampled from a normal distribution of a 5% standard deviation about their nominal values. Both the core k-eigenvalue and pinwise core fission rate distribution were considered as quantities of interest.

Chapter 6 summarizes the progress made in these four manuscripts and presents possibilities for future research.

A VARIANCE DECONVOLUTION ESTIMATOR FOR EFFICIENT UNCERTAINTY QUANTIFICATION IN MONTE CARLO RADIATION TRANSPORT APPLICATIONS

Kayla B. Clements, Gianluca Geraci, Aaron J. Olson, Todd S. Palmer

Journal of Quantitative Spectroscopy and Radiative Transfer
Vol. 319, pp. 108958, Jun 2024.
https://doi.org/10.1016/j.jqsrt.2024.108958

Chapter 2: A variance deconvolution estimator for efficient uncertainty quantification in Monte Carlo radiation transport applications

Abstract

Monte Carlo simulations are at the heart of many high-fidelity simulations and analyses for radiation transport systems. As is the case with any complex computational model, it is important to propagate sources of input uncertainty and characterize how they affect model output. Unfortunately, uncertainty quantification (UQ) is made difficult by the stochastic variability that Monte Carlo transport solvers introduce. The standard method to avoid corrupting the UQ statistics with the transport solver noise is to increase the number of particle histories, resulting in very high computational costs. In this contribution, we propose and analyze a sampling estimator based on the law of total variance to compute UQ variance even in the presence of residual noise from Monte Carlo transport calculations. We rigorously derive the statistical properties of the new variance estimator, compare its performance to that of the standard method, and demonstrate its use on neutral particle transport model problems involving both attenuation and scattering physics. We illustrate, both analytically and numerically, the estimator's statistical performance as a function of available computational budget and the distribution of that budget between UQ samples and particle histories. We show analytically and corroborate numerically that the new estimator is unbiased, unlike the standard approach, and is more accurate and precise than the standard estimator for the same computational budget.

2.1 Introduction

As computational modeling becomes more important to scientific and engineering communities, so does the necessity of quantifying and analyzing model reliability, accuracy, and robustness [18, 24, 42]. These requirements can be met using uncertainty quantification (UQ), the mathematical characterization of how sources of input uncertainty affect model

output [34]. UQ can be used to assess the confidence of calculations that inform decisions or to motivate experimental or computational work to reduce key uncertainties. It is also an important step in rigorous code validation, which provides confidence in software's ability to predict the behavior of new systems [24]. UQ is often performed in conjunction with sensitivity analysis, a related field which aims to compute the degree to which model output is sensitive to different inputs or to identify how output uncertainty can be apportioned to different sources of input uncertainty [97]. However, the scope of this work is specifically UQ to compute output variance and does not include techniques to compute sensitivities. We focus in particular on forward UQ using Monte Carlo (MC) sampling [79], in which sources of uncertainty are propagated through the computational model to calculate mean, variance, and possibly higher-order moments of the model response over the entire range of parameter uncertainty [47] (as opposed to inverse UQ to characterize input distributions; see [111]). MC UQ satisfies the need for a non-intrusive, robust, and efficient UQ approach; its convergence rate is independent of both the dimensionality of the problem and the smoothness of the model's response to its input variability [42, 78]. Some of the concepts developed here could be extended to non-MC UQ approaches such as the construction of accurate surrogates for UQ, as demonstrated in [29, 33]. Forward UQ often requires a large number of code evaluations corresponding to independent realizations of the uncertain input, which are then used to compute statistics of interest such as failure probabilities or moments like mean and variance. In practice, just a single code evaluation for realistic models of complex physics, as is the case in radiation transport [27, 94], is very computationally expensive. Even if high-performance computing resources are available, the requirement to perform multiple evaluations for forward UQ compounds this issue. Over the last few decades, a number of algorithmic advancements have been introduced to reduce the number of required simulations, for instance with the use of surrogates like polynomial chaos [19, 105], stochastic collocation [22, 66], and Gaussian process approaches [38]. More recently, multilevel and multifidelity approaches have been developed to optimally fuse simulations from different approximations of a problem, e.g., combining fine and coarse spatial/temporal resolutions in numerical solutions of systems of partial differential equations, for accurate statistics estimation with a computational cost one or two orders of magnitude lower compared to single fidelity methods [35, 37, 81, 82].

UQ methods typically treat model output variability as being caused exclusively by input variability [34, 73], implicitly assuming that the underlying solver is deterministic and will produce the same output when queried with the same input (e.g., the discrete ordinates method [62]). However, non-deterministic methods that produce a *stochastic* output with some associated variability are used in a variety of disciplines such as compute networks [20, 32], turbulent flows [61], financial modeling [88], disease prediction [112], and radiation transport [62]. Monte Carlo radiation transport (MC RT) solvers, for example, model average particle behavior by sampling probability distributions that describe physical phenomena and averaging over the behavior of those particles [62]. MC RT methods are well-suited to handling time-dependent problems with complex geometries, as they do not require discretization across phase space, and are also valuable for their ability to model physical data continuously as a function of particle energy [62, 58]. Unfortunately, results of UQ studies applied to problems that use stochastic solvers are in a sense 'polluted' by the variability introduced by the solver itself; it is widely known that the overall variance is comprised of the stochastic solver variance and the MC UQ variance [94, 5]. A brute-force treatment to handle the stochasticity of the solver when estimating the parametric variance is to increase the number of particle histories N, knowing that the MC RT variance will approach zero at the limit of an infinite number of particle histories [23, 114]. While a number of variance-reduction techniques have been introduced for MC RT simulations, the standard error of the result will still only decrease proportionally with $1/\sqrt{N}$, leaving some remaining solver uncertainty [58]. The disadvantage of the brute-force approach is that the stochastic solver's variance needs to be made much smaller than the parametric variance in order to accurately estimate the latter, and the high computational cost of doing so must be paid for each of the multiple code evaluations required for MC UQ.

Nevertheless, MC UQ has been used in conjunction with MC RT simulations to estimate the output uncertainty caused by the input uncertainty (the combination of MC UQ and MC RT is sometimes referred to as Total Monte Carlo [54]). SCALE, a comprehensive modeling and simulation suite for nuclear safety analysis and design, includes the SAMPLER module for performing general uncertainty and sensitivity analysis [115]. However, the uncertainty of an individual output parameter due to uncertain input parameters is taken to be the variance of the output parameter over multiple code evaluations, therefore including the

'pollution' of the solver variance [7]. The Monte Carlo N-Particle (MCNP) code, used for general-purpose transport simulations of particles such as neutrons, photons, electrons, elementary particles, etc. includes mcnp-pstudy, a tool to automate the setup, execution, and collection of results from a series of MCNP calculations for convenient uncertainty analysis [5]. The theory manual for mcnp-pstudy points out that the total variance will approach the variance due solely to the uncertain parameter space as the number of histories increases; in an example problem, the tool uses batch statistics on a problem without parameter uncertainty to confirm that the solver variance is low relative to the total observed variance of problems with parameter uncertainty, in that case an order of magnitude smaller. A number of studies have suggested that rather than rely on the brute-force approach to ensure that the MC RT variance is a sufficiently small portion of the total variance, it would be useful to explicitly compute how much the MC RT variance contributes to the total observed variance when the problem contains uncertain parameters [27, 94, 41, 85, 89]. In [94], the authors present the fast Total Monte Carlo method to compute the parametric variance by using different random number seeds to remove the average MC RT variance from the total observed variance so long as the average MC RT variance is less than 50% of the total observed variance, an important improvement over existing methods. In [41], the authors developed an analytical method (rather than a MC UQ method) for estimating the MC RT variance using the analysis-of-variance (ANOVA) approach for uncertainty in geometric configurations and nuclear data.

In this contribution, we study the evaluation of moments of the QoI (namely mean and variance) due only to the variability introduced by uncertain parameters when combining MC UQ and stochastic solvers (discussed here as MC RT solvers). We demonstrate both theoretically and numerically how to correct the UQ statistics by explicitly computing and removing the variability introduced by the MC RT solver. This approach leads to statistical estimators with a significantly reduced mean-squared error compared to the brute-force approach of reducing the solver's variability by increasing the number of particle histories. Moreover, by deriving the statistical properties of these estimators, we are able to discuss their statistical performance in terms of resource allocation amongst the number of MC UQ realizations and the number of MC RT particle histories per realization. We develop analytical solutions for UQ statistics of transmittance through an attenuation-only 1D slab

as a reference radiation-transport problem and use them to verify numerical results; we also corroborate our findings with numerical results for a problem with scattering, for which we do not have an analytical solution.

The remainder of this manuscript is organized as follows. In Section 2.2, we introduce the mathematical background for Monte Carlo estimation of statistics in UQ. In Section 2.3 we introduce our novel estimator, named *variance deconvolution*, and discuss its statistical properties, including its mean-squared error as a function of the total number of particle histories. Both Sections 2.2 and 2.3 are presented assuming a generic stochastic solver, i.e., our approach is not limited by the particular stochastic solver employed and, in the context of radiation transport, is applicable to any MC-based transport solver. In Section 2.4, we briefly introduce MC RT methods and our numerical problem, including the verification test case. In Section 2.5, we provide numerical results and compare to analytical results or a reference solution. In Section 2.6, we conclude by discussing current and future research directions.

2.2 Mathematical background

We focus on quantifying statistics for a scalar quantity of interest (QoI) $Q : \mathbb{R}^d \to \mathbb{R}$, which is a function of a vector of uncertain variables $\xi \in \Xi \subset \mathbb{R}^d$, where the number of uncertain variables $d \in \mathbb{N}$ can be arbitrarily large. We consider arbitrary joint distribution functions $p(\xi)$ for the input parameters, including the case of correlated (i.e., non-independent) variables. The goal of the analysis is the precise quantification of the first two statistical moments of Q, i.e., the mean and variance of Q, which are defined as

$$\begin{aligned} \mathbb{E}\left[Q\right] &= \int_{\Xi} Q(\xi)\, p(\xi)\, \mathrm{d}\xi \quad \text{and} \\ \mathbb{V}ar\left[Q\right] &= \int_{\Xi} \left(Q(\xi) - \mathbb{E}\left[Q\right]\right)^2 p(\xi)\, \mathrm{d}\xi, \end{aligned} \tag{2.1}$$

respectively. In particular, we design estimators capable of efficiently resolving the variance of Q for stochastic solvers. When using stochastic solvers, direct observations of Q as a function of ξ are not possible, either because the response is corrupted by noise or because

the quantity of interest is defined as a statistic of events associated with the solver [79]. The latter case emerges naturally when using MC RT solvers; without loss of generality, we use the MC RT application as the motivation for this paper. For each realization of the random uncertainty parameters ξ, Q is obtained by post-processing statistics associated with individual particle histories. We notionally represent the stochasticity of the MC RT solver with a random variable $\eta \in H \subset \mathbb{R}^{d'}$, where the series of random events constituting a single particle history is represented as a single realization of η. The distribution of η is unknown (i.e., cannot be directly sampled) but its events $f : H \to \mathbb{R}$ are observable. For instance, an event f could be defined as a single particle transmitting through a slab. We can define the QoI in terms of the events f and the conditional variance of f, which characterize the solver's variability, as

$$\begin{aligned} Q(\xi_i) &= \mathbb{E}\left[f(\xi,\eta) \mid \xi = \xi_i\right] \overset{\text{def}}{=} \mathbb{E}_\eta\left[f(\xi_i,\eta)\right] \\ \sigma_\eta^2(\xi_i) &= \mathbb{V}ar\left[f(\xi,\eta) \mid \xi = \xi_i\right] \overset{\text{def}}{=} \mathbb{V}ar_\eta\left[f(\xi_i,\eta)\right]. \end{aligned} \tag{2.2}$$

From this point forward, we indicate the variable of integration with a subscript. To evaluate the statistics of Q with respect to the uncertain parameters ξ in Eq. (2.1), the definitions from Eq. (2.2) are necessary. Unfortunately, accurate convergence of Eq. (2.2) with MC RT solvers requires a large collection of events f, particularly for high-fidelity simulations of practical applications. UQ requires evaluating Q for multiple realizations of ξ, and the computational cost compounds when this is paired with use of MC RT solvers. We illustrate this challenge specifically for UQ using MC sampling in the next section.

2.2.1 Monte Carlo sampling estimation

MC sampling estimation is one of several UQ techniques that allow for efficient computation of statistics like those in Eq. (2.1). Despite its slow convergence rate, MC sampling is the most robust choice in the presence of large dimensional spaces and noisy QoIs, like those of interest for MC RT. In the context of this work, MC simply consists of drawing samples of ξ from $p(\xi)$ and evaluating the corresponding QoI $Q(\xi)$ a total of N_ξ times, then

post-processing those values to evaluate the statistics in Eq. (2.1) as

$$\begin{aligned} \mathbb{E}[Q] &\approx \frac{1}{N_\xi}\sum_{i=1}^{N_\xi} Q(\xi_i) \overset{\text{def}}{=} \hat{Q}_\xi \quad \text{and} \\ \mathbb{V}ar[Q] &\approx \frac{1}{N_\xi - 1}\sum_{i=1}^{N_\xi}\left(Q(\xi_i) - \frac{1}{N_\xi}\sum_{k=1}^{N_\xi} Q(\xi^{(k)})\right)^2 \overset{\text{def}}{=} \hat{\sigma}_\xi^2. \end{aligned} \tag{2.3}$$

Since the MC estimators depend on a finite number of realizations for $Q(\xi)$, a different set of N_ξ realizations would correspond to a different value for the estimator. Hence, the MC estimators in Eq. (2.3) are themselves random variables; as such, it is important to characterize these estimators with their statistical properties of bias and variance, which correspond respectively to their accuracy and precision. Both estimators presented in Eq. (2.3) are unbiased, i.e., $\mathbb{E}\left[\hat{Q}_\xi\right] = \mathbb{E}[Q]$ and $\mathbb{E}\left[\hat{\sigma}_\xi^2\right] = \mathbb{V}ar[Q]$ (for the variance, Bessel's correction is introduced to achieve this property; see [79]).

When using MC RT to evaluate the QoI, we introduce an additional estimator that approximates Eq. (2.2) using N_η independent particle histories,

$$Q(\xi_i) \approx \frac{1}{N_\eta}\sum_{j=1}^{N_\eta} f(\xi_i, \eta^{(j)}) \overset{\text{def}}{=} \tilde{Q}_{N_\eta}(\xi_i)\,. \tag{2.4}$$

As the sample mean of $f(\xi_i, \eta)$, the estimator presented in Eq. (2.4) is also unbiased, i.e., $\mathbb{E}_\eta\left[\tilde{Q}_{N_\eta}(\xi_i)\right] = Q(\xi_i)$. While this does indicate that the standard error of the estimator will tend to 0 as $N_\eta \to \infty$, it is also known that the standard error will converge as ${N_\eta}^{-1/2}$ [79]. Rather than assume that N_η will be large enough to render the standard error of the approximation negligible, we include the approximation in evaluating the statistics

of Eq. (2.3). Inserting Eq. (2.4) into Eq. (2.3), we obtain

$$\begin{aligned}
\mathbb{E}_\xi\left[Q\right] \approx \mathbb{E}_\xi\left[\tilde{Q}_{N_\eta}\right] \approx \frac{1}{N_\xi}\sum_{i=1}^{N_\xi}\tilde{Q}_{N_\eta}(\xi_i) = \frac{1}{N_\xi}\sum_{i=1}^{N_\xi}\left(\frac{1}{N_\eta}\sum_{j=1}^{N_\eta} f(\xi_i,\eta^{(j)})\right) &\overset{\text{def}}{=} \left\langle \tilde{Q}_{N_\eta}\right\rangle \\
\mathbb{V}ar_\xi\left[Q\right] \approx \mathbb{V}ar_\xi\left[\tilde{Q}_{N_\eta}\right] \approx \frac{1}{N_\xi-1}\sum_{i=1}^{N_\xi}\left(\tilde{Q}_{N_\eta}(\xi_i) - \frac{1}{N_\xi}\sum_{k=1}^{N_\xi}\tilde{Q}_{N_\eta}(\xi^{(k)})\right)^2 &\overset{\text{def}}{=} \tilde{S}^2,
\end{aligned} \tag{2.5}$$

where, because $\tilde{Q}_{N_\eta}$ depends on both ξ and η, we have now specified the variable of integration ξ for clarity. Since the estimators in Eqs. (2.5) are based on an approximation of Q using a finite number of N_η evaluations for f, we refer to these estimators as *polluted*. Our main focus in this work is to obtain an efficient estimation of $\mathbb{V}ar_\xi\left[Q\right]$ from its approximation, the total polluted variance $\tilde{S^2}$; we introduce our novel estimator to do so in Section 2.3. First, we summarize below some statistical properties of $\left\langle \tilde{Q}_{N_\eta}\right\rangle$ (previously introduced in [33, 11]).

Proposition 2.2.1. *The polluted estimator* $\left\langle \tilde{Q}_{N_\eta}\right\rangle$ *is unbiased, i.e.,* $\mathbb{E}\left[\left\langle \tilde{Q}_{N_\eta}\right\rangle\right] = \mathbb{E}_\xi\left[Q\right]$.

Proof. This result follows directly from the linearity of expected value.

$$\begin{aligned}
\mathbb{E}\left[\left\langle \tilde{Q}_{N_\eta}\right\rangle\right] &= \mathbb{E}_\xi\left[\mathbb{E}_\eta\left[\left\langle \tilde{Q}_{N_\eta}\right\rangle\right]\right] \\
&= \mathbb{E}_\xi\left[\mathbb{E}_\eta\left[\frac{1}{N_\xi}\sum_{i=1}^{N_\xi}\left(\frac{1}{N_\eta}\sum_{j=1}^{N_\eta} f(\xi_i,\eta^{(j)})\right)\right]\right] \\
&= \frac{1}{N_\xi}\frac{1}{N_\eta}\sum_{i=1}^{N_\xi}\sum_{j=1}^{N_\eta}\mathbb{E}_\xi\left[\mathbb{E}_\eta\left[f(\xi_i,\eta^{(j)})\right]\right] \\
&= \frac{1}{N_\xi}\frac{1}{N_\eta}\sum_{i=1}^{N_\xi}\sum_{j=1}^{N_\eta}\mathbb{E}_\xi\left[Q(\xi_i)\right] \\
&= \frac{1}{N_\xi}\frac{1}{N_\eta}\sum_{i=1}^{N_\xi}\sum_{j=1}^{N_\eta}\mathbb{E}_\xi\left[Q\right] \\
&= \mathbb{E}_\xi\left[Q\right]
\end{aligned}$$

□

Proposition 2.2.2. *The variance of* $\left\langle \tilde{Q}_{N_\eta} \right\rangle$ *is equal to*

$$\mathbb{V}ar\left[\left\langle \tilde{Q}_{N_\eta} \right\rangle\right] = \frac{\mathbb{V}ar\left[\tilde{Q}_{N_\eta}\right]}{N_\xi}, \tag{2.6}$$

where

$$\mathbb{V}ar\left[\tilde{Q}_{N_\eta}\right] = \mathbb{V}ar_\xi\left[Q\right] + \frac{\mathbb{E}_\xi\left[\sigma_\eta^2\right]}{N_\eta}. \tag{2.7}$$

Proof. Eq. (2.6) follows from the definition of $\left\langle \tilde{Q}_{N_\eta} \right\rangle$, a sampling estimator for the mean of $\tilde{Q}_{N_\eta}$ from N_ξ evaluations [10]. The remaining result follows from the law of total variance,

$$\mathbb{V}ar\left[\cdot\right] = \mathbb{V}ar_\xi\left[\mathbb{E}_\eta\left[\cdot\right]\right] + \mathbb{E}_\xi\left[\mathbb{V}ar_\eta\left[\cdot\right]\right],$$

applied to $\mathbb{V}ar\left[\tilde{Q}_{N_\eta}\right]$,

$$\begin{aligned}
\mathbb{V}ar\left[\tilde{Q}_{N_\eta}\right] &= \mathbb{V}ar_\xi\left[\mathbb{E}_\eta\left[\tilde{Q}_{N_\eta}\right]\right] + \mathbb{E}_\xi\left[\mathbb{V}ar_\eta\left[\tilde{Q}_{N_\eta}\right]\right] \\
&= \mathbb{V}ar_\xi\left[Q\right] + \mathbb{E}_\xi\left[\mathbb{V}ar_\eta\left[\frac{1}{N_\eta}\sum_{j=1}^{N_\eta} f(\xi_i, \eta^{(j)})\right]\right] \\
&= \mathbb{V}ar_\xi\left[Q\right] + \mathbb{E}_\xi\left[\frac{1}{{N_\eta}^2}\sum_{j=1}^{N_\eta} \mathbb{V}ar_\eta\left[f(\xi_i, \eta^{(j)})\right]\right] \\
&= \mathbb{V}ar_\xi\left[Q\right] + \frac{\mathbb{E}_\xi\left[\sigma_\eta^2\right]}{N_\eta}.
\end{aligned}$$

□

Corollary 2.2.1. *Let independent realizations of* η*, i.e., independent particle histories, require the same computational effort independent of parameter* ξ*. Then, for a prescribed total computational budget equal to* $C = N_\xi \times N_\eta$*, the variance of estimator* $\left\langle \tilde{Q}_{N_\eta} \right\rangle$ *is minimized at* $N_\eta = 1$*.*

Proof. This follows from Proposition 2.2.2 (see also [33]), i.e.,

$$\mathbb{V}ar\left[\left\langle \tilde{Q}_{N_\eta}\right\rangle\right] = \frac{\mathbb{V}ar_\xi\left[Q\right] + \frac{\mathbb{E}_\xi\left[\sigma_\eta^2\right]}{N_\eta}}{N_\xi} = \frac{N_\eta \mathbb{V}ar_\xi\left[Q\right] + \mathbb{E}_\xi\left[\sigma_\eta^2\right]}{N_\xi N_\eta} = \frac{N_\eta \mathbb{V}ar_\xi\left[Q\right] + \mathbb{E}_\xi\left[\sigma_\eta^2\right]}{C},$$

where $C = N_\xi \times N_\eta$. Given C = constant, $\mathbb{V}ar\left[\left\langle \tilde{Q}_{N_\eta}\right\rangle\right]$ increases with N_η. It follows that its minimum is obtained for $N_\eta = 1$. □

Corollary 2.2.1 shows that the sampling estimator for the mean, $\left\langle \tilde{Q}_{N_\eta}\right\rangle$, is most precise when $N_\eta = 1$, corresponding to the case in which the UQ parameters are re-sampled for each particle history. This indicates that, when estimating the mean value, it is more advantageous to invest the computational budget in exploring the UQ parameter space than it is to invest the computational budget in explicitly controlling the solver noise with a large N_η. We have obtained this result by considering an ideal cost model in which the costs of data transfer or restart are considered negligible. In the next section we demonstrate that even for this simplistic cost scenario, this result does not hold for our novel variance estimator; the variance of the variance deconvolution estimator is not minimized when $N_\eta = 1$, but rather an optimal value of N_η can be selected to minimize the variance of the estimator for a fixed computational budget C.

2.3 Variance deconvolution estimator for QoIs from stochastic solvers

2.3.1 A variance deconvolution estimator

Having explored the statistical properties of the polluted mean estimator $\left\langle \tilde{Q}_{N_\eta}\right\rangle$, we now turn to the polluted variance estimator $\tilde{S^2}$. To start, we can draw an important theoretical conclusion from Eq. (2.7) in the proof of Proposition 2.2.2. By applying the law of total variance to $\tilde{Q}_{N_\eta}$, we decompose it into $\mathbb{V}ar_\xi\left[Q\right]$, the contribution from parameter uncertainty, and $\mathbb{E}_\xi\left[\sigma_\eta^2\right]/N_\eta$, the contribution from the MC RT variance. Using this relationship, we examine the effect of using polluted estimator $\tilde{S^2}$ to estimate $\mathbb{V}ar_\xi\left[Q\right]$.

Theorem 2.3.1. *The total polluted variance $\tilde{S^2}$ is an unbiased estimator for $\mathbb{V}ar\left[\tilde{Q}_{N_\eta}\right]$,*

i.e., $\mathbb{E}\left[\tilde{S^2}\right] = \mathbb{V}ar\left[\tilde{Q}_{N_\eta}\right]$.

Proof. Provided in 2.7. □

Corollary 2.3.2. *Given any finite number of particle histories N_η used at each sample of ξ and $\mathbb{E}_\xi\left[\sigma_\eta^2\right] > 0$, $\tilde{S^2}$ is a* biased *estimator for $\mathbb{V}ar_\xi\left[Q\right]$.*

Proof. This follows from Theorem 2.3.1 and Proposition 2.2.2,

$$\mathbb{E}\left[\tilde{S^2}\right] = \mathbb{V}ar\left[\tilde{Q}_{N_\eta}\right] = \mathbb{V}ar_\xi\left[Q\right] + \frac{\mathbb{E}_\xi\left[\sigma_\eta^2\right]}{N_\eta}.$$

Therefore, $\mathbb{E}\left[\tilde{S^2}\right] = \mathbb{V}ar_\xi\left[Q\right]$ if and only if $\mathbb{E}_\xi\left[\sigma_\eta^2\right] = 0$, which is not the case for any finite N_η. □

Corollary 2.3.2 presents a closed-form representation of the brute-force approach: the bias of $\tilde{S^2}$ approaches 0 as N_η increases and σ_η^2 decreases. We introduce an alternative to the brute-force approach, accounting outright for the variance introduced by the MC RT simulations and removing it from the polluted variance. This idea was introduced in a series of prior contributions [11, 13, 74] and was coined *variance deconvolution* in [74], a designation we adopt in this article. Assuming the number of particle histories N_η is constant for each sample of ξ, we estimate the *average solver variance*:

$$\frac{\mathbb{E}_\xi\left[\sigma_\eta^2\right]}{N_\eta} \approx \frac{1}{N_\xi}\sum_{i=1}^{N_\xi}\frac{\hat{\sigma}_\eta^2(\xi_i)}{N_\eta} \stackrel{\text{def}}{=} \hat{\mu}_{\sigma^2_{RT,N_\eta}}, \tag{2.8}$$

where

$$\sigma_\eta^2(\xi_i) \approx \frac{1}{N_\eta - 1}\sum_{j=1}^{N_\eta}\left(f(\xi_i, \eta^{(j)}) - \tilde{Q}_{N_\eta}(\xi_i)\right)^2 \stackrel{\text{def}}{=} \hat{\sigma}_\eta^2(\xi_i). \tag{2.9}$$

We define the variance deconvolution estimator S^2 as

$$\begin{aligned}\mathbb{V}ar_\xi\left[Q\right] &= \mathbb{V}ar\left[\tilde{Q}_{N_\eta}\right] - \frac{\mathbb{E}_\xi\left[\sigma_\eta^2\right]}{N_\eta} \\ &\approx \tilde{S^2} - \hat{\mu}_{\sigma^2_{RT,N_\eta}} \stackrel{\text{def}}{=} S^2,\end{aligned} \tag{2.10}$$

providing a means to estimate $\mathbb{V}ar_{\xi}\left[Q\right]$ without requiring over-resolution of the MC RT simulation.

2.3.2 Statistical properties of the deconvolution estimator

The statistical properties (mean and variance) of the variance deconvolution estimator are necessary to understand its behavior. They also allow for comparison between the variance deconvolution estimator and the standard estimator, i.e., the estimator obtained by explicitly over-resolving the MC RT statistics.

Theorem 2.3.3. *The deconvolution estimator is unbiased, i.e.,*

$$\mathbb{E}\left[S^2\right] = \mathbb{V}ar_{\xi}\left[Q\right]. \tag{2.11}$$

Proof. From the linearity of the expected value,

$$\mathbb{E}\left[S^2\right] = \mathbb{E}\left[\tilde{S^2}\right] - \mathbb{E}\left[\hat{\mu}_{\sigma^2_{RT,N_\eta}}\right].$$

In Theorem 2.3.1, we showed that $\mathbb{E}\left[\tilde{S^2}\right] = \mathbb{V}ar\left[\tilde{Q}_{N_\eta}\right]$. All that remains is to show that

$$\mathbb{E}\left[\hat{\mu}_{\sigma^2_{RT,N_\eta}}\right] = \mathbb{E}\left[\frac{1}{N_\eta}\frac{1}{N_\xi}\sum_{i=1}^{N_\xi}\hat{\sigma}^2_\eta(\xi_i)\right] = \frac{1}{N_\eta}\mathbb{E}\left[\hat{\sigma}^2_\eta\right] = \frac{1}{N_\eta}\mathbb{E}_\xi\left[\sigma^2_\eta\right]. \tag{2.12}$$

Therefore,

$$\mathbb{E}\left[S^2\right] = \mathbb{V}ar_\xi\left[\tilde{Q}_{N_\eta}\right] - \frac{1}{N_\eta}\mathbb{E}_\xi\left[\sigma^2_\eta\right] = \mathbb{V}ar_\xi\left[Q\right]. \tag{2.13}$$

□

Theorem 2.3.4. *The variance of the deconvolution estimator is*

$$\mathbb{V}ar\left[S^2\right] = \mathbb{V}ar\left[\tilde{S^2}\right] + \mathbb{V}ar\left[\hat{\mu}_{\sigma^2_{RT,N_\eta}}\right] - 2\mathbb{C}ov\left[\tilde{S^2}, \hat{\mu}_{\sigma^2_{RT,N_\eta}}\right], \tag{2.14}$$

where

$$\mathbb{V}ar\left[\tilde{S^2}\right] = \frac{\mu_4\left[\tilde{Q}_{N_\eta}\right]}{N_\xi} - \frac{\sigma^4\left[\tilde{Q}_{N_\eta}\right](N_\xi - 3)}{N_\xi(N_\xi - 1)},$$
$$\mathbb{V}ar\left[\hat{\mu}_{\sigma^2_{RT,N_\eta}}\right] = \frac{1}{N_\xi {N_\eta}^2}\mathbb{V}ar\left[\hat{\sigma}^2_\eta\right], \qquad \textit{and}$$
$$\mathbb{C}ov\left[\tilde{S^2}, \hat{\mu}_{\sigma^2_{RT,N_\eta}}\right] = \mathbb{E}\left[\tilde{S^2}\hat{\mu}_{\sigma^2_{RT,N_\eta}}\right] - \mathbb{E}\left[\tilde{S^2}\right]\mathbb{E}\left[\hat{\mu}_{\sigma^2_{RT,N_\eta}}\right].$$

Proof. Equation 2.14 follows from the definition of variance. We define $\mathbb{V}ar\left[\tilde{S^2}\right]$, $\mathbb{V}ar\left[\hat{\mu}_{\sigma^2_{RT,N_\eta}}\right]$, and $\mathbb{C}ov\left[\tilde{S^2}, \hat{\mu}_{\sigma^2_{RT,N_\eta}}\right]$ here in terms of polluted quantities for brevity, where μ_4 indicates the fourth moment and σ^4 indicates the second moment squared. The proof in 2.8 shows $\mathbb{V}ar\left[\tilde{S^2}\right]$, $\mathbb{V}ar\left[\hat{\mu}_{\sigma^2_{RT,N_\eta}}\right]$, and $\mathbb{C}ov\left[\tilde{S^2}, \hat{\mu}_{\sigma^2_{RT,N_\eta}}\right]$ in terms of un-polluted quantities $f(\xi,\eta)$ and $Q(\xi)$. □

Corollary 2.3.5. *The MSE of the variance deconvolution estimator is equal to its variance*

$$MSE\left[S^2\right] = \mathbb{V}ar\left[\tilde{S^2}\right] + \mathbb{V}ar\left[\hat{\mu}_{\sigma^2_{RT,N_\eta}}\right] - 2\mathbb{C}ov\left[\tilde{S^2}, \hat{\mu}_{\sigma^2_{RT,N_\eta}}\right]. \tag{2.15}$$

Proof. This result follows from the definition of the MSE of an estimator,

$$MSE\left[S^2\right] = \left(\mathbb{E}\left[S^2\right] - \mathbb{V}ar_\xi\left[Q\right]\right)^2 + \mathbb{V}ar\left[S^2\right] \tag{2.16}$$
$$= Bias\left[S^2\right] + \mathbb{V}ar\left[S^2\right] \tag{2.17}$$

and the results in Theorems 2.3.3 and 2.3.4. □

2.3.3 Variance deconvolution algorithm

In Algorithm 1, we show pseudo-code for implementing variance deconvolution to compute parametric variance. In this pseudo-code, the *STOCHASTIC SOLVER* function (lines 3-10) represents *any* stochastic solver that takes uncertain parameters ξ as input and uses N_η solver samples to compute QoI $\tilde{Q}_{N_\eta}$ and solver variance $\hat{\sigma}^2_\eta$. In our example problems, the stochastic solver is a MC RT solver and $f(\xi_i, \eta^{(j)})$ is a single particle tally. Each execution

of the *STOCHASTIC SOLVER* must use an independent sequence of random numbers. The variance deconvolution algorithm can be implemented in software with existing batch-statistic capabilities with a couple modifications: assigning re-sampled parameters to each batch and adding the computation and removal of the average solver variance from the total variance once all of the batch executions are complete.

Algorithm 1 Compute parametric variance with variance deconvolution

for $i \leftarrow 1, N_\xi$ **do**
  $\xi_i \leftarrow$ Re-sample uncertain parameters
  function STOCHASTIC SOLVER(ξ_i)
    for $j \leftarrow 1, N_\eta$ **do**
      $f(\xi_i, \eta^{(j)}) \leftarrow$ single-sample response
    end for
    $\tilde{Q}_{N_\eta}(\xi_i) \leftarrow \frac{1}{N_\eta} \sum_{j=1}^{N_\eta} f(\xi_i, \eta^{(j)})$
    $\hat{\sigma}^2_\eta(\xi_i) \leftarrow \frac{1}{N_\eta - 1} \sum_{j=1}^{N_\eta} \left(f(\xi_i, \eta^{(j)}) - \tilde{Q}_{N_\eta}(\xi_i) \right)^2$
    return $\tilde{Q}_{N_\eta}(\xi_i)$, $\hat{\sigma}^2_\eta(\xi_i)$
  end function
end for
$\left\langle \tilde{Q}_{N_\eta} \right\rangle \leftarrow \frac{1}{N_\xi} \sum_{i=1}^{N_\xi} \tilde{Q}_{N_\eta}(\xi_i)$ ▷ Unbiased QoI, Eq. (2.5)
$\tilde{S^2} \leftarrow \frac{1}{N_\xi - 1} \sum_{i=1}^{N_\xi} \left(\tilde{Q}_{N_\eta}(\xi_i) - \left\langle \tilde{Q}_{N_\eta} \right\rangle \right)^2$ ▷ Total polluted variance, Eq. (2.5)
$\hat{\mu}_{\sigma^2_{RT,N_\eta}} \leftarrow \frac{1}{N_\xi} \sum_{i=1}^{N_\xi} \frac{\hat{\sigma}^2_\eta(\xi_i)}{N_\eta}$ ▷ Average solver variance, Eq. (2.8)
$S^2 = \tilde{S^2} - \hat{\mu}_{\sigma^2_{RT,N_\eta}}$ ▷ Parametric variance, Eq. (2.10)

2.4 Monte Carlo radiation transport methods

While general MC sampling estimation and MC RT solvers were introduced in Section 2.2, we describe the MC RT methods used in this paper in more detail here. MC RT simulations treat the physical system of interest as a statistical process, using nuclear data to construct probability distributions that describe the various ways particles can behave in the system.

Individual particles are simulated and their behavior (e.g., moving through, interacting with, and exiting the system) is tallied based on user-defined output quantities [58]. Applying the Central Limit Theorem [59], the tallied behavior of the simulated particles can then be extrapolated as the average behavior of all particles in the system, with some associated uncertainty on the order of $N_\eta^{-1/2}$, as discussed in Section 2.2. In contrast, deterministic radiation transport methods solve an approximation to the transport equation, analytically or numerically, for average particle behavior across an entire phase space [58]. While deterministic solvers introduce bias via the discretization scheme or numerical method used, stochastic solvers introduce variability via the use of a finite number of samples. MC RT methods are useful depending on the information needed by the user, the problem space, or the complexity of the equations governing the system. For example, because MC RT methods are event-based rather than phase space-based, they can be used to solve time-dependent problems in complicated geometries without requiring an accurate discretization scheme or numerical method for a complex system of differential equations [58].

This work uses analog MC RT methods, which use probability distributions constructed directly from physical data such that a simulated particle's behavior is directly analogous to the physical behavior of a particle in a real system [58]. Non-analog methods, in general, forego the exact physics of the problem to reduce computation time, improve scaling with problem size, or as a variance reduction technique. The variance deconvolution estimator is equally applicable when non-analog methods are used so long as the definitions introduced in Eqs. (2.2) and (2.4) remain true. Particle behavior is sampled using macroscopic cross sections, material-dependent properties with units of inverse-distance that define the probability per unit distance that a given reaction will occur [25]. For example, the total cross section Σ_t measures the probability per unit distance that any reaction will occur, while the absorption cross section Σ_a measures the probability per unit distance that an interacting particle will be absorbed. The random walk of a neutral particle[1] begins with some initial conditions, and the particle is moved through the system by computing the

[1]Transport for charged-particles like electrons and protons is more complex due to electrostatic interactions, and interested readers can refer to [104] for more details.

distance to its next collision[2] d_c ,

$$d_c = \frac{-\ln(\Gamma)}{\Sigma_t},\ \Gamma \in [0,1)\ , \tag{2.18}$$

where Γ is a randomly sampled number on [0,1) [58]. The computed distance to collision remains accurate as long as Σ_t is constant, as in homogeneous media[3]. The particle will eventually exit the system, either through geometric boundaries or via absorption, and a new particle history is initiated. Once all particle histories have been terminated, tallies are averaged over the particle histories. As the systems modeled using MC RT become more complex, a single simulation of the model becomes more computationally expensive. Even for neutral particles, transport can become restrictively computationally expensive as higher-fidelity geometries or physics are modeled. For example, if the tally of interest is located where few particles end up traveling, it can take a large number of histories to obtain a statistically significant result [58]. When considering charged-particle transport, accurate simulation requires modeling even more complex physics and often more computational expense.

2.4.1 Verification problem

To show applicability of the variance deconvolution estimator, we consider an example radiation transport problem solved using MC RT methods. We solve the one-dimensional, neutral-particle, mono-energetic, isotropic scattering, source-free steady-state radiation transport problem with a normally incident beam source of magnitude one:

$$\mu \frac{\partial \psi\ (x,\mu)}{\partial x} + \Sigma_t\ (x)\ \psi\ (x,\mu) = \frac{\Sigma_s\ (x)}{2} \int_{-1}^{1} d\mu' \psi\ (x,\mu')\ , \tag{2.19}$$

$$0 \leq x \leq L; \quad \psi(0, \mu > 0) = 1. \tag{2.20}$$

[2]Readers interested in the derivation of the distance to collision can see ref [58].

[3]This is a common simplifying assumption, but in reality macroscopic cross section data can vary with energy, temperature, density, or changing material composition [65].

Dependence on space and angle are represented by x and μ, respectively; $\psi(x, \mu)$ is the angular neutron flux; $\Sigma_t(x)$ is the total cross section; and $\Sigma_s(x)$ is the scattering cross section integrated over all angles. Because we only consider two possible particle interactions, absorption or scattering, the total cross section is the sum of the absorption and scattering cross sections, $\Sigma_t = \Sigma_a + \Sigma_s$. The geometry of the problem is a 1D slab sectioned into M material regions, the boundaries between which are fixed. We consider two quantities of interest: the percentage of incident particles that exit the system through the opposite surface, transmittance $T = \psi\ (x = L, \mu < 0)$, and the percentage of incident particles that exit the system through the incident surface, reflectance $R = \psi\ (x = 0, \mu)$. Stochasticity, represented by ξ[4], is introduced to the problem via the total cross section and the scattering ratio $c = \Sigma_s/\Sigma_t$. The stochastic total cross section for material region m is given by

$$\Sigma_{t,m}\left(\xi_m\right) = \Sigma^0_{t,m} + \Sigma^\Delta_{t,m}\xi_m, \quad \xi_m \sim \mathcal{U}\left[-1, 1\right]\ , \tag{2.21}$$

where $\Sigma^0_{t,m}$ represents its mean and $\Sigma^\Delta_{t,m}$ represents its deviation from the mean. It follows from this definition that $\Sigma_{t,m} \sim \mathcal{U}\left[\Sigma^0_{t,m} - \Sigma^\Delta_{t,m}, \Sigma^0_{t,m} + \Sigma^\Delta_{t,m}\right]$. Similarly to the total cross section, we model the scattering ratio as a uniform random variable $c_m \sim \mathcal{U}\left(c_m - c^\Delta_m, c_m + c^\Delta_m\right)$, defined by

$$c_m(\xi_{m+M}) = c^0_m + c^\Delta_m\xi_{m+M}, \quad \xi_{m+M} \sim \mathcal{U}[-1, 1]\,. \tag{2.22}$$

Both QoIs are functions of particle behavior, which is affected by the uncertain material properties. With two uncertain parameters per material region, a single realization of $T(\xi)$ and $R(\xi)$ corresponds to a single realization of $\xi \in \mathbb{R}^{2M}$. The goal is to estimate the variances of the QoIs induced by uncertainty in the material properties, $\mathbb{V}ar_\xi\left[T\right]$ and $\mathbb{V}ar_\xi\left[R\right]$. We also examine an attenuation-only version of this test case, in which $\Sigma_s = 0$. Without a scattering ratio to consider, our only QoI is $T(\xi)$, $\xi \in \mathbb{R}^M$.

[4]The variable ξ is often used in nuclear engineering texts to represent angular dependence in 2D or 3D problems, so we point out that in our context, ξ is a vector of random variables. See Sec. 2.2.

2.5 Numerical Experiments on MC RT problems

In this section, we demonstrate use of the variance deconvolution estimator on a MC RT verification problem and compare its performance to that of a brute-force estimator for variance. In Sec. 2.5.1 we derive analytic reference solutions for the attenuation-only case, then in Sec. 2.5.2 present numerical results for both the attenuation-only and scattering cases.

2.5.1 Analytic solution derivations

With $\Sigma_s = 0$, the total cross section and absorption cross section are equivalent and we are able to derive analytic solutions to serve as verification for numerical results. Because there is no scattering, particle motion is restricted to the forward direction $\mu = 1$. The transmittance $T(\xi) = \psi\left(x = L, \mu = 1, \xi\right)$ is a function of the optical thickness of each material region,

$$T\left(\xi\right) = \exp\left[-\sum_{m=1}^{M} \Sigma_{t,m}\left(\xi_m\right) \Delta x_m\right] . \tag{2.23}$$

Olson *et al.* [76] derived an analytic solution for the pth raw moment of Eq. (2.23) with respect to ξ,

$$\mathbb{E}_{\xi}\left[T^p\right] = \prod_{m=1}^{M} \exp\left[-p\Sigma_{t,m}^{0}\Delta x\right] \frac{\sinh\left[p\Sigma_{t,m}^{\Delta}\Delta x\right]}{p\Sigma_{t,m}^{0}\Delta x}. \tag{2.24}$$

We verify our variance estimate S^2 by comparing to the standard raw-to-central moment conversion for variance, $\mathbb{V}ar_{\xi}\left[T\right] = \mathbb{E}_{\xi}\left[T^2\right] - \mathbb{E}_{\xi}\left[T\right]^2$. We can also verify estimates for $\hat{\mu}_{\sigma^2_{RT,N_\eta}}$ and $\tilde{S^2}$ by deriving a reference solution for the average solver variance[5] and summing it with that of $\mathbb{V}ar_{\xi}\left[T\right]$. Additionally, we can use the closed-form expression for the variance of the variance deconvolution estimator from Theorem 2.3.4 to derive an expression[5] for the variance deconvolution estimator's MSE as a function of N_η.

[5] See 2.9 for details.

2.5.2 Numerical results

We have arbitrarily chosen a 1D slab with 3 material regions, though our results could be extended to any number of material regions. In Table 2.1, we present the width, total cross section average and deviation, and scattering ratio average and deviation for each material region. UQ is performed using N_ξ sample realizations, where each model realization is a MC RT simulation using N_η histories, for a total computational cost of $C = N_\xi \times N_\eta$. We solved each problem using an array of total computational costs $C = 200, 500, 1000, 2000,$ and 5000 and also varied the factor pairs within each C. To generate statistics of estimator performance and distribution of results, we repeated each experiment 25 000 times.

2.5.2.1 Attenuation-only

From Eq. (2.24), the analytic transmittance with the parameters listed in Table 2.1 is $\mathbb{E}_\xi[T] = 0.08378$. Our variance deconvolution method does not introduce any novelty in computing the QoI of transmittance; over all estimator costs and (N_ξ, N_η) configurations, we estimate $\mathbb{E}_\xi[T]$ within $\pm 8 \times 10^{-5}\%$ (using 25 000 repetitions). The brute-force approach

Problem Parameters				Scattering Parameters	
	Δx	$\Sigma_{t,m}^0$	$\Sigma_{t,m}^\Delta$	$c_{s,m}^0$	$c_{s,m}^\Delta$
m = 1	2.0	0.90	0.70	0.50	0.40
m = 2	3.0	0.15	0.12	0.50	0.40
m = 3	1.0	0.60	0.50	0.50	0.40

Table 2.1: Problem parameters.

approximates $\mathbb{V}ar_\xi[Q]$ with $\tilde{S^2}$; the variance deconvolution approach approximates it with S^2. From Eq. (2.24), the analytic variance with the parameters listed in Table 2.1 is $\mathbb{V}ar_\xi[T] = 5.504 \times 10^{-3}$. In Figure 2.1, we show the distributions of S^2 and $\tilde{S^2}$, as well as their means, using a total cost of $C = 2000$ for selected factor pairs. For all four factor pairs, we see that the mean of S^2 over 25 000 repetitions overlaps with the analytic $\mathbb{V}ar_\xi[T]$ result; this is consistent with the fact that this estimator is unbiased. As the number of particle histories per UQ sample increases, in order from Figure 2.1(a) to Figure 2.1(d),

we see the bias of the $\tilde{S^2}$ estimator reduce as it converges to $\mathbb{V}ar_\xi[T]$. These distributions are a visualization of the efficiency of the variance deconvolution estimator compared to a brute-force approach, and we gain insight into how computational resources must be spent on resolving the stochasticity of the MC RT solver. For the same computational cost, one can instead spend more computational resource on improving the precision of the S^2 estimator.

In Figure 2.2, we show the MSE, variance, and bias of both estimators as logarithmic heat maps for all tested total computational costs. We can see from the MSE and $Bias$ maps that S^2 is a more accurate estimator for $\mathbb{V}ar_\xi[T]$ than $\tilde{S^2}$ at every factor pair and every computational cost, only approaching equality as we increase N_η at the expense of UQ resolution. We see similar profiles and order of magnitude in the variance, therefore the precision, of the two estimators. This is also visible from the similarity in the shapes of their distributions in Figure 2.1. As expected, $MSE[S^2] = \mathbb{V}ar\left[S^2\right]$ (note that the scale has shifted between the two maps). Additionally, the observed bias is on the order of 10^{-10}, and has a maximum on the order of 10^{-9}. Though this result is non-zero, it is statistically insignificant compared to the standard error of the S^2 result, which is on the order of 10^{-5}. The bias of the brute-force estimator, however, is statistically significant compared to $\mathbb{V}ar_\xi[T]$ itself and we see, as expected, that the bias term is a function entirely of N_η.

As a final analysis of estimator behavior, we evaluate the behavior of estimator statistics as a function of N_η. Using the analytic expressions for the statistics derived in Section 2.5.1, we can explicitly derive the dependency of $\mathbb{V}ar\left[S^2\right]$ on N_η and evaluate its minimum in closed-form. In Figures 2.3 and 2.4, we show these results for a variety of total computational costs. The analytic expressions for $\mathbb{V}ar\left[S^2\right]$, $\mathbb{V}ar\left[\tilde{S^2}\right]$, $\mathbb{V}ar\left[\hat{\mu}_{\sigma^2_{RT,N_\eta}}\right]$, $MSE\left[S^2\right]$, and $MSE\left[\tilde{S^2}\right]$ are plotted with dashed lines, with numerical results from the 25 000 repetitions and their confidence intervals superimposed. The analytic minimum is marked with a star in each plot. We can see clearly here that, unlike the result for the mean estimator in Corollary 2.2.1, $\mathbb{V}ar\left[S^2\right]$ is not minimized at $N_\eta = 1$, suggesting there is an efficiency trade-off between exploration of the parameter space via N_ξ and solver noise reduction via N_η for a prescribed computational cost[6]. If the statistics of the QoI cannot

[6]Incorporating more complex cost dependencies on N_ξ and N_η would give different results; see, e.g., [29].

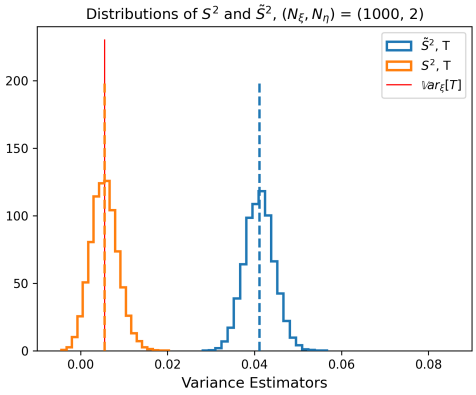

(a) $C = 2000$, $N_\eta = 2$.

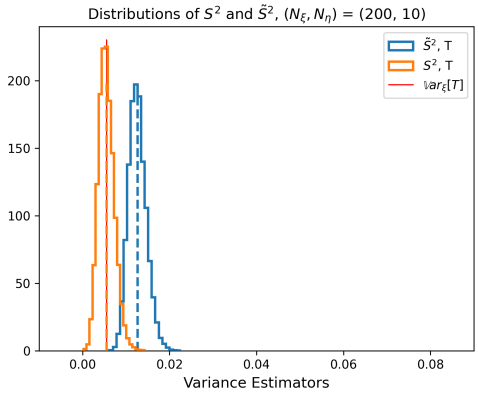

(b) $C = 2000$, $N_\eta = 10$.

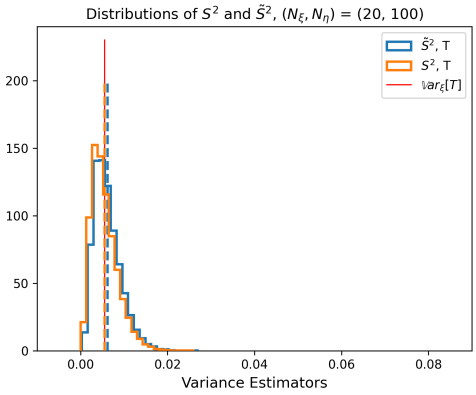

(c) $C = 2000$, $N_\eta = 100$.

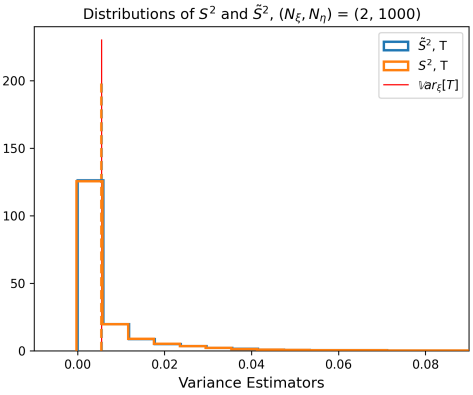

(d) $C = 2000$, $N_\eta = 1000$.

Figure 2.1: Comparing the variance estimate with a brute-force approach to the estimate with the variance deconvolution approach for an attenuation-only 1D radiation transport problem ($d = 3$). PDF created with 25 000 repetitions, averages reported with dashed lines. Exact $\mathbb{V}ar_\xi[T]$ is reported as solid vertical line. $\tilde{S^2}$ converges to $\mathbb{V}ar_\xi[T]$ as the number of particles per UQ sample increases, while S^2 is accurate even with $N_\eta = 2$.

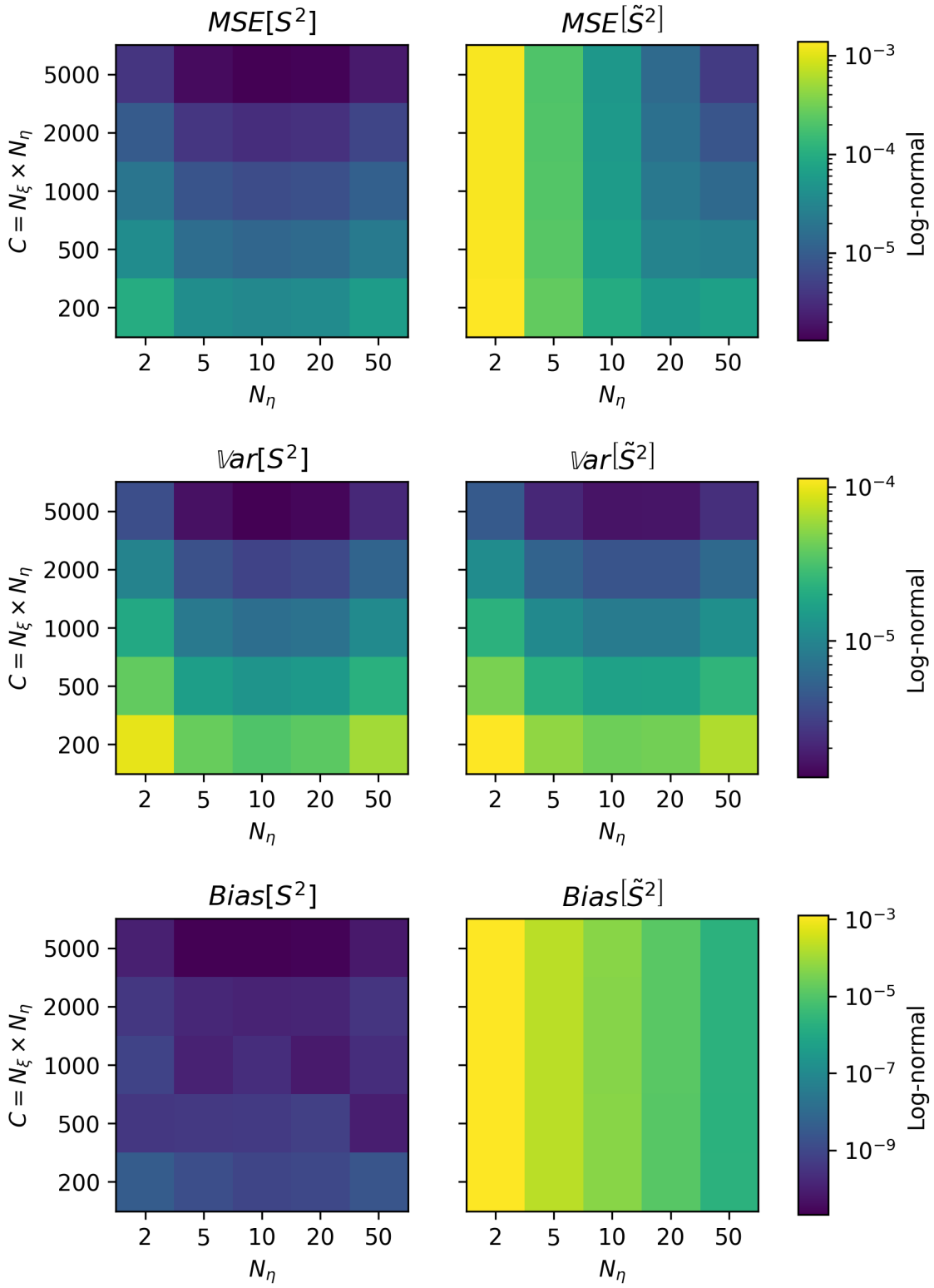

Figure 2.2: Comparing statistics of S^2 and $\tilde{S^2}$ as estimators for $\mathbb{V}ar_\xi[T] = 5.504 \times 10^{-3}$. Logarithmic scales.

be evaluated in closed form, one would need to estimate them by employing a procedure based on pilot runs. Therefore, it is possible to envision a numerical procedure that automatically discovers and selects the best resource allocation for a fixed computational cost. Developing such a procedure is beyond the present scope of the manuscript and we leave it to future contributions.

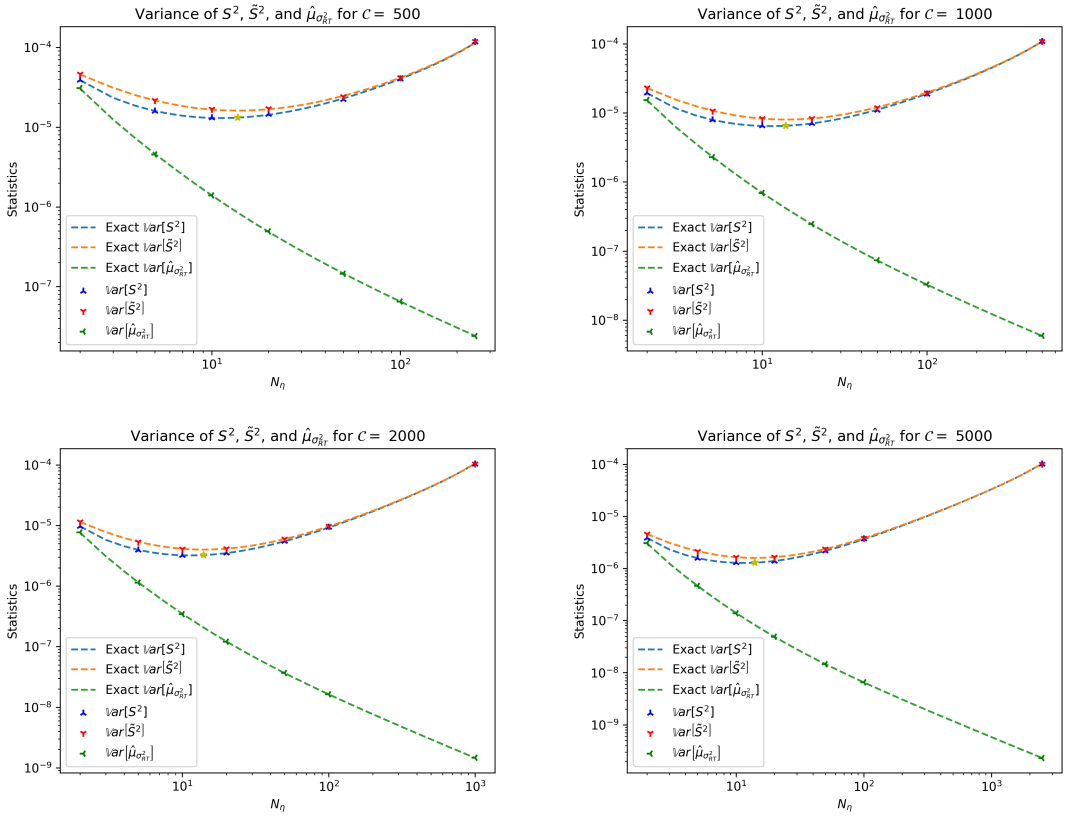

Figure 2.3: Comparing analytic functions of $\mathbb{V}ar\left[S^2\right]$, $\mathbb{V}ar\left[\tilde{S}^2\right]$, and $\mathbb{V}ar\left[\hat{\mu}_{\sigma^2_{RT,N_\eta}}\right]$ to numerical results. The star indicates the minimum $\mathbb{V}ar\left[S^2\right]$. Note that axes are different for each plot.

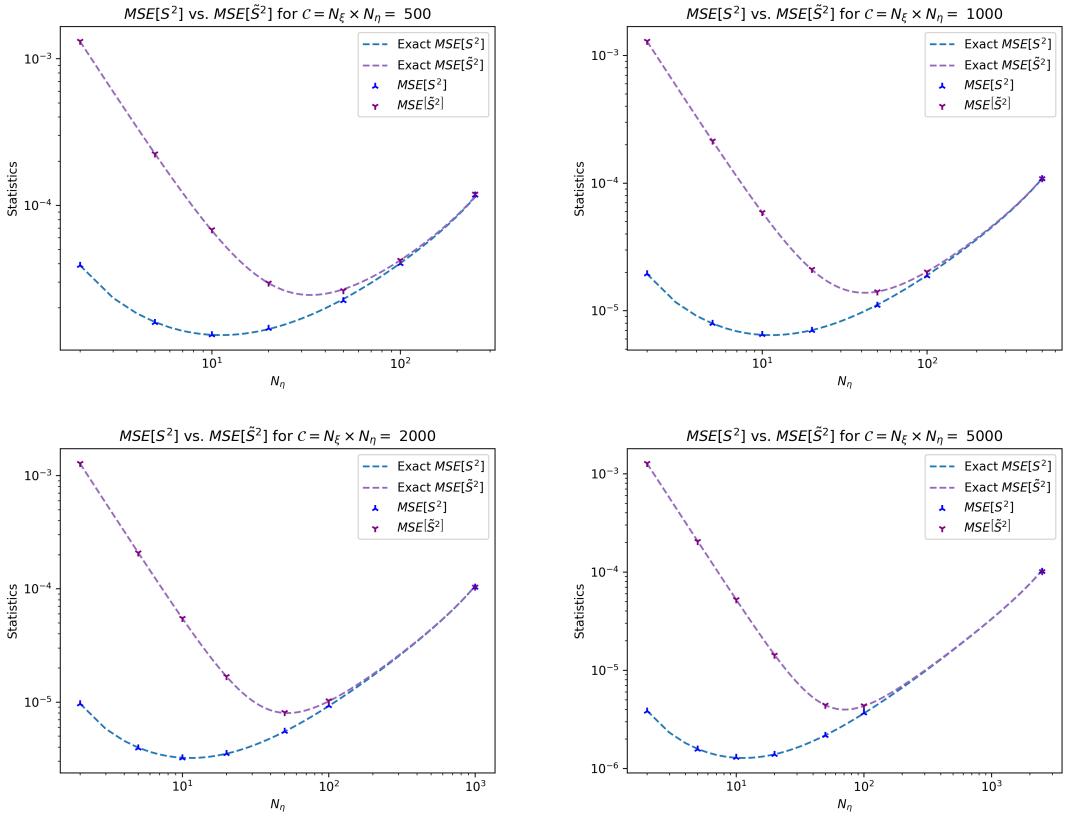

Figure 2.4: Comparing analytic functions of $MSE\left[S^2\right]$ and $MSE\left[\tilde{S}^2\right]$ to numerical results. Note that axes are different for each plot.

2.5.2.2 Scattering

We now move to the scattering case, for which analytical solutions are unavailable for both the QoI and its statistics. Instead, we generate over-resolved reference solutions of S^2 using $(N_\xi, N_\eta) = (10^5, 20)$ for comparison. The reference solution variances are $\mathbb{V}ar_\xi[T] = 9.348(7) \times 10^{-3}$ and $\mathbb{V}ar_\xi[R] = 8.033(6) \times 10^{-3}$, where the parenthetical indicates the standard deviation of the last digit. For both QoIs, the MSE, $\mathbb{V}ar$, and $Bias$ of $\tilde{S^2}$ and S^2 follow the same trends as those shown in Figure 2.2. In Figure 2.5, we show the distributions of S^2 and $\tilde{S^2}$ over 25 000 independent repetitions for both the transmittance and reflectance. These results are qualitatively the same as the attenuation-only case, and we similarly see $\tilde{S^2}$ converge to the mean of S^2. Finally, in Figures 2.6 and 2.7, we evaluate the behavior of estimator statistics as a function of N_η for both $\mathbb{V}ar_\xi[T]$ and $\mathbb{V}ar_\xi[R]$. The trends of $\mathbb{V}ar\left[S^2\right]$ and $\mathbb{V}ar\left[\tilde{S^2}\right]$ for both QoIs are similar to what we saw in the attenuation-only case. From numerical results, shown in Table 2.2, $\mathbb{V}ar\left[S^2\right]$ for $\mathbb{V}ar_\xi[T]$ appears to be minimized at the same N_η for both the scattering and attenuation-only cases. However, when approximating $\mathbb{V}ar_\xi[R]$ in Table 2.3, we find that $\mathbb{V}ar\left[S^2\right]$ is minimized at $N_\eta = 20$ rather than $N_\eta = 10$. This demonstrates that the optimal factor pair $(N_\xi \times N_\eta)$ can differ between different QoIs even within the same problem, motivating further investigation to allow the analyst to choose these parameters in an informed way.

Scattering Problem – $\mathbb{V}ar\left[S^2\right]$, Transmittance				
N_η	Estimator Cost			
	200	500	2000	5000
2	1.757E-04	6.976E-05	1.730E-05	6.973E-06
5	7.512E-05	2.968E-05	7.422E-06	2.891E-06
10	**6.411E-05**	**2.486E-05**	**6.191E-06**	**2.439E-06**
20	7.283E-05	2.789E-05	6.947E-06	2.714E-06
25	8.030E-05	3.079E-05	7.399E-06	2.967E-06
100	2.891E-04	8.558E-05	1.883E-05	7.525E-06

Table 2.2: The variance of the estimate of S^2 over 25 000 repetitions for transmittance in the scattering problems.

Scattering Problem – $\mathbb{V}ar\left[S^2\right]$, Reflectance				
N_η	Estimator Cost			
	200	500	2000	5000
2	1.809E-04	7.041E-05	1.803E-05	7.222E-06
5	6.617E-05	2.628E-05	6.549E-06	2.612E-06
10	4.837E-05	1.869E-05	4.592E-06	1.840E-06
20	**4.639E-05**	**1.774E-05**	**4.212E-06**	**1.686E-06**
25	4.935E-05	1.842E-05	4.437E-06	1.773E-06
100	1.682E-04	4.044E-05	8.478E-06	3.287E-06

Table 2.3: The variance of the estimate of S^2 over 25 000 repetitions for reflectance in the scattering problems.

2.6 Conclusions

Monte Carlo sampling-based methods for UQ are non-intrusive, robust, and efficient. However, when coupled with a stochastic computational model such as a Monte Carlo radiation transport solver, Monte Carlo UQ methods propagate both the intended uncertainty and the additional variance introduced by the stochastic model. In this work, we applied the law of total variance to present in closed-form how the UQ variance and stochastic solver variance contribute to the total observed variance. Our primary outcome was the development of a *variance deconvolution* approach to accurately and precisely estimate the UQ variance. Rather than the standard method of over-resolving the stochastic solver for each UQ evaluation, variance deconvolution explicitly computes the stochastic solver variance and removes it from the total observed variance. We showed both in theory and numerically, with an example neutral-particle radiation transport problem, that the variance deconvolution estimator is unbiased and more efficient than the standard approach for the same computational cost. Statistical analysis of the estimator and numerical results suggest an efficiency trade-off between the number of UQ samples and number of stochastic model samples (e.g., particle histories) for a prescribed computational budget. We used the analytic solution of the example radiation transport problem to find the cost-optimal distribution between UQ samples and stochastic model samples, and ongoing work focuses on constructing a pilot study to numerically estimate the cost-optimal distribution without an analytic solution, for application to more complex and realistic problems. While the

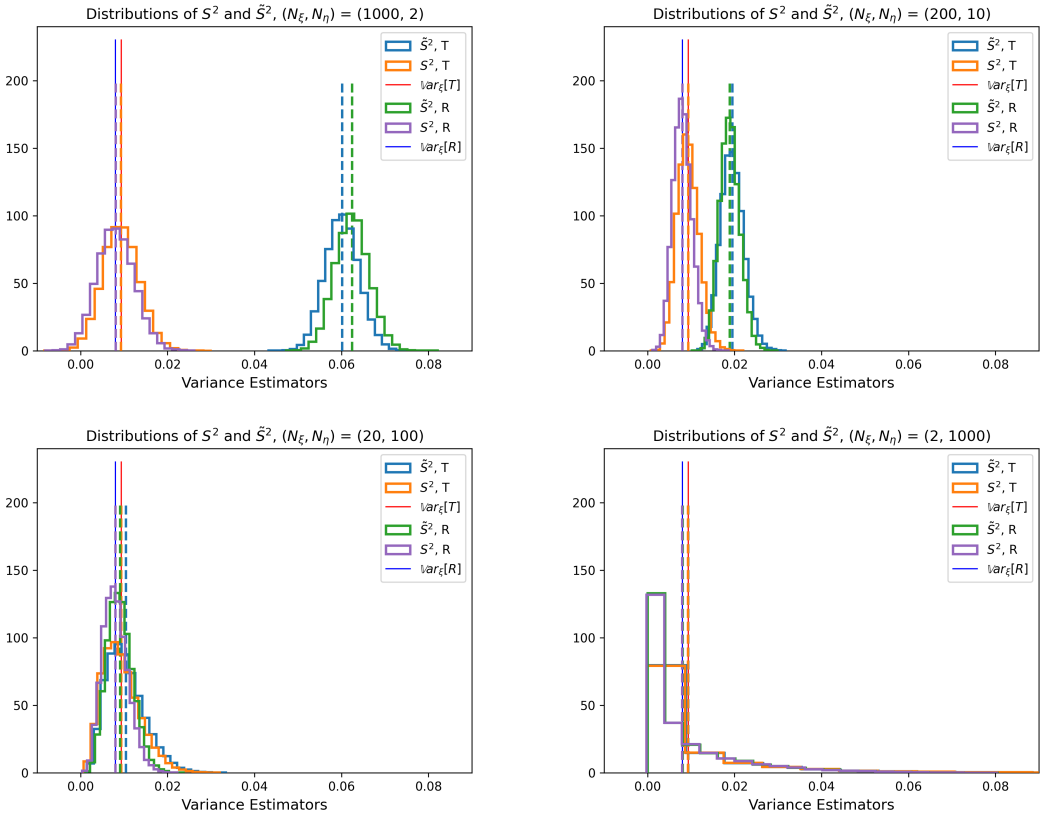

Figure 2.5: Comparing the variance estimates for $\mathbb{V}ar_\xi[T]$ and $\mathbb{V}ar_\xi[R]$ from a brute-force approach to the estimates from the variance deconvolution approach for a 1D radiation transport problem with scattering ($d = 6$). PDF created with 25 000 repetitions, averages reported with dashed lines.

presented test problem applied variance deconvolution to Monte Carlo radiation transport methods, the statistical analysis and theoretical conclusions of the variance deconvolution estimator are applicable to Monte Carlo UQ coupled with any stochastic computational model. In ongoing work, we incorporate variance deconvolution into Saltelli's method for global sensitivity analysis [97] to rank the importance of uncertain random inputs to a MC RT problem, again without having to over-resolve the stochastic solver [77, 15].

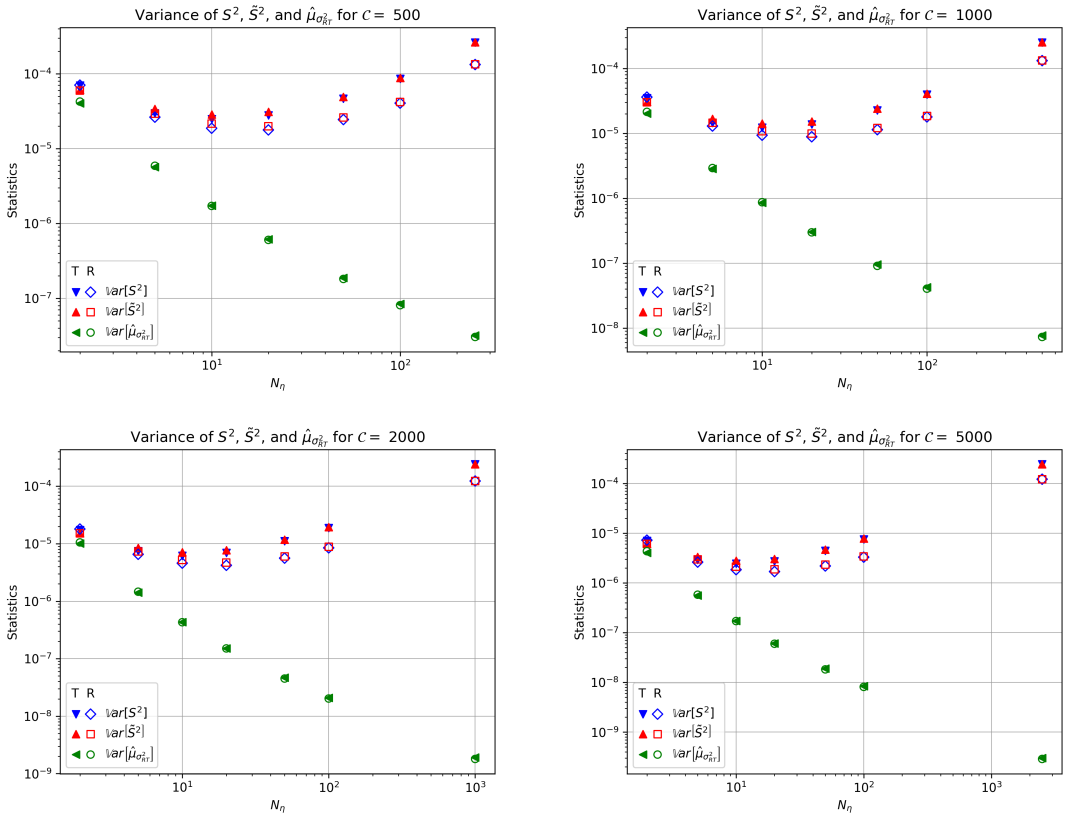

Figure 2.6: Comparing numerical results for $\mathbb{V}ar\left[S^2\right]$, $\mathbb{V}ar\left[\tilde{S^2}\right]$, and $\mathbb{V}ar\left[\hat{\mu}_{\sigma^2_{RT,N_\eta}}\right]$ when approximating $\mathbb{V}ar_\xi\left[T\right]$ and $\mathbb{V}ar_\xi\left[R\right]$. Note that axes are different for each plot.

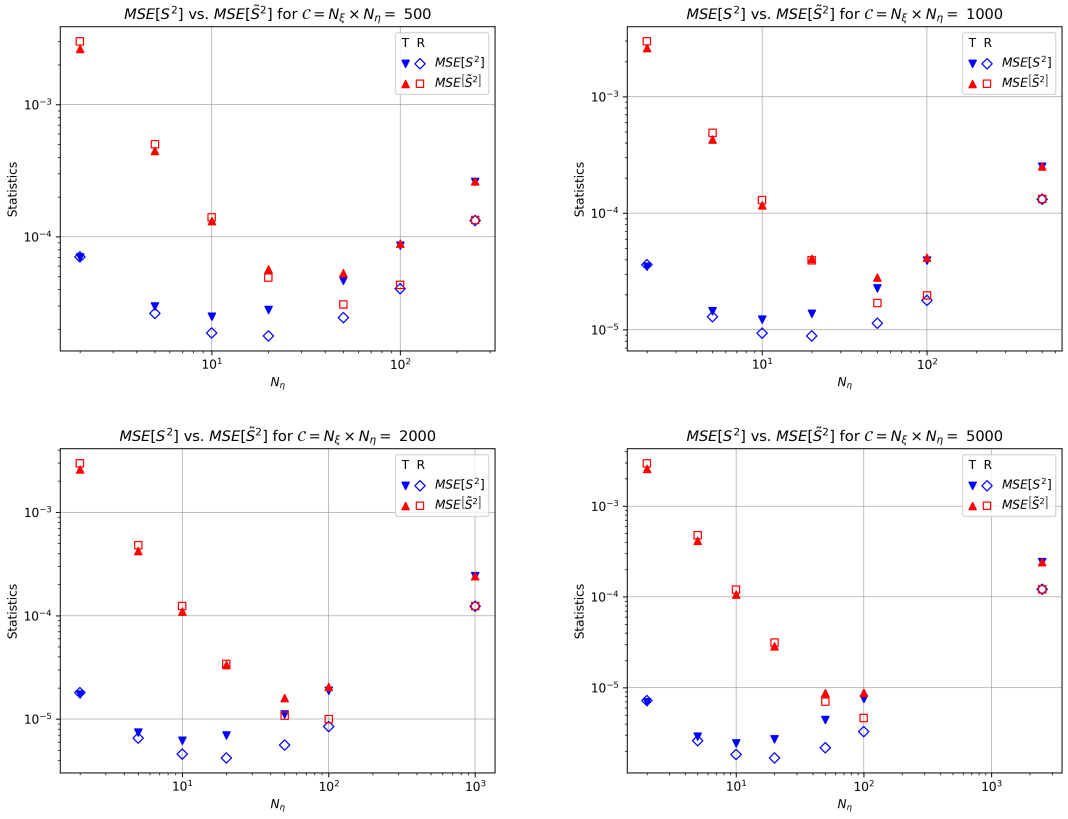

Figure 2.7: Comparing numerical results for $MSE\,[S^2]$ and $MSE\,[\tilde{S^2}]$ when approximating $\mathbb{V}ar_{\xi}\,[T]$ and $\mathbb{V}ar_{\xi}\,[R]$. Note that axes are different for each plot.

Acknowledgment

This work was supported by the Laboratory Directed Research and Development program at Sandia National Laboratories, a multimission laboratory managed and operated by National Technology and Engineering Solutions of Sandia LLC, a wholly owned subsidiary of Honeywell International Inc. for the U.S. Department of Energy's National Nuclear Security Administration under contract DE-NA0003525. This paper describes objective technical results and analysis. Any subjective views or opinions that might be expressed in the paper do not necessarily represent the views of the U.S. Department of Energy or the United States Government. This article has been authored by an employee of National Technology & Engineering Solutions of Sandia, LLC under Contract No. DE-NA0003525 with the U.S. Department of Energy (DOE). The employee owns all right, title and interest in and to the article and is solely responsible for its contents. The United States Government retains and the publisher, by accepting the article for publication, acknowledges that the United States Government retains a non-exclusive, paid-up, irrevocable, world-wide license to publish or reproduce the published form of this article or allow others to do so, for United States Government purposes. The DOE will provide public access to these results of federally sponsored research in accordance with the DOE Public Access Plan https://www.energy.gov/downloads/doe-public-access-plan. This work was supported by the Center for Exascale Monte-Carlo Neutron Transport (CEMeNT) a PSAAP-III project funded by the Department of Energy, grant number DE-NA003967.

2.7 Appendix: Proof of Theorem 2.3.1

We show that $\tilde{S^2}$ is an unbiased estimator for $\mathbb{V}ar\left[\tilde{Q}_{N_\eta}\right]$.

$$\tilde{S^2} = \frac{1}{N_\xi - 1}\sum_{i=1}^{N_\xi}\left(\tilde{Q}_{N_\eta}(\xi_i) - \left\langle\tilde{Q}_{N_\eta}\right\rangle\right)^2 = \frac{1}{N_\xi - 1}\sum_{i=1}^{N_\xi}\left(\tilde{Q}^2_{N_\eta}(\xi_i) - 2\tilde{Q}_{N_\eta}(\xi_i)\left\langle\tilde{Q}_{N_\eta}\right\rangle + \left\langle\tilde{Q}_{N_\eta}\right\rangle^2\right)$$

$$= \frac{1}{N_\xi - 1}\sum_{i=1}^{N_\xi}\left(\tilde{Q}^2_{N_\eta}(\xi_i) - \left\langle\tilde{Q}_{N_\eta}\right\rangle^2\right)$$

$$\begin{aligned}\mathbb{E}\left[\tilde{S^2}\right] &= \mathbb{E}\left[\frac{1}{N_\xi - 1}\sum_{i=1}^{N_\xi}\left(\tilde{Q}_{N_\eta}^2(\xi_i) - \left\langle\tilde{Q}_{N_\eta}\right\rangle^2\right)\right] \\ &= \frac{1}{N_\xi - 1}\sum_{i=1}^{N_\xi}\mathbb{E}\left[\tilde{Q}_{N_\eta}^2(\xi_i) - \left\langle\tilde{Q}_{N_\eta}\right\rangle^2\right] \\ &= \frac{N_\xi}{N_\xi - 1}\left(\mathbb{E}\left[\tilde{Q}_{N_\eta}^2\right] - \mathbb{E}\left[\left\langle\tilde{Q}_{N_\eta}\right\rangle^2\right]\right). \end{aligned} \tag{2.25}$$

We first handle $\mathbb{E}\left[\left\langle\tilde{Q}_{N_\eta}\right\rangle^2\right]$. Using combination theory,

$$\left\langle\tilde{Q}_{N_\eta}\right\rangle^2 = \left(\frac{1}{N_\xi}\sum_{i=1}^{N_\xi}\tilde{Q}_{N_\eta}(\xi_i)\right)^2 = \frac{1}{{N_\xi}^2}\left(\sum_{i=1}^{N_\xi}\tilde{Q}_{N_\eta}^2(\xi_i) + \sum_{i=1}^{N_\xi}\sum_{k=1,\neq i}^{N_\xi}\tilde{Q}_{N_\eta}(\xi_i)\tilde{Q}_{N_\eta}(\xi^{(k)})\right).$$

The distinction between $\tilde{Q}_{N_\eta}^2(\xi_i)$ and $\tilde{Q}_{N_\eta}(\xi_i)\tilde{Q}_{N_\eta}(\xi^{(k)})$ becomes apparent when taking the expected value over ξ. Because ξ_i and $\xi^{(k)}$ are independent realizations, $\mathbb{E}_\xi\left[\tilde{Q}_{N_\eta}(\xi_i)\tilde{Q}_{N_\eta}(\xi^{(k)})\right] = \mathbb{E}_\xi\left[\tilde{Q}_{N_\eta}(\xi_i)\right]\mathbb{E}_\xi\left[\tilde{Q}_{N_\eta}(\xi^{(k)})\right]$. Then,

$$\begin{aligned}\mathbb{E}\left[\left\langle\tilde{Q}_{N_\eta}\right\rangle^2\right] &= \frac{1}{{N_\xi}^2}\left(\sum_{i=1}^{N_\xi}\mathbb{E}\left[\tilde{Q}_{N_\eta}^2(\xi_i)\right] + \sum_{i=1}^{N_\xi}\sum_{k\neq i}^{N_\xi}\mathbb{E}\left[\tilde{Q}_{N_\eta}(\xi_i)\tilde{Q}_{N_\eta}(\xi^{(k)})\right]\right) \\ &= \frac{1}{{N_\xi}^2}\left(N_\xi\mathbb{E}\left[\tilde{Q}_{N_\eta}^2\right] + N_\xi(N_\xi - 1)\mathbb{E}\left[\tilde{Q}_{N_\eta}\right]^2\right) \\ &= \frac{1}{N_\xi}\left(\mathbb{E}\left[\tilde{Q}_{N_\eta}^2\right] + (N_\xi - 1)\mathbb{E}\left[\tilde{Q}_{N_\eta}\right]^2\right) \\ &= \frac{1}{N_\xi}\mathbb{E}\left[\tilde{Q}_{N_\eta}^2\right] + \frac{N_\xi - 1}{N_\xi}\mathbb{E}_\xi\left[Q\right]^2. \end{aligned} \tag{2.26}$$

Plugging this result into Eq. (2.25),

$$\begin{aligned}\mathbb{E}\left[\tilde{S^2}\right] &= \frac{N_\xi}{N_\xi - 1}\left(\mathbb{E}\left[\tilde{Q}_{N_\eta}^2\right] - \frac{1}{N_\xi}\mathbb{E}\left[\tilde{Q}_{N_\eta}^2\right] - \frac{N_\xi - 1}{N_\xi}\mathbb{E}_\xi\left[Q\right]^2\right) \\ &= \mathbb{E}\left[\tilde{Q}_{N_\eta}^2\right] - \mathbb{E}_\xi\left[Q\right]^2 \end{aligned} \tag{2.27}$$

We now handle $\mathbb{E}\left[\tilde{Q}^2_{N_\eta}\right]$ by first introducing the variable transformation $f(\xi,\eta) = Q(\xi) + Z(\eta)$ such that

$$\begin{aligned}\mathbb{E}_\eta\left[f(\xi,\eta)\right] = \mathbb{E}_\eta\left[Q(\xi) + Z(\eta)\right] = Q(\xi)\\ \rightarrow \mathbb{E}_\eta\left[Z(\eta)\right] = 0.\end{aligned}$$

It follows that $\tilde{Q}_{N_\eta}$ can also be written

$$\begin{aligned}\tilde{Q}_{N_\eta}(\xi) &= \frac{1}{N_\eta}\sum_{j=1}^{N_\eta} f(\xi,\eta^{(j)})\\ &= \frac{1}{N_\eta}\sum_{j=1}^{N_\eta}\left(Q(\xi) + Z(\eta^{(j)})\right)\\ &= Q(\xi) + \frac{1}{N_\eta}\sum_{j=1}^{N_\eta} Z(\eta^{(j)}).\end{aligned} \tag{2.28}$$

Applying this definition and combination theory,

$$\begin{aligned}\tilde{Q}^2_{N_\eta}(\xi) &= Q^2(\xi) + \frac{2Q(\xi)}{N_\eta}\sum_{j=1}^{N_\eta} Z(\eta^{(j)}) + \left(\frac{1}{N_\eta}\sum_{j=1}^{N_\eta} Z(\eta^{(j)})\right)^2\\ &= Q^2(\xi) + \frac{2Q(\xi)}{N_\eta}\sum_{j=1}^{N_\eta} Z(\eta^{(j)}) + \frac{1}{{N_\eta}^2}\left(\sum_{j=1}^{N_\eta} Z^2(\eta^{(j)}) + \sum_{j=1}^{N_\eta}\sum_{k=1,\neq j}^{N_\eta} Z(\eta^{(j)})Z(\eta^{(k)})\right).\end{aligned} \tag{2.29}$$

Again, because $\eta^{(j)}$ and $\eta^{(k)}$ are independent realizations, $\mathbb{E}_\eta\left[Z(\eta^{(j)})Z(\eta^{(k)})\right] = \mathbb{E}_\eta\left[Z(\eta^{(j)})\right]\mathbb{E}_\eta\left[Z(\eta^{(k)})\right]$. Finally,

$$\begin{aligned}
\mathbb{E}\left[\tilde{Q}^2_{N_\eta}\right] &= \mathbb{E}_\xi\left[\mathbb{E}_\eta\left[\tilde{Q}^2_{N_\eta}\right]\right] \\
&= \mathbb{E}_\xi\left[Q^2 + 0 + \frac{1}{{N_\eta}^2}\sum_{j=1}^{N_\eta}\mathbb{E}_\eta\left[Z^2\right] + 0\right] \\
&= \mathbb{E}_\xi\left[Q^2\right] + \frac{1}{N_\eta}\mathbb{E}_\xi\left[\mathbb{E}_\eta\left[Z^2\right]\right]
\end{aligned}$$

Plugging in our variable transformation, we see that $\mathbb{E}_\eta\left[Z^2\right] = \mathbb{E}_\eta\left[(f-Q)^2\right] = \mathbb{E}_\eta\left[\left(f - \mathbb{E}_\eta\left[f\right]\right)^2\right] = \sigma^2_\eta$. Therefore,

$$\mathbb{E}\left[\tilde{Q}^2_{N_\eta}\right] = \mathbb{E}_\xi\left[Q^2\right] + \frac{1}{N_\eta}\mathbb{E}_\xi\left[\sigma^2_\eta\right]. \tag{2.30}$$

Finally, combining Eq. (2.27) and Eq. (2.30),

$$\begin{aligned}
\mathbb{E}\left[\tilde{S^2}\right] &= \mathbb{E}_\xi\left[Q^2\right] + \frac{1}{N_\eta}\mathbb{E}_\xi\left[\sigma^2_\eta\right] - \mathbb{E}_\xi\left[Q\right]^2 \\
&= \mathbb{V}ar_\xi\left[Q\right] + \frac{1}{N_\eta}\mathbb{E}_\xi\left[\sigma^2_\eta\right], \qquad (2.31)
\end{aligned}$$

which we recognize from Proposition 2.2.2 as $\mathbb{V}ar\left[\tilde{Q}_{N_\eta}\right]$. Therefore, $\tilde{S^2}$ is an unbiased estimator for $\mathbb{V}ar\left[\tilde{Q}_{N_\eta}\right]$.

2.8 Appendix: Proof of Theorem 2.3.4

Before presenting the derivation for the terms appearing in the previous equations, we introduce some notation for central moments:

$$\begin{aligned}
\mu_k\left[X\right] &\overset{\text{def}}{=} \mathbb{E}\left[\left(X - \mathbb{E}\left[X\right]\right)^k\right] \\
\mu_{\eta,k}\left[X\right] &\overset{\text{def}}{=} \mathbb{E}_\eta\left[\left(X - \mathbb{E}_\eta\left[X\right]\right)^k\right] \\
\sigma^4\left[X\right] &= \Big(\mu_2\left[X\right]\Big)^2 \\
\sigma_\eta^4\left[X\right] &= \left(\mu_{\eta,2}\left[X\right]\right)^2.
\end{aligned} \tag{2.32}$$

We refer to the variable transformation from 2.7 and the useful property it gives rise to,

$$\begin{aligned}
\mathbb{E}_\eta\left[f(\xi,\eta)\right] = \mathbb{E}_\eta\left[Q(\xi) + Z(\eta)\right] &= Q(\xi) \\
\rightarrow \mathbb{E}_\eta\left[Z(\eta)\right] &= 0, \\
\mathbb{E}_\eta\left[Z^k\right] = \mathbb{E}_\eta\left[(f-Q)^k\right] &= \mu_{\eta,k}.
\end{aligned}$$

The following is also useful; we use the notation $Z_j \overset{\text{def}}{=} Z(\eta^{(j)})$ for brevity.

$$\left(\sum_{j=1}^{N_\eta} Z_j\right)^2 = \sum_{j=1}^{N_\eta} Z_j^2 + \sum_{j=1}^{N_\eta}\sum_{\substack{k=1,\\ \neq j}}^{N_\eta} Z_j Z$$

$$\left(\sum_{j=1}^{N_\eta} Z_j\right)^3 = \sum_{j=1}^{N_\eta} Z_j^3 + 3\sum_{j=1}^{N_\eta}\sum_{\substack{k=1,\\ \neq j}}^{N_\eta} Z_j^2 Z_k + \sum_{j=1}^{N_\eta}\sum_{\substack{k=1,\\ \neq j}}^{N_\eta}\sum_{\substack{q=1,\\ \neq j,\\ \neq k}}^{N_\eta} Z_j Z_k Z_q$$

$$\left(\sum_{j=1}^{N_\eta} Z_j\right)^4 = \sum_{j=1}^{N_\eta} Z_j^4 + 4\sum_{j=1}^{N_\eta}\sum_{\substack{k=1,\\ \neq j}}^{N_\eta} Z_j^3 Z_k + 3\sum_{j=1}^{N_\eta}\sum_{\substack{k=1,\\ \neq j}}^{N_\eta} Z_j^2 Z_k^2 + 6\sum_{j=1}^{N_\eta}\sum_{\substack{k=1,\\ \neq j}}^{N_\eta}\sum_{\substack{q=1,\\ \neq j,\\ \neq k}}^{N_\eta} Z_j^2 Z_k Z_q + \sum_{j=1}^{N_\eta}\sum_{\substack{k=1,\\ \neq j}}^{N_\eta}\sum_{\substack{q=1,\\ \neq j,\\ \neq k}}^{N_\eta}\sum_{\substack{r=1,\\ \neq j,\\ \neq k,\\ ,\neq q}}^{N_\eta} Z_j Z_k Z_q Z_r.$$

The variance of the deconvolution estimator S^2 can be written as

$$\mathbb{V}ar\left[S^2\right] = \underbrace{\mathbb{V}ar\left[\tilde{S}^2\right]}_{\text{Term 1}} + \underbrace{\mathbb{V}ar\left[\hat{\mu}_{\sigma^2_{RT,N_\eta}}\right]}_{\text{Term 2}} - 2\underbrace{\mathbb{C}ov\left[\tilde{S}^2, \hat{\mu}_{\sigma^2_{RT,N_\eta}}\right]}_{\text{Term 3}}. \tag{2.33}$$

Term 1

$\tilde{S}^2$ is a sampling estimator for the variance of $\tilde{Q}_{N_\eta}$ from N_ξ evaluations. The variance of a sampling estimator for variance is [10],

$$\mathbb{V}ar\left[\tilde{S}^2\right] = \frac{\overbrace{\mu_4\left[\tilde{Q}_{N_\eta}\right]}^{1.1}}{N_\xi} - \frac{\overbrace{\sigma^4\left[\tilde{Q}_{N_\eta}\right]}^{1.2}(N_\xi - 3)}{N_\xi(N_\xi - 1)}. \tag{2.34}$$

Expanding Term 1.1,

$$\begin{aligned}
\mu_4\left[\tilde{Q}_{N_\eta}\right] &= \mathbb{E}\left[\left(\tilde{Q}_{N_\eta} - \mathbb{E}\left[\tilde{Q}_{N_\eta}\right]\right)^4\right] = \mathbb{E}\left[\left(\tilde{Q}_{N_\eta} - \mathbb{E}_\xi\left[Q\right]\right)^4\right] \\
&= \mathbb{E}\left[\tilde{Q}^4_{N_\eta}\right] - 4\mathbb{E}\left[\tilde{Q}^3_{N_\eta}\right]\mathbb{E}_\xi\left[Q\right] + 6\mathbb{E}\left[\tilde{Q}^2_{N_\eta}\right]\mathbb{E}_\xi\left[Q\right]^2 - 4\mathbb{E}\left[\tilde{Q}_{N_\eta}\right]\mathbb{E}_\xi\left[Q\right]^3 + \mathbb{E}_\xi\left[Q\right]^4 \\
&= \mathbb{E}\left[\tilde{Q}^4_{N_\eta}\right] - 4\mathbb{E}\left[\tilde{Q}^3_{N_\eta}\right]\mathbb{E}_\xi\left[Q\right] + 6\mathbb{E}\left[\tilde{Q}^2_{N_\eta}\right]\mathbb{E}_\xi\left[Q\right]^2 - 3\mathbb{E}_\xi\left[Q\right]^4.
\end{aligned} \tag{2.35}$$

We solved for $\mathbb{E}\left[\tilde{Q}^2_{N_\eta}\right]$ in 2.7, resulting in Eq. (2.30) (repeated below as (2.36)). Applying the same process to $\mathbb{E}\left[\tilde{Q}^3_{N_\eta}\right]$ and $\mathbb{E}\left[\tilde{Q}^4_{N_\eta}\right]$,

$$\mathbb{E}\left[\tilde{Q}^2_{N_\eta}\right] = \mathbb{E}_\xi\left[Q^2\right] + \frac{1}{N_\eta}\mathbb{E}_\xi\left[\sigma^2_\eta\right], \tag{2.36}$$

$$\mathbb{E}\left[\tilde{Q}^3_{N_\eta}\right] = \mathbb{E}_\xi\left[Q^3\right] + \frac{3}{N_\eta}\mathbb{E}_\xi\left[Q\sigma^2_\eta\right] + \frac{1}{{N_\eta}^2}\mathbb{E}_\xi\left[\mu_{\eta,3}\right], \tag{2.37}$$

$$\mathbb{E}\left[\tilde{Q}^4_{N_\eta}\right] = \mathbb{E}_\xi\left[Q^4\right] + \frac{6}{N_\eta}\mathbb{E}_\xi\left[Q^2\sigma^2_\eta\right] + \frac{4}{{N_\eta}^2}\mathbb{E}_\xi\left[Q\mu_{\eta,3}\right] + \frac{1}{{N_\eta}^3}\mathbb{E}_\xi\left[\mu_{\eta,4}\right] + \frac{3\left(N_\eta - 1\right)}{{N_\eta}^3}\mathbb{E}_\xi\left[\sigma^4_\eta\right]. \tag{2.38}$$

Expanding Term 1.2,

$$\sigma^4\left[\tilde{Q}_{N_\eta}\right] = \left(\sigma^2\left[\tilde{Q}_{N_\eta}\right]\right)^2 = \left(\mathbb{V}ar\left[\tilde{Q}_{N_\eta}\right]\right)^2$$
$$= \left(\mathbb{V}ar_\xi\left[Q\right] + \frac{1}{N_\eta}\mathbb{E}_\xi\left[\sigma_\eta^2\right]\right)^2. \tag{2.39}$$

Term 2

$$\mathbb{V}ar\left[\hat{\mu}_{\sigma^2_{RT,N_\eta}}\right] = \mathbb{V}ar\left[\frac{1}{N_\xi}\sum_{i=1}^{N_\xi}\frac{\hat{\sigma}_\eta^2(\xi_i)}{N_\eta}\right] = \frac{1}{{N_\xi}^2{N_\eta}^2}\sum_{i=1}^{N_\xi}\mathbb{V}ar\left[\hat{\sigma}_\eta^2(\xi_i)\right] = \frac{1}{N_\xi{N_\eta}^2}\mathbb{V}ar\left[\hat{\sigma}_\eta^2\right]. \tag{2.40}$$

Applying the law of total variance and the variance of a sample variance [10],

$$\mathbb{V}ar\left[\hat{\sigma}_\eta^2\right] = \mathbb{V}ar_\xi\left[\mathbb{E}_\eta\left[\hat{\sigma}_\eta^2\right]\right] + \mathbb{E}_\xi\left[\mathbb{V}ar_\eta\left[\hat{\sigma}_\eta^2\right]\right]$$
$$= \mathbb{V}ar_\xi\left[\sigma_\eta^2\right] + \mathbb{E}_\xi\left[\frac{\mu_{\eta,4}[f]}{N_\eta} - \frac{\sigma_\eta^4[f]\left(N_\eta - 3\right)}{N_\eta\left(N_\eta - 1\right)}\right].$$

Combining,

$$\mathbb{V}ar\left[\hat{\mu}_{\sigma^2_{RT,N_\eta}}\right] = \frac{\mathbb{V}ar_\xi\left[\sigma_\eta^2\right]}{N_\xi{N_\eta}^2} + \frac{1}{N_\xi{N_\eta}^3}\mathbb{E}_\xi\left[\mu_{\eta,4}[f] - \frac{\sigma_\eta^4[f]\left(N_\eta - 3\right)}{\left(N_\eta - 1\right)}\right] \tag{2.41}$$

Term 3

From the definition of covariance,

$$\mathbb{C}ov\left[\tilde{S}^2, \hat{\mu}_{\sigma^2_{RT,N_\eta}}\right] = \mathbb{E}\left[\tilde{S}^2\hat{\mu}_{\sigma^2_{RT,N_\eta}}\right] - \mathbb{E}\left[\tilde{S}^2\right]\mathbb{E}\left[\hat{\mu}_{\sigma^2_{RT,N_\eta}}\right].$$

We have shown in Proposition 2.3.1 that $\mathbb{E}\left[\tilde{S}^2\right] = \mathbb{V}ar\left[\tilde{Q}_{N_\eta}\right]$, and in Theorem 2.3.3 that $\mathbb{E}\left[\hat{\mu}_{\sigma^2_{RT,N_\eta}}\right] = \frac{1}{N_\eta}\mathbb{E}_\xi\left[\sigma^2_\eta\right]$. What remains is to evaluate $\mathbb{E}\left[\tilde{S}^2\hat{\mu}_{\sigma^2_{RT,N_\eta}}\right]$:

$$\mathbb{E}\left[\tilde{S}^2\hat{\mu}_{\sigma^2_{RT,N_\eta}}\right] = \frac{1}{N_\xi N_\eta}\left(\mathbb{E}\left[\tilde{Q}^2_{N_\eta}\hat{\sigma}^2_\eta\right] + \mathbb{E}_\xi\left[\sigma^2_\eta\right]\mathbb{E}_\xi\left[Q\right]^2\right) - \frac{2}{N_\xi N_\eta}\mathbb{E}_\xi\left[Q\right]\mathbb{E}\left[\tilde{Q}_{N_\eta}\hat{\sigma}^2_\eta\right] + \frac{\left(N_\xi - 1\right)}{N_\xi N_\eta}\mathbb{V}ar\left[\tilde{Q}_{N_\eta}\right]\mathbb{E}_\xi\left[\sigma^2_\eta\right].$$

Combining,

$$\mathbb{C}ov\left[\tilde{S}^2, \hat{\mu}_{\sigma^2_{RT,N_\eta}}\right] = \frac{1}{N_\xi N_\eta}\left(\mathbb{E}\left[\tilde{Q}^2_{N_\eta}\hat{\sigma}^2_\eta\right] + \mathbb{E}_\xi\left[\sigma^2_\eta\right]\mathbb{E}_\xi\left[Q\right]^2\right) - \frac{2}{N_\xi N_\eta}\mathbb{E}_\xi\left[Q\right]\mathbb{E}\left[\tilde{Q}_{N_\eta}\hat{\sigma}^2_\eta\right] - \frac{1}{N_\xi N_\eta}\mathbb{E}_\xi\left[\sigma^2_\eta\right]\mathbb{V}ar\left[\tilde{Q}_{N_\eta}\right], \tag{2.42}$$

where

$$\mathbb{E}\left[\tilde{Q}^2_{N_\eta}\hat{\sigma}^2_\eta\right] = \mathbb{E}_\xi\left[Q^2\sigma^2_\eta\right] + \frac{2}{N_\eta}\mathbb{E}_\xi\left[Q\mu_{\eta,3}\right] + \frac{1}{{N_\eta}^2}\mathbb{E}_\xi\left[\mu_{\eta,4} + \left(N_\eta - 3\right)\sigma^4_\eta\right],$$

$$\mathbb{E}\left[\tilde{Q}_{N_\eta}\hat{\sigma}^2_\eta\right] = \mathbb{E}_\xi\left[Q\sigma^2_\eta\right] + \frac{1}{N_\eta}\mathbb{E}_\xi\left[\mu_{\eta,3}\right], \text{ and}$$

$$\mathbb{V}ar\left[\tilde{Q}_{N_\eta}\right] = \mathbb{V}ar_\xi\left[Q\right] + \frac{1}{N_\eta}\mathbb{E}_\xi\left[\sigma^2_\eta\right].$$

2.9 Appendix: Analytic Solutions for Section 2.5.1

We can derive reference solutions for the average solver variance and total polluted variance by assuming that elementary event f is valued 1 to indicate transmittance, or 0 to indicate absorption. This assumption excludes weighted MC RT approaches, but our primary interest here is to develop analytic solutions to verify the estimators introduced in this

work. It follows that $f = f^2$, from which we can show that

$$\begin{aligned}
\frac{1}{N_\eta}\mathbb{E}_\xi\left[\sigma_\eta^2\right] &= \frac{1}{N_\eta}\mathbb{E}_\xi\left[\mathbb{E}_\eta\left[(f-Q)^2\right]\right] \\
&= \frac{1}{N_\eta}\mathbb{E}_\xi\left[\mathbb{E}_\eta\left[f^2 - 2fQ + Q^2\right]\right] \\
&= \frac{1}{N_\eta}\mathbb{E}_\xi\left[\mathbb{E}_\eta\left[f - 2fQ + Q^2\right]\right] \\
&= \frac{1}{N_\eta}\mathbb{E}_\xi\left[Q - 2Q^2 + Q^2\right] \\
&= \frac{\mathbb{E}_\xi\left[Q\right] - \mathbb{E}_\xi\left[Q^2\right]}{N_\eta}. \\
\mathbb{V}ar\left[\tilde{Q}_{N_\eta}\right] &= \mathbb{V}ar_\xi\left[Q\right] + \frac{\mathbb{E}_\xi\left[Q\right] - \mathbb{E}_\xi\left[Q^2\right]}{N_\eta}.
\end{aligned} \tag{2.43}$$

Additionally, we can use the closed-form expression for the variance of the variance deconvolution estimator from Theorem 2.3.4 to derive an expression for the variance deconvolution estimator's MSE as a function of N_η. By adopting the same assumption that $f = f^2$, tedious computations lead us to the following expressions, which simply express all statistics needed for Eq. (2.33) in terms of raw moments of the transmittance up to the fourth order.

$$\begin{aligned}
\mathbb{E}_\xi\left[\sigma_\eta^2\right] &= \mathbb{E}_\xi\left[Q\right] - \mathbb{E}_\xi\left[Q^2\right] \\
\mathbb{E}_\xi\left[\left(\sigma_\eta^2\right)^2\right] &= \mathbb{E}_\xi\left[Q^2\right] - 2\mathbb{E}_\xi\left[Q^3\right] + \mathbb{E}_\xi\left[Q^4\right] \\
\mathbb{E}_\xi\left[\mu_{\eta,3}\right] &= \mathbb{E}_\xi\left[Q\right] - 3\mathbb{E}_\xi\left[Q^2\right] + 2\mathbb{E}_\xi\left[Q^3\right] \\
\mathbb{E}_\xi\left[\mu_{\eta,4}\right] &= \mathbb{E}_\xi\left[Q\right] - 4\mathbb{E}_\xi\left[Q^2\right] + 6\mathbb{E}_\xi\left[Q^3\right] - 3\mathbb{E}_\xi\left[Q^4\right] \\
\mathbb{E}_\xi\left[Q\sigma_\eta^2\right] &= \mathbb{E}_\xi\left[Q^2(1-Q)\right] = \mathbb{E}_\xi\left[Q^2\right] - \mathbb{E}_\xi\left[Q^3\right] \\
\mathbb{E}_\xi\left[Q^2\sigma_\eta^2\right] &= \mathbb{E}_\xi\left[Q^3\left(1-Q\right)\right] = \mathbb{E}_\xi\left[Q^3\right] - \mathbb{E}_\xi\left[Q^4\right] \\
\mathbb{E}_\xi\left[Q\mu_{\eta,3}\right] &= \mathbb{E}_\xi\left[Q^2\right] - 3\mathbb{E}_\xi\left[Q^3\right] + 2\mathbb{E}_\xi\left[Q^4\right] \\
\mathbb{V}ar_\xi\left[Q\right] &= \mathbb{E}_\xi\left[Q^2\right] - \left(\mathbb{E}_\xi\left[Q\right]\right)^2.
\end{aligned} \tag{2.44}$$

GLOBAL SENSITIVITY ANALYSIS IN MONTE CARLO RADIATION TRANSPORT

Kayla B. Clements, Gianluca Geraci, Aaron J. Olson, Todd S. Palmer

Presented at *The International Conference on Mathematics and Computational Methods Applied to Nuclear Science and Engineering*
Proceedings, Aug 2023.

Chapter 3: Global Sensitivity Analysis in Monte Carlo Radiation Transport

Abstract

We consider *Global Sensitivity Analysis* (GSA) for Monte Carlo (MC) radiation transport (RT) applications. GSA is usually combined with Uncertainty Quantification (UQ), where the latter (among other goals) quantifies the variability of a model output in the presence of uncertain inputs and the former attributes this variability to the inputs. The additional noise inherent to MC RT solvers due to the finite number of particle histories presents an additional challenge to GSA and UQ, which are well-established for deterministic solvers. In this contribution, we apply variance deconvolution to Saltelli's method to address MC RT solver noise without having to over-resolve the MC RT simulation.

3.1 Introduction

Global sensitivity analysis (GSA) aims to apportion, or divide and allocate, variability in model output to different sources of uncertainty in model input [102]. GSA is useful to understand the relative importance of each of a model's uncertain inputs, and their interactions with one another, to the behavior of model output. It is typically paired with uncertainty quantification (UQ), which deals with characterizing and propagating uncertainty sources through computational models. For an exhaustive introduction to GSA in the scientific computing context, see Saltelli's book [102]. This work focuses on sampling-based GSA applied to stochastic solvers, specifically Monte Carlo radiation transport (MC RT) solvers. Typically, UQ and GSA assume that the computational model itself is deterministic, *i.e.*, , that given identical inputs, the model will produce identical outputs. From this assumption, it follows that any output variability characterized by UQ or apportioned by GSA is a result of some uncertain input to the solver, not variability inherent to the solver itself. Despite the abundant literature produced on GSA over the last few decades, there is a gap in the quantification and control of the intrinsic randomness

introduced by non-deterministic solvers.

Stochastic solvers are widely used and important for many applications depending on the information needed by the user, the problem space, and the complexity of the modeled system. Unlike deterministic methods, which require phase-space discretization and approximate solutions to continuous equations, MC RT methods are event based and can faithfully model complex physics. This makes MC RT methods well-suited to solve, for example, complicated three-dimensional, time-dependent problems [64]. However, results from MC RT solvers are always approximate, constrained by the finite number of particle histories that can be used in a simulation. While it is certainly possible to apply UQ and GSA to stochastic solvers, this invalidates the assumption that output uncertainty can be analyzed solely in the context of input uncertainty. Statistical analysis can be considered "polluted" by the variability introduced by the solver itself. It is possible to rigorously show [12, 14] that the stochastic solver increases the observed model output variance, possibly causing an analyst to over-estimate the model's response to an uncertain input. A brute-force method to address this complication and "de-pollute" statistics of interest is to over-resolve the stochastic solver, *e.g.*, , increase the number of particles in the simulation, until the solver variance is rendered negligible compared to the effects of the uncertain inputs [9]. Resolving stochastic models to this extent is already computationally expensive and folding that into the UQ and GSA workflow, which requires repeated evaluation of numerical codes, increases the computational expense to the point of intractability. Our goal is to gain an understanding of how GSA can be performed in the context of MC RT solvers by explicitly accounting for the stochastic variability they introduce.

This work builds on a recently-derived *variance deconvolution* approach [12, 14]. We have introduced variance deconvolution to quantify the variance contribution from a stochastic solver and effectively remove it from the total polluted variance, accurately estimating the desired variance induced by uncertain input parameters (referred to from here as *parametric variance*). This is far more cost effective than the brute-force approach, and uses an unbiased estimator for the variance introduced by the solver and for the parametric variance. We apply this variance deconvolution UQ workflow here to MC RT problems, but as we will show, the method is not specific to radiation transport and is widely applicable to stochastic solvers. Also in recent work, we integrated variance deconvolution

in sampling-based GSA for stochastic media [75] and surrogate [31, 28] approaches. Detailed derivation and analysis for UQ with variance deconvolution is available in [14], and is summarized below. In this paper, we apply variance deconvolution to a general GSA case and compare its performance to the straightforward application of Saltelli's method, without any particular correction for the solver's noise.

3.2 Global Sensitivity Analysis: Background Theory

We consider a generic QoI $Q = Q(\boldsymbol{\xi})$, which expresses a mapping from the vector of d uncertain input parameters $\xi \in \Xi \subset \mathbb{R}^d$, with joint probability density function (PDF) $p(\xi)$, to scalar Q. In standard UQ, we are concerned with estimating statistics for Q with respect to the input parameters, *e.g.* moments like the mean and variance:

$$\mathbb{E}_\xi[Q] \stackrel{\text{def}}{=} \int_\Xi Q(\xi)p(\xi)d\xi \quad \text{and} \quad \mathbb{V}ar_\xi[Q] \stackrel{\text{def}}{=} \int_\Xi \left(Q(\xi) - \mathbb{E}_\xi[Q]\right)^2 p(\xi)d\xi. \tag{3.1}$$

In this work, we consider variance-based GSA[1], quantifying the uncertainty of model output by studying how each parameter (or group of parameters) ξ_i affects the output's variance. We start by considering that ξ_i is fixed to some value in its PDF ξ_i^*. To compute the mean of Q conditional on $\xi_i = \xi_i^*$, we take the expected value of Q over all parameters *except* ξ_i, denoted $\xi_{\sim i}$. The conditional variance over all possible values of ξ_i^*, $\mathbb{V}_{\xi_i}\left[\mathbb{E}_{\xi_{\sim i}}\left[Q \mid \xi_i\right]\right] \stackrel{\text{def}}{=} \mathbb{V}_i$, is known as the first-order effect of ξ_i on Q, a measure of the variance introduced by parameter ξ_i. To simplify notation, we write this as $\mathbb{V}ar\left[\mathbb{E}\left[Q \mid \xi_i\right]\right]$, where the parameters of integration can be assumed from the fixed parameter. We can also consider higher order effects, known as interaction effects, which captures that Q's response to a set of parameters cannot be fully described by the sum of their individual first-order effects. For example, the second-order effect of the pair (ξ_i, ξ_j) can be written using Sobol's decomposition [103] by removing their individual first-order effects from their joint effect, $\mathbb{V}_{ij} = \mathbb{V}ar\left[\mathbb{E}\left[Q \mid \xi_i, \xi_j\right]\right] - \mathbb{V}_i - \mathbb{V}_j$. While $\mathbb{V}_i$ is a measure of the effect of ξ_i on Q, the second-order effect $\mathbb{V}_{ij}$ is a measure of the effect of the interaction between ξ_i and ξ_j on Q.

Sensitivity indices, sometimes referred to as Sobol' indices (SI), provide a measure of

[1] We limit ourselves here to variance-based strategies, although other approaches are also possible [80, 30].

how important a parameter (or set of parameters) is in contributing to the overall variance. This sensitivity can range between 0 and 1, where importance increases as a SI approaches 1. A SI can be computed for any of a parameter's arbitrary-order effects. We are typically interested in computing the first-order SI S_i and total SI S_{Ti},

$$S_i = \frac{\mathbb{V}_{\xi_i}\left[\mathbb{E}_{\xi_{\sim i}}\left[Q \mid \xi_i\right]\right]}{\mathbb{V}ar_{\xi}\left[Q\right]}, \qquad S_{Ti} = 1 - \frac{\mathbb{V}_{\xi_{\sim i}}\left[\mathbb{E}_{\xi_i}\left[Q \mid \xi_{\sim i}\right]\right]}{\mathbb{V}ar_{\xi}\left[Q\right]}, \tag{3.2}$$

where total SI accounts for the individual effect of ξ_i and all of its interaction effects. For a model with three uncertain input factors, the total effect SI of ξ_1 is the sum of its first-order, second-order, and third-order SIs, $S_{T1} = S_1 + S_{12} + S_{13} + S_{123}$.

3.2.1 Saltelli's method

Saltelli introduced a widely used sampling method [102] that provides the benchmark for any subsequent GSA development, which we briefly summarize here. Assuming d random inputs and N sampling realizations, Saltelli's algorithm reads as follows:

1. Define two (N, d) matrices, A and B, which contain independent input samples.

$$A = \begin{bmatrix} \xi_1^{(1)} & \cdots & \xi_i^{(1)} & \cdots & \xi_d^{(1)} \\ \vdots & & \ddots & & \vdots \\ \xi_1^{(N)} & \cdots & \xi_i^{(N)} & \cdots & \xi_d^{(N)} \end{bmatrix}, \qquad B = \begin{bmatrix} \xi_{d+1}^{(1)} & \cdots & \xi_{d+i}^{(1)} & \cdots & \xi_{2d}^{(1)} \\ \vdots & & \ddots & & \vdots \\ \xi_{d+1}^{(N)} & \cdots & \xi_{d+i}^{(N)} & \cdots & \xi_{2d}^{(N)} \end{bmatrix}. \tag{3.3}$$

2. For each ith random input, define a matrix C_i using all columns of B except for the ith column, which comes from A.

$$C_i = \begin{bmatrix} \xi_{d+1}^{(1)} & \cdots & \xi_i^{(1)} & \cdots & \xi_{2d}^{(1)} \\ \vdots & & \ddots & & \vdots \\ \xi_{d+1}^{(N)} & \cdots & \xi_i^{(N)} & \cdots & \xi_{2d}^{(N)} \end{bmatrix}. \tag{3.4}$$

3. Compute model output for A, B, and all C_i to obtain vectors of model output y of

dimension $(N, 1)$.

4. Estimate the first-order and total sensitivity indices via sampling:

$$S_i = \frac{\mathbb{V}ar\left[\mathbb{E}\left[Q \mid \xi_i\right]\right]}{\mathbb{V}ar_{\xi}\left[Q\right]} \approx \frac{\frac{1}{N}\sum_{j=1}^{N} y_A^{(j)} y_{C_i}^{(j)} - \left(\frac{1}{N}\sum_{j=1}^{N} y_A^{(j)}\right)^2}{\frac{1}{N}\sum_{j=1}^{N}\left(y_A^{(j)}\right)^2 - \left(\frac{1}{N}\sum_{j=1}^{N} y_A^{(j)}\right)^2}, \tag{3.5}$$

$$S_{T_i} = 1 - \frac{\mathbb{V}ar\left[\mathbb{E}\left[Q \mid \xi_{\sim i}\right]\right]}{\mathbb{V}ar_{\xi}\left[Q\right]} \approx 1 - \frac{\frac{1}{N}\sum_{j=1}^{N} y_B^{(j)} y_{C_i}^{(j)} - \left(\frac{1}{N}\sum_{j=1}^{N} y_A^{(j)}\right)^2}{\frac{1}{N}\sum_{j=1}^{N}\left(y_A^{(j)}\right)^2 - \left(\frac{1}{N}\sum_{j=1}^{N} y_A^{(j)}\right)^2}. \tag{3.6}$$

While in this paper we only consider the baseline Saltelli method as in [102], a number of modifications and extensions have been made to the method, for example as discussed in [103].

3.3 Computing Sobol' Indices with Stochastic Solvers

The Saltelli method is well-established when the computational model is deterministic. We propose a modified application of the Saltelli method for use with stochastic computational models by applying variance deconvolution.

When the computational model is a stochastic solver, the QoI Q can only be approximated by averaging a finite number of elementary event realizations f (see [14] for details). For instance, in MC RT applications, we indicate with f an event resulting from a single particle history, and approximate Q using N_η particle histories:

$$Q(\xi) \stackrel{\text{def}}{=} \mathbb{E}_\eta\left[f(\xi, \eta)\right] \approx \frac{1}{N_\eta}\sum_{j=1}^{N_\eta} f(\xi, \eta^{(j)}) \stackrel{\text{def}}{=} \tilde{Q}_{N_\eta}(\xi). \tag{3.7}$$

The additional variable η is introduced only to notionally represent the randomness in a MC RT solver. In practice η, unlike ξ, is neither controlled nor assumed to be known, and merely reflects that even for identical systems defined by the same ξ, individual particle histories will follow different trajectories. Because Q is approximated by $\tilde{Q}_{N_\eta}$, parametric

variance is not directly accessible. With the variance deconvolution approach [14], we approximate the parametric variance $\mathbb{V}ar_{\xi}\left[Q\right]$ from observable quantities via Eq. (3.8), where $\mathbb{V}ar\left[\tilde{Q}_{N_\eta}\right]$ represents the total variance (polluted by the MC RT noise) and $\mathbb{E}_{\xi}\left[\sigma_\eta^2\right]$ represents the average contribution from the solver's stochasticity $\sigma_\eta^2 \overset{\text{def}}{=} \mathbb{V}ar_{\eta}\left[f\right]$

$$\mathbb{V}ar_{\xi}\left[Q\right] = \mathbb{V}ar\left[\tilde{Q}_{N_\eta}\right] - \frac{\mathbb{E}_{\xi}\left[\sigma_\eta^2\right]}{N_\eta}. \tag{3.8}$$

In [75], we applied this variance deconvolution strategy to GSA in the case where the QoI was the conditional expectation of Q over stochastic media realizations. Here, we focus on the general case, wherein we desire to compute first-order and total SIs (Eq. (3.2)) for the QoI Q but can only access $\tilde{Q}_{N_\eta}$. We develop an expression for the first-order effect $\mathbb{V}ar\left[\mathbb{E}\left[Q \mid \xi_i\right]\right]$ by first applying the law of total variance to the polluted total variance,

$$\mathbb{V}ar\left[\tilde{Q}_{N_\eta}\right] = \mathbb{V}_{\xi_i}\left[\mathbb{E}_{\xi_{\sim i},\eta}\left[\tilde{Q}_{N_\eta}\right]\right] + \mathbb{E}_{\xi_i}\left[\mathbb{V}_{\xi_{\sim i},\eta}\left[\tilde{Q}_{N_\eta}\right]\right]. \tag{3.9}$$

We apply variance deconvolution and the law of total variance as needed and, after a few manipulations, arrive at an expression for the first-order effect of ξ_i,

$$\mathbb{V}_{\xi_i}\left[\mathbb{E}_{\xi_{\sim i}}\left[Q\right]\right] = \mathbb{V}ar\left[\tilde{Q}_{N_\eta}\right] - \mathbb{E}_{\xi_i}\left[\mathbb{V}_{\xi_{\sim i}}\left[\tilde{Q}_{N_\eta}\right]\right], \tag{3.10}$$

where we have refrained from including the full derivation details in the interest of space. It follows that the first-order effect of $\xi_{\sim i}$, needed to compute the total SI, can be written

$$\mathbb{V}_{\xi_{\sim i}}\left[\mathbb{E}_{\xi_i}\left[Q\right]\right] = \mathbb{V}ar\left[\tilde{Q}_{N_\eta}\right] - \mathbb{E}_{\xi_{\sim i}}\left[\mathbb{V}_{\xi_i}\left[\tilde{Q}_{N_\eta}\right]\right]. \tag{3.11}$$

When applying variance deconvolution to UQ [14], we computed the parametric variance by removing the average solver variance from the total polluted variance. Applied here for GSA, however, we do not need to explicitly compute the average solver variance to compute the parametric conditional variances. Instead, we do so by removing the polluted conditional means, *e.g.*, , $\mathbb{E}\left[\mathbb{V}ar\left[\tilde{Q}_{N_\eta}|\xi_i\right]\right]$ from the total polluted variance.

3.3.1 Modifying Saltelli's method for stochastic solvers

We use the sampling scheme from Saltelli's method to compute sample estimates of Eqs. (3.10) and (3.11), analogous to the sampling estimators in Eqs. (3.5) and (3.6) for the deterministic-solver case. We consider matrices of random numbers A, B, and C_i as defined in Eqs. (3.3) and (3.4), and output vectors $\tilde{y}_A$, $\tilde{y}_B$, and $\tilde{y}_{C_i}$ that contain outputs of an MC RT solver $\tilde{Q}_{N_\eta}(\xi_1, \ldots, \xi_d)$. The only new information to collect for our modification is a vector of solver variances

$$\tilde{y}_{\sigma^2_\eta, A} \stackrel{\text{def}}{=} \begin{bmatrix} \hat{\sigma}^2_\eta\left(\xi_1^{(1)}, \cdots, \xi_i^{(1)}, \cdots, \xi_d^{(1)}\right) \\ \hat{\sigma}^2_\eta\left(\xi_1^{(2)}, \cdots, \xi_i^{(2)}, \cdots, \xi_d^{(2)}\right) \\ \vdots \\ \hat{\sigma}^2_\eta\left(\xi_1^{(N)}, \cdots, \xi_i^{(N)}, \cdots, \xi_d^{(N)}\right) \end{bmatrix}, \tag{3.12}$$

where $\hat{\sigma}^2_\eta$ is the sampling estimator for σ^2_η,

$$\hat{\sigma}^2_\eta\left(\xi^{(k)}\right) \stackrel{\text{def}}{=} \frac{1}{N_\eta} \sum_{j=1}^{N_\eta} \left(f\left(\xi^{(k)}, \eta^{(j)}\right) - \tilde{Q}_{N_\eta}\left(\xi^{(k)}\right)\right)^2. \tag{3.13}$$

We define sampling estimator counterparts for the terms in Eq. (3.10) and (3.11). The total polluted variance,

$$\mathbb{V}ar\left[\tilde{Q}_{N_\eta}\right] \approx \tilde{S}^2 \stackrel{\text{def}}{=} \frac{1}{N-1} \sum_{j=1}^{N} \left(\tilde{y}_A^{(j)} - \sum_{k=1}^{N} \tilde{y}_A^{(k)}\right)^2, \tag{3.14}$$

is used to estimate the parametric variance,

$$\mathbb{V}ar_\xi\left[Q\right] \approx S^2 \stackrel{\text{def}}{=} \tilde{S}^2 - \frac{1}{N_\eta N_\xi} \sum_{j=1}^{N} \tilde{y}^{(j)}_{\sigma^2_\eta, A}. \tag{3.15}$$

We estimate the conditional variances as

$$\mathbb{V}_{\xi_{\sim i}}\left[\tilde{Q}_{N_\eta}^{(j)}\right] \approx \left(\tilde{S}^2_{\xi_{\sim i}}\right)^{(j)} \stackrel{\text{def}}{=} \left(\tilde{y}_A^{(j)}\right)^2 + \left(\tilde{y}_{C_i}^{(j)}\right)^2 - \frac{\left(\tilde{y}_A^{(j)} + \tilde{y}_{C_i}^{(j)}\right)^2}{2}, \tag{3.16}$$

$$\mathbb{V}_{\xi_i}\left[\tilde{Q}_{N_\eta}^{(j)}\right] \approx \left(\tilde{S}^2_{\xi_i}\right)^{(j)} \stackrel{\text{def}}{=} \left(\tilde{y}_B^{(j)}\right)^2 + \left(\tilde{y}_{C_i}^{(j)}\right)^2 - \frac{\left(\tilde{y}_B^{(j)} + \tilde{y}_{C_i}^{(j)}\right)^2}{2} \tag{3.17}$$

such that the sample estimators for first-order and total SI using stochastic solvers are:

$$S_i = \frac{\mathbb{V}ar\left[\mathbb{E}\left[Q \mid \xi_i\right]\right]}{\mathbb{V}ar_\xi\left[Q\right]} \approx \frac{\tilde{S}^2 - \frac{1}{N}\sum_{j=1}^{N}\left(\tilde{S}^2_{\xi_{\sim i}}\right)^{(j)}}{S^2} \tag{3.18}$$

$$S_{T_i} = 1 - \frac{\mathbb{V}ar\left[\mathbb{E}\left[Q \mid \xi_{\sim i}\right]\right]}{\mathbb{V}ar_\xi\left[Q\right]} \approx 1 - \frac{\tilde{S}^2 - \frac{1}{N}\sum_{j=1}^{N}\left(\tilde{S}^2_{\xi_i}\right)^{(j)}}{S^2}. \tag{3.19}$$

3.4 Results

As a test radiation transport problem, we consider a neutral-particle, attenuation-only, mono-energetic steady-state radiation transport problem. A beam source of magnitude one is incident on a 1D slab of length 3 that is separated into three material regions. The problem QoI $Q\left(\boldsymbol{\xi}\right)$ is transmittance through the slab. We introduce six uniformly distributed uncertain parameters, grouped into three uncertainty sources of interest: 1) Cosine of beam-source incidence angle $\mu \sim \mathcal{U}\left[0.6, 1.0\right]$; 2) Boundary locations between material regions $x_1 \sim \mathcal{U}\left[0.3, 1.7\right]$ and $x_2 \sim \mathcal{U}\left[1.7, 2.3\right]$; and 3) Total cross sections of the slab materials $\Sigma_{t,1} \sim \mathcal{U}\left[0.1, 0.9\right], \Sigma_{t,2} \sim \mathcal{U}\left[0.2, 0.4\right], \Sigma_{t,3} \sim \mathcal{U}\left[0.07, 1.03\right]$.

To investigate our variance deconvolution modification of Saltelli's method (denoted Saltelli-VarD for brevity), we compute first-order and total SIs for the three groups of parametric uncertainty with both Saltelli-VarD and the straightforward Saltelli method. For benchmark reference solutions, we solve for SIs using Saltelli's method with $N = 10^8$ sample realizations, computing transmittance analytically with optical thickness.

GSA is performed using $N = N_\xi$ sample realizations, where each model realization is

a MC RT simulation using N_η particle histories. We perform two GSA tests, one using $(N_\xi = 1000, N_\eta = 10)$, and another using $(N_\xi = 1000, N_\eta = 1000)$. We repeat this numerical experiment 1000 times to construct histograms of estimator output, shown in Figure 3.1. Across all of the histograms in Figure 3.1, we can see that applying Saltelli's method, developed for deterministic solvers, to a stochastic solver does indeed produce biased results for first-order and total SI compared to the benchmark result. This is most visible in S_3 and S_{T1}, Figures 3.1e and 3.1b. For every SI, we can see that the Saltelli-VarD result is unbiased compared to the benchmark solution, corroborating our theoretical finding that the conditional variance is accessible using variance deconvolution. In using Saltelli's method with a stochastic solver, one could increase the number of particle histories per simulation to drive down the MC RT variance. We can see the effect of this approach looking at the $N_\eta = 1000$ case, where we see that all of the results are converging to the benchmark mean, confirming that over-resolving the MC RT simulation will eventually drive down the solver variance and cause the bias term to approach 0. However, in every case, the Saltelli-VarD results with $N_\eta = 10$ are distributed similarly to Saltelli's method with $N_\eta = 1000$. For this particular example problem, we observe that Saltelli-VarD produces results comparable to Saltelli's method with 100× fewer particles per sample. Comparing Saltelli-VarD's $N_\eta = 1000$ results to Saltelli's $N_\eta = 1000$ results, we see that Saltelli-VarD achieves a much tighter distribution around the benchmark solution for all first-order and total SIs.

To quantify these effects, we compute the mean-squared error (MSE) for both methods compared to the benchmark result. Eq. (3.20) shows MSE of estimator value $\hat{X}$ with respect to a known result X, from which we can see that MSE captures both the variance and the bias of the estimator,

$$MSE\left[\hat{X}\right] = \mathbb{E}\left[\left(\hat{X} - X\right)^2\right] = \mathbb{V}ar\left[\hat{X}\right] + Bias^2\left[\hat{X}, X\right]. \tag{3.20}$$

In Table 3.1 we compare the SIs computed with Saltelli and Saltelli-VarD (averaged over 1000 repetitions) and the benchmark SI values. Using $N_\eta = 10$, Saltelli-VarD well-approximates the benchmark result, while Saltelli's method has statistically significant deviation from the benchmark results. In Table 3.2, we report the variance, bias, and MSE

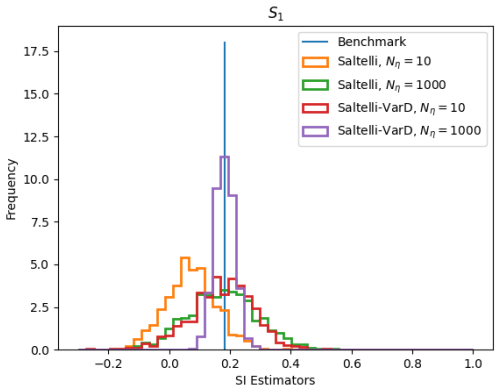

(a) First-order SI for cosine of beam incident angle

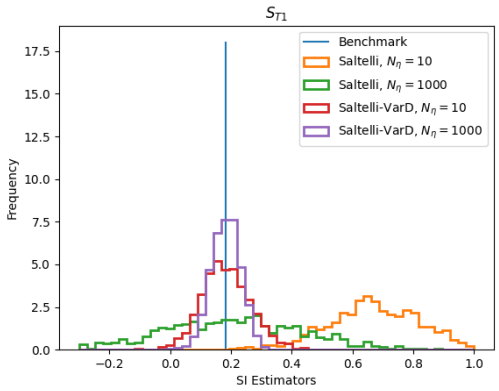

(b) Total SI for cosine of beam incident angle

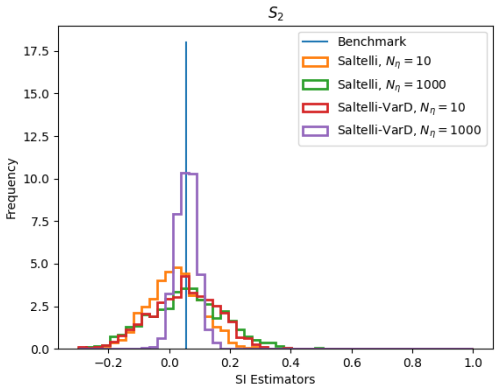

(c) First-order SI for material boundary location

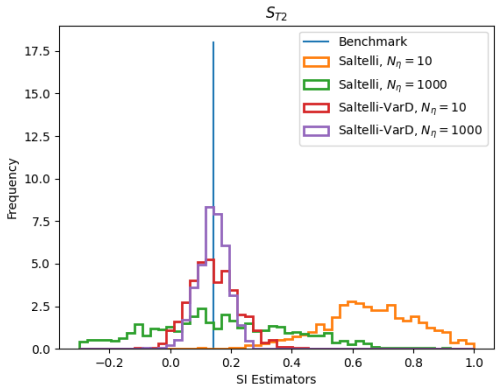

(d) Total SI for material boundary location

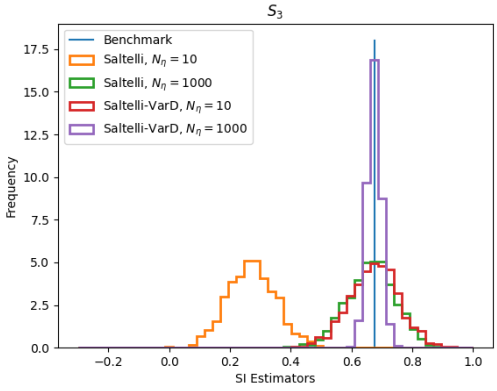

(e) First-order SI for total cross section

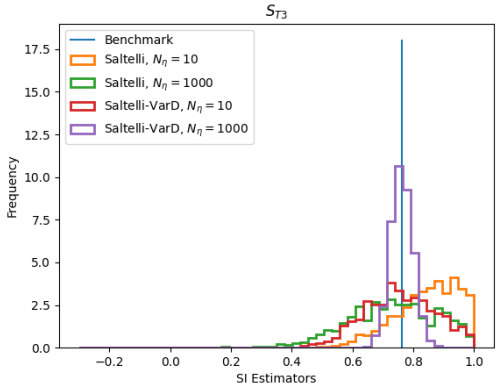

(f) Total SI for total cross section

Figure 3.1: First-order and total sensitivity indices for the three groups of parametric uncertainty. Comparing using the straightforward Saltelli approach and Saltelli with variance deconvolution (Saltelli-VarD) over 1000 repetitions. MC RT simulations performed with Sandia National Laboratories research code PlaybookMC.

of each SI from both methods. For Saltelli's method, going from $N_\eta = 10$ to $N_\eta = 1000$ does reduce the bias term, corresponding to how one might hope to over-resolve the MC RT solution by increasing the number of particle histories. This comparison between $N_\eta = 10$ and $N_\eta = 1000$ is for a simple 1D slab and attenuation-only physics, and the computational cost of MC RT resolution will only increase with problem complexity. While we do see non-zero bias results for Saltelli-VarD, the standard deviation indicates zero-bias is within a 1σ confidence interval, corroborating our theoretical finding that the Saltelli-VarD approach provides an unbiased estimate of SIs.

Table 3.1: Comparing Saltelli's method to Saltelli-VarD for computing first-order and total SIs when using a MC RT solver. Saltelli and Saltelli-VarD results averaged over 1000 repetitions, using $N_\xi = 1000$ for every case. Results indicate mean(std dev).

	Benchmark	Saltelli		Saltelli-VarD	
N_η		10	1000	10	1000
S_1	0.1824(4)	0.07(8)	0.2(1)	0.2(1)	0.18(3)
S_2	0.0549(4)	0.02(9)	0.1(1)	0.0(1)	0.06(3)
S_3	0.6752(2)	0.27(8)	0.66(8)	0.67(8)	0.67(2)
S_{T1}	0.1835(8)	0.7(2)	0.2(2)	0.18(8)	0.18(5)
S_{T2}	0.1424(8)	0.7(2)	0.2(3)	0.14(8)	0.14(5)
S_{T3}	0.7623(7)	0.9(1)	0.8(2)	0.8(1)	0.76(4)

3.5 Conclusions

The Saltelli method is a well-defined approach for global sensitivity analysis (GSA), but assumes that analysis is performed using a deterministic solver. In this paper, we consider the effects on GSA results of using a stochastic solver, namely a Monte Carlo radiation transport solver. We have incorporated our previously-developed variance deconvolution approach [14] to the Saltelli method for GSA and compared its performance to the unmodified approach. Applied to a test 1D radiation transport problem with three independent sources of parametric variance, our approach accurately estimated first-order and total sensitivity indices for significantly less computational cost than the unmodified Saltelli method and, for the same computational cost, out-performed the unmodified Saltelli

Table 3.2: MSE, variance, and bias of Saltelli and Saltelli-VarD methods. Comparing performance using $N_\eta = 10$ to using $N_\eta = 1000$ with a constant $N_\xi = 1000$, over 1000 repetitions.

		MSE		Var		Bias	
	N_η	10	1000	10	1000	10	1000
Saltelli	S_1	0.0194	0.0130	0.0068	0.0129	-0.1121	-0.0077
	S_2	0.0089	0.0155	0.0075	0.0155	-0.0368	-0.0006
	S_3	0.1693	0.0064	0.0062	0.0063	-0.4038	-0.0111
	S_{T1}	0.2626	0.0562	0.0233	0.0560	0.4892	0.0151
	S_{T2}	0.2914	0.0639	0.0252	0.0638	0.5160	0.0115
	S_{T3}	0.0396	0.0313	0.0189	0.0313	0.1437	0.0047
		MSE		Var		Bias	
	N_η	10	1000	10	1000	10	1000
Saltelli-VarD	S_1	0.0109	0.0010	0.0108	0.0010	-0.0099	-0.0013
	S_2	0.0124	0.0012	0.0123	0.0012	-0.0091	0.0008
	S_3	0.0066	0.0005	0.0066	0.0005	-0.0007	-0.0010
	S_{T1}	0.0064	0.0023	0.0064	0.0023	0.0004	-0.0015
	S_{T2}	0.0063	0.0024	0.0063	0.0024	0.0016	-0.0024
	S_{T3}	0.0187	0.0013	0.0186	0.0013	0.0104	0.0003

method in terms of accuracy.

Acknowledgments

This article has been authored by an employee of National Technology & Engineering Solutions of Sandia, LLC under Contract No. DE-NA0003525 with the U.S. Department of Energy (DOE). The employee owns all right, title and interest in and to the article and is solely responsible for its contents. The United States Government retains and the publisher, by accepting the article for publication, acknowledges that the United States Government retains a non-exclusive, paid-up, irrevocable, world-wide license to publish or reproduce the published form of this article or allow others to do so, for United States Government purposes. The DOE will provide public access to these results of federally sponsored research in accordance with the DOE Public Access Plan

https://www.energy.gov/downloads/doe-public-access-plan.

This work was supported by the Center for Exascale Monte-Carlo Neutron Transport (CEMeNT), a PSAAP-III project funded by the Department of Energy, grant number DE-NA003967.

SAMPLING-BASED SENSITIVITY INDICES FOR STOCHASTIC SOLVERS WITH APPLICATION TO MONTE CARLO RADIATION TRANSPORT

Kayla B. Clements, Todd S. Palmer

To be submitted to *Journal of Computational Physics*

Chapter 4: Sampling-based Sensitivity Indices for Stochastic Solvers with Application to Monte Carlo Radiation Transport

Abstract

In computational modeling, global sensitivity analysis aims to characterize how input variability affects output variability. Sobol' indices, a variance-based tool for global sensitivity analysis, rank parameters in order of importance to model response across the entire combined input parameter space. Accurate and efficient methods for computing Sobol' indices have been widely researched for deterministic simulators, in which multiple evaluations of the same input will produce identical outputs. Stochastic simulators, on the hand, have an intrinsic randomness and produce different outputs for multiple evaluations of the same input. This introduces additional variability to model output, complicating the use of traditional methods for computing Sobol' indices. In this paper, we focus on computing Sobol' indices that are unbiased by solver noise without needing to over-resolve each evaluation of the stochastic simulator. We propose doing so using variance deconvolution, in which we explicitly calculate the variance due to the solver and remove it from the total observed variance. The proposed method is applied to two examples: the Ishigami function that is commonly used as a test case for Sobol' indices and a neutron-transport case study. The results confirm the convergence of the approach and highlight the approach's utility particularly when the indices are not near-zero and when there is a large amount of solver noise.

4.1 Introduction

In computational modeling, uncertainty and sensitivity analyses are essential to quantify and analyze the reliability, accuracy, and robustness of a model and its outputs [18, 24, 42]. Uncertainty analysis focuses on quantifying uncertainty in model output by calculating statistics of the quantity of interest such as mean and variance [97, 34]; it is also referred

to as uncertainty quantification (UQ). Sensitivity analysis (SA), a related practice, is the study of how uncertainty in model output can be ascribed to different sources of input uncertainty [99]. *Local* SA characterizes a system's response to small perturbations around some nominal parameter value by computing partial derivatives of the model response at that value [47, 8]. On the other hand, *global* sensitivity analysis (GSA) aims to rank parameters in order of importance to model response across the entire input parameter space. There are many statistics that can be used as measures of importance for parameter ranking; what statistic is used depends on what question the practitioner hopes to answer, defined in [97] as the SA *setting*. For an exhaustive introduction to GSA in the scientific computing context, see Saltelli's book [97].

In this paper we focus on variance-based GSA, in which sensitivity indices are used to determine which factor or set of factors has the largest impact on output variance. Sensitivity indices (SIs), also commonly referred to as Sobol' indices, arise from the ANOVA (ANalysis Of VAriance) decomposition of the output [108, 43]. Many methods have been introduced to compute SIs, either by approximating the ANOVA decomposition via meta-modeling (surrogate modeling) or directly by using a sampling-based approach. In the former, the ANOVA decomposition of the output is approximated via a surrogate model, such as the polynomial chaos expansion [19]. Meta-modeling approaches typically require fewer model evaluations than sampling-based approaches and are therefore attractive for computational models with a large single-simulation time; however, they can be susceptible to any lack of smoothness or regularity of the underlying function [97, 19] and suffer from the 'curse of dimensionality' [56, 19]. In the latter, indices are computed directly using sampling-based estimators in combination with sampling schemes such as Monte Carlo (MC), quasi-MC, or Latin Hypercube [108, 43, 57]. Sampling-based methods are useful because they do not make any *a priori* assumptions about the linearity, smoothness, or regularity of the model [1, 8]. They do assume that the input factors are mutually independent [95], though treatments exist for the more complex case of correlated input factors [97]. Their primary drawback is the high computational cost associated with the multiple code evaluations needed to compute a full suite of sensitivity indices, and efficient numerical algorithms for computing SIs is an area of ongoing research [86].

The vast majority of the large body of work on GSA [97, 42, 47, 8] has been designed

with deterministic solvers in mind, inherently assuming that output variability results exclusively from propagated input variability. Additional complication arises when performing sensitivity analysis in the context of stochastic solvers, which are used in a variety of disciplines such as compute networks [20, 32], turbulent flows [61], financial modeling [88], disease prediction [112], and radiation transport [62]. Multiple evaluations of a stochastic solver using the same input will produce different outputs, akin to different realizations of a random variable whose probability distribution is unknown [59]. In computer codes, stochastic solvers simulate randomness using (pseudo-)random number generators, where the initial seed could be chosen by the analyst but the random number stream cannot [79]. When the inputs of a stochastic simulator have some associated uncertainty, as is the case for GSA, the total observed output variance is a combination of the variability of the solver itself (referred to from here as solver variance) and the variability of the inputs (referred to from here as parametric variance) [94, 16]. A standard approach to approximate the parametric variance using a stochastic solver is to increase the number of solver realizations, knowing that the total variance will approach the parametric variance in the limit of an infinite number of solver samples [90]. However, doing this for each of the multiple code evaluations needed to calculate sampling-based SIs exacerbates the already-high computational cost.

Over the past decade or so, there have been a number of methods introduced to extend Sobol' indices to stochastic simulators, which are reviewed thoroughly in [116]. The macroparameter method [48] considers the solver's random seed to be an additional input parameter and computes Sobol' indices as if there are $(k + 1)$ parameters, explicitly treating the covariances [21] of the sets of k now-correlated inputs (similar methods exist for sampling-based UQ with stochastic solvers, *e.g.*, , Total Monte Carlo [54, 55]). Other methods have defined the Sobol' indices themselves as random variables by treating them as functions of the solver stochasticity, then analyzed the statistical properties of the SIs [40, 53]. Many of the proposed methods mitigate the expense of resolving the stochastic solver by instead emulating the stochastic solver with a surrogate model, then calculating Sobol' indices using the constructed surrogate at a reduced computational cost [116]. One such class of methods uses joint meta-models to deterministically represent the statistics of the stochastic outputs such as mean and variance [48, 68], alpha-quantile [6], and

differential entropy [2]. Most recently, Zhu and Sudret [116] presented a framework for creating a surrogate that captures entire response distribution of the stochastic solver by using their generalized lambda model.

In recent publications [74], as an alternative to the standard approach, we proposed a novel method for UQ with stochastic solvers called *variance deconvolution* to compute parametric variance without a surrogate by explicitly quantifying and removing the solver variance from the total observed variance. In Clements, *et al.* [16], we rigorously showed that variance deconvolution is accurate and far more cost effective than the standard approach for computing parametric variance. In previous work, we integrated variance deconvolution in sampling-based GSA for stochastic media [74] and surrogate [33, 29] approaches. The goal of this paper is to present a clear framework to compute Sobol' indices using stochastic solvers without stochastic emulators or the expensive standard approach by using variance deconvolution. We examine the biases introduced when using stochastic solvers to compute parametric SIs, discuss how and when to use variance deconvolution, and analyze the impact of combining it with existing sampling-based methods for SIs.

The remainder of the paper is structured as follows. In Section 4.2, we review ANOVA decomposition and Sobol' indices. In Section 4.3, we review existing sampling-based estimators for sensitivity indices. In Section 4.4, we summarize variance deconvolution as presented in [16]. Then, in Section 4.5, we discuss the impact of computing SIs with stochastic solvers and how using variance deconvolution compares to a standard approach. In Section 4.6, we show variance deconvolution's performance and compare it to that of the standard approach for two examples, the analytical Ishigami function and a neutral-particle radiation transport example problem with energy-dependence and fission. Finally, we summarize the main findings of the paper and discuss possible future applications in Section 4.7.

4.2 Background and theory on ANOVA

In this section, we give a brief review of Sobol's variance decomposition [108] and how it is used to define variance-based sensitivity indices [108, 43].

4.2.1 Sobol' decomposition

Consider a generic scalar quantity of interest (QoI) $Q = Q(\boldsymbol{\xi}), \boldsymbol{\xi} = (\xi_1, \ldots, \xi_k) \in \Xi \subset \mathbb{R}^k$, where $\xi_1, \ldots, \xi_k$ are independent random variables with arbitrary joint distribution function $p(\boldsymbol{\xi})$. The mean and variance of Q can be computed as

$$\mathbb{E}_\xi[Q] = \int_\Xi Q(\boldsymbol{\xi})\, p(\boldsymbol{\xi}) d\boldsymbol{\xi} \qquad \text{and} \qquad \mathbb{V}ar_\xi[Q] = \int_\Xi \Big(Q(\boldsymbol{\xi}) - \mathbb{E}_\xi[Q]\Big)^2 p(\boldsymbol{\xi}) d\boldsymbol{\xi}, \quad (4.1)$$

respectively, where we have used a subscript to indicate the expectation and variance over ξ. Sobol' considered [108] an expansion of Q into 2^k orthogonal terms of increasing dimension,

$$Q = Q_0 + \sum_i Q_i + \sum_i \sum_{j>i} Q_{ij} + \cdots + Q_{12\ldots k}, \quad (4.2)$$

in which each term is a function only of the factors in its subscript, *i.e.*, , $Q_i = Q_i(\xi_i)$, $Q_{ij} = Q_{ij}(\xi_i, \xi_j)$. In particular, Sobol' considered the case in which each term could be defined recursively using the conditional expectations of Q,

$$Q_0 = \mathbb{E}_\xi[Q] \quad (4.3)$$

$$Q_i = \mathbb{E}_{\xi_{\sim i}}\big[Q \mid \xi_i\big] - \mathbb{E}_\xi[Q] \quad (4.4)$$

$$Q_{ij} = \mathbb{E}_{\xi_{\sim i}, \xi_{\sim j}}\big[Q \mid \xi_i, \xi_j\big] - Q_i - Q_j - \mathbb{E}_\xi[Q], \quad (4.5)$$

where $\mathbb{E}_{\xi_{\sim i}}\big[Q \mid \xi_i\big]$ indicates the expected value of Q conditional on some fixed value ξ_i and $\mathbb{E}_{\xi_{\sim i}, \xi_{\sim j}}\big[Q \mid \xi_i, \xi_j\big]$ indicates the expected value of Q conditional on the pair of values (ξ_i, ξ_j). The variances of the terms in Eq. (4.2) give rise to the measures of importance being sought. The conditional variance $\mathbb{V}ar_\xi[Q_i] = \mathbb{V}ar_{\xi_i}\Big[\mathbb{E}_{\xi_{\sim i}}\big[Q \mid \xi_i\big]\Big] \overset{\text{def}}{=} \mathbb{V}_i$ is called the first-order effect of ξ_i on Q. The second-order effect $\mathbb{V}ar_\xi\big[Q_{ij}\big] = \mathbb{V}ar\big[\mathbb{E}(Q \mid \xi_i, \xi_j)\big] - \mathbb{V}_i - \mathbb{V}_j \overset{\text{def}}{=} \mathbb{V}_{ij}$ is the difference between the combined effect of the pair (ξ_i, ξ_j) and both of their individual effects; it captures the effect solely of their interaction with one another. Higher-order effects can be defined analogously to quantify the effects of higher-order interactions, up to the final term $\mathbb{V}_{12\ldots k}$. Sobol's variance decomposition

expands $\mathbb{V}ar_{\xi}\left[Q\right]$ into variance terms of increasing order,

$$\mathbb{V}ar_{\xi}\left[Q\right] = \sum_{i} \mathbb{V}_{i} + \sum_{i} \sum_{j>i} \mathbb{V}_{ij} + \cdots + \mathbb{V}_{12\ldots k}. \tag{4.6}$$

Sensitivity indices (SIs), also referred to as Sobol' indices, result directly from dividing Eq. (4.6) by the unconditional variance $\mathbb{V}ar\left[Q\right]$ and provide measures of importance used to, e.g., rank the parameters in GSA; this is discussed in the next section.

4.2.2 Sensitivity indices

A sensitivity index is the ratio of the conditional variance of a parameter or set of parameters to the unconditional variance, which can be used as a measure of importance of the parameter(s) to the QoI [108, 43, 44, 49, 46]. The first-order sensitivity index of parameter ξ_i is the ratio of its first-order effect to the unconditional variance,

$$\mathbb{S}_{i} = \frac{\mathbb{V}ar_{\xi_i}\left[\mathbb{E}_{\xi_{\sim i}}\left[Q \mid \xi_i\right]\right]}{\mathbb{V}ar_{\xi}\left[Q\right]}. \tag{4.7}$$

The k first-order SIs represent the main effect contributions of each input factor to the variance of the output. All first-order SIs are between 0 and 1 and $\sum_{i=1}^{k} \mathbb{S}_{i} \leq 1$, with equality for purely additive models. Analogously to the higher-order variance terms in Eq. (4.6), higher-order SIs represent the contribution only of the interactions amongst a set of variables. Dividing Eq. (4.6) by $\mathbb{V}ar\left[Q\right]$ results in the summation of all of the first- and higher-order SIs to 1:

$$\sum_{i} \mathbb{S}_{i} + \sum_{i} \sum_{j>i} \mathbb{S}_{ij} + \cdots + \mathbb{S}_{12\ldots k} = 1. \tag{4.8}$$

In addition to its first-order SI, a parameter can be described by its total-order SI $\mathbb{T}_{I}$, which accounts for its total contribution to the output variance by combining its first-order effect and all of its higher-order interaction effects. For example, in a model with three parameters, the total effect of ξ_1 would be the sum of all of the terms in Eq. (4.8) that

contain a 1: $\mathbb{T}_1 = \mathbb{S}_1 + \mathbb{S}_{12} + \mathbb{S}_{13} + \mathbb{S}_{123}$. The total-order SI of ξ_i can also be expressed [43, 95] by conditioning on the set $\boldsymbol{\xi}_{\sim i}$, which contains all factors except ξ_i, as

$$\mathbb{T}_i = \frac{\mathbb{E}_{\xi_{\sim i}}\left[\mathbb{V}ar_{\xi_i}\left[Q \mid \boldsymbol{\xi}_{\sim i}\right]\right]}{\mathbb{V}ar_{\xi}\left[Q\right]} = 1 - \frac{\mathbb{V}ar_{\xi_{\sim i}}\left[\mathbb{E}_{\xi_i}\left[Q \mid \boldsymbol{\xi}_{\sim i}\right]\right]}{\mathbb{V}ar_{\xi}\left[Q\right]}. \tag{4.9}$$

Since $\mathbb{V}ar_{\xi_i}\left[\mathbb{E}_{\xi_{\sim i}}\left[Q \mid \boldsymbol{\xi}_{\sim i}\right]\right]$ can be understood as the main effect of everything that is not ξ_i, the remaining $\mathbb{E}_{\xi_{\sim i}}\left[\mathbb{V}ar_{\xi_i}\left[Q \mid \boldsymbol{\xi}_{\sim i}\right]\right] = \mathbb{V}ar\left[Q\right] - \mathbb{V}ar_{\xi_{\sim i}}\left[\mathbb{E}_{\xi_i}\left[Q \mid \boldsymbol{\xi}_{\sim i}\right]\right] \stackrel{\text{def}}{=} \mathbb{E}_{\sim i}$ is the effect of any terms that do contain ξ_i. Rather than compute all higher-order terms, it is customary to compute the set of first- and total-order indices for a good description of the importance of parameters and their interactions at a reasonable cost [97]. In the next section, we summarize sampling-based methods for estimating the full set of first- and total-order SIs.

4.3 Sampling-based estimators for sensitivity indices

The development of efficient numerical algorithms for computing the full suite of first- and total-order SIs has been an ongoing area of research since MC estimators for $\mathbb{S}_i$ and $\mathbb{T}_i$ were first proposed [108, 43, 95], and a number of sampling schemes and estimators exist to do so. The various methods follow the same general structure: sample the parameter space, evaluate the computational model at the sampled parameters, then approximate $\mathbb{S}_i$ and $\mathbb{T}_i$ using MC estimators. We outline the general algorithm, the Saltelli approach [96, 95], here, assuming k uncertain parameters:

1. Define two (N_ξ, k) matrices, $\boldsymbol{A}$ and $\boldsymbol{B}$, which contain independent input samples.

$$\boldsymbol{A} = \begin{bmatrix} \xi_1^{(1)} & \cdots & \xi_i^{(1)} & \cdots & \xi_k^{(1)} \\ \vdots & & \ddots & & \vdots \\ \xi_1^{(N)} & \cdots & \xi_i^{(N_\xi)} & \cdots & \xi_k^{(N_\xi)} \end{bmatrix}, \qquad \boldsymbol{B} = \begin{bmatrix} \xi_{k+1}^{(1)} & \cdots & \xi_{k+i}^{(1)} & \cdots & \xi_{2k}^{(1)} \\ \vdots & & \ddots & & \vdots \\ \xi_{k+1}^{(N_\xi)} & \cdots & \xi_{k+i}^{(N_\xi)} & \cdots & \xi_{2k}^{(N_\xi)} \end{bmatrix}. \tag{4.10}$$

2. For each i-th parameter, define matrix $\boldsymbol{A}_{\boldsymbol{B}}^{(\boldsymbol{i})}$ ($\boldsymbol{B}_{\boldsymbol{A}}^{(\boldsymbol{i})}$), which is a copy of $\boldsymbol{A}$ ($\boldsymbol{B}$) except

for the i-th column, which comes from $\boldsymbol{B}$ ($\boldsymbol{A}$).

$$\boldsymbol{A}_{\boldsymbol{B}}^{(\boldsymbol{i})} = \begin{bmatrix} \xi_1^{(1)} & \cdots & \xi_{k+i}^{(1)} & \cdots & \xi_k^{(1)} \\ \vdots & & \ddots & & \vdots \\ \xi_1^{(N_\xi)} & \cdots & \xi_{k+i}^{(N_\xi)} & \cdots & \xi_k^{(N_\xi)} \end{bmatrix}. \tag{4.11}$$

3. Compute model output for $\boldsymbol{A}$, $\boldsymbol{B}$, and all $\boldsymbol{A}_{\boldsymbol{B}}^{(\boldsymbol{i})}$ ($\boldsymbol{B}_{\boldsymbol{A}}^{(\boldsymbol{i})}$) to obtain vectors of model output $Q(\boldsymbol{A})$, $Q(\boldsymbol{B})$, $Q(\boldsymbol{A}_{\boldsymbol{B}}^{(\boldsymbol{i})})$, and/or $Q(\boldsymbol{B}_{\boldsymbol{A}}^{(\boldsymbol{i})})$ of dimension $(N_\xi, 1)$.

4. Approximate the full set of $\mathbb{S}_i$ and $\mathbb{T}_i$ using $Q(\boldsymbol{A})$, $Q(\boldsymbol{B})$, $Q(\boldsymbol{A}_{\boldsymbol{B}}^{(\boldsymbol{i})})$, and/or $Q(\boldsymbol{B}_{\boldsymbol{A}}^{(\boldsymbol{i})})$.

Specific methods for computing SIs are defined by two components [83]: 1) the sampling scheme used to populate matrices $\boldsymbol{A}$ and $\boldsymbol{B}$ from the parameter space, such as purely random MC or a quasi-random scheme like the Sobol' sequence [106, 107] or Latin hypercube [70]; and 2) the MC estimators used to approximate Eqs. (4.7) and (4.9). Though some estimators require a specific sampling scheme, quasi-random sampling as a default choice has been shown to be the best for a function of unknown behavior [57, 87]. This is by no means intended as an exhaustive review of estimator design; a few notable works include [97, 108, 43, 95, 96, 36, 51, 63, 67, 69, 78, 84, 91, 110, 52, 3, 109, 71, 92, 93]. For a review, see, *e.g.*, , [86, 96].

For simplicity when examining the effects of variance deconvolution, we limit discussion to using purely random MC sampling. With purely random MC sampling, there is no difference between using triplet $\left(\boldsymbol{A}, \boldsymbol{B}, \boldsymbol{A}_{\boldsymbol{B}}^{(\boldsymbol{i})}\right)$ or triplet $\left(\boldsymbol{B}, \boldsymbol{A}, \boldsymbol{B}_{\boldsymbol{A}}^{(\boldsymbol{i})}\right)$ in the estimators, as long as they are used consistently within the estimator [96]. We also limit discussion to one first- and one total-order estimator, shown in Section 4.3.1. Later, we discuss how the presented variance deconvolution analysis can be extended to other SI estimators.

4.3.1 Sampling estimators for $\mathbb{S}_i$ and $\mathbb{T}_i$

As recommended by Saltelli et al. (2012) [98], we use the the sampling estimator for $\mathbb{S}_i$ from Sobol' et al. (2007) [110] and for $\mathbb{T}_i$ from Jansen et al. (1999) [52]. Letting $Q(\boldsymbol{A})_v$

indicates the v-th element of the vector $Q(\boldsymbol{A})$, *i.e.*, one function evaluation of Q,

$$\mathbb{S}_i \approx \frac{\frac{1}{N_\xi}\sum_{v=1}^{N_\xi} Q(\boldsymbol{B})_v\left[Q(\boldsymbol{A}_{\boldsymbol{B}}^{(\boldsymbol{i})})_v - Q(\boldsymbol{A})_v\right]}{\frac{1}{2N_\xi}\sum_{v=1}^{N_\xi}\left(Q(\boldsymbol{A})_v - Q(\boldsymbol{B})_v\right)^2} \stackrel{\text{def}}{=} \hat{\mathbb{S}}_i, \tag{4.12}$$

$$\mathbb{T}_i \approx \frac{\frac{1}{2N_\xi}\left[Q(\boldsymbol{B}_{\boldsymbol{A}}^{(\boldsymbol{i})})_v - Q(\boldsymbol{B})_v\right]^2}{\frac{1}{2N_\xi}\sum_{v=1}^{N_\xi}\left(Q(\boldsymbol{A})_v - Q(\boldsymbol{B})_v\right)^2} \stackrel{\text{def}}{=} \hat{\mathbb{T}}_i. \tag{4.13}$$

In the following, we analyze how to compute the statistical quantities introduced above when the underlying QoI is computed using a stochastic solver.

4.4 Introduction to variance deconvolution

Variance deconvolution was introduced [16, 74] as a means to efficiently and accurately estimate the parametric variance of QoI Q in the presence of an additional variance contribution from a stochastic solver. In this section, we summarize the concept and notation of variance deconvolution before extending it to GSA in Section 4.5. For a detailed presentation of variance deconvolution, see [16].

We consider the same generic QoI defined in Section 4.1, $Q = Q\left(\boldsymbol{\xi}\right), \boldsymbol{\xi} = (\xi_1, \ldots, \xi_k) \in \Xi \subset \mathbb{R}^k$, with mean $\mathbb{E}_\xi\left[Q\right]$ and variance $\mathbb{V}ar_\xi\left[Q\right]$. We now introduce an additional random variable η to represent the inherent variability of the stochastic solver, and define our QoI Q as the expectation over η of a function $f(\boldsymbol{\xi}, \eta)$, $Q(\boldsymbol{\xi}) \stackrel{\text{def}}{=} \mathbb{E}_\eta\left[f(\boldsymbol{\xi}, \eta)\right]$. The function $f(\boldsymbol{\xi}, \eta)$ can be directly evaluated as the output from the stochastic solver with input $\boldsymbol{\xi}$, but the expectation $\mathbb{E}_\eta\left[f(\boldsymbol{\xi}, \eta)\right]$ and variance $\sigma_\eta^2(\boldsymbol{\xi}) \stackrel{\text{def}}{=} \mathbb{V}ar_\eta\left[f(\boldsymbol{\xi}, \eta)\right]$ are not directly available. Instead, we approximate $Q(\boldsymbol{\xi})$ as the sample mean of N_η independent evaluations of f, $Q\left(\boldsymbol{\xi}\right) \approx \frac{1}{N_\eta}\sum_{j=1}^{N_\eta} f(\boldsymbol{\xi}, \eta^{(j)}) \stackrel{\text{def}}{=} \tilde{Q}_{N_\eta}(\boldsymbol{\xi})$.

In [16], we present that the total variance of $\tilde{Q}_{N_\eta}$ decomposes into the effect of the uncertain parameters and the effect of the stochastic solver,

$$\mathbb{V}ar_\xi\left[Q\right] = \mathbb{V}ar\left[\tilde{Q}_{N_\eta}\right] - \frac{1}{N_\eta}\mathbb{E}_\xi\left[\sigma_\eta^2\right], \tag{4.14}$$

and propose an unbiased estimator for the parametric variance using MC estimators

for $\mathbb{V}ar\left[\tilde{Q}_{N_\eta}\right]$ and $\mathbb{E}_\xi\left[\sigma_\eta^2\right]$. Using the Saltelli method summarized in Section 4.3, variance deconvolution requires tallying the variance of the model output $\hat{\sigma}_\eta^2(\boldsymbol{A}) \stackrel{\text{def}}{=} \frac{1}{N_\eta - 1}\sum_{j=1}^{N_\eta}\left(f^2(\boldsymbol{\xi}, \eta^{(j)}) - \tilde{Q}_{N_\eta}^2(\boldsymbol{\xi})\right)$ in addition to model output $\tilde{Q}_{N_\eta}(\boldsymbol{A})$. Then, to estimate $\mathbb{V}ar_\xi\left[Q\right]$ using N_ξ samples,

$$\mathbb{V}ar_\xi\left[Q\right] \approx S_{(A)}^2 \stackrel{\text{def}}{=} \tilde{S}_{(A)}^2 - \frac{1}{N_\eta}\left\langle\hat{\sigma}_\eta^2\right\rangle_{(A)}, \tag{4.15}$$

$$\text{where } \tilde{S}_{(A)}^2 \stackrel{\text{def}}{=} \frac{1}{N_\xi - 1}\sum_{v=1}^{N_\xi}\left(\tilde{Q}_{N_\eta}^2(\boldsymbol{A})_v - \left\langle\tilde{Q}_{N_\eta}\right\rangle_{(A)}^2\right), \tag{4.16}$$

$$\left\langle\tilde{Q}_{N_\eta}\right\rangle_{(A)} = \frac{1}{N_\xi}\sum_{v=1}^{N_\xi}\tilde{Q}_{N_\eta}(\boldsymbol{A})_v \quad \text{and} \quad \left\langle\hat{\sigma}_\eta^2\right\rangle_{(A)} = \frac{1}{N_\xi}\sum_{v=1}^{N_\xi}\hat{\sigma}_\eta^2(\boldsymbol{A}).$$

A standard approach is to estimate $\mathbb{V}ar_\xi\left[Q\right]$ as $\tilde{S}_{(A)}^2$, where $\tilde{S}_{(A)}^2 \to \mathbb{V}ar_\xi\left[Q\right]$ as $N_\eta, N_\xi \to \infty$. This standard approach is reliably accurate but computationally expensive, as large N_η is needed for each function evaluation. In [16], we showed that for the same linear computational cost $\mathbb{C} = N_\xi \times N_\eta$, $S_{(A)}^2$ was a more accurate estimate of $\mathbb{V}ar_\xi\left[Q\right]$ than the biased estimator $\tilde{S}_{(A)}^2$. In the next section, we extend the variance deconvolution approach to computation of Sobol' indices.

4.5 GSA with variance deconvolution

In this section, we first analyze how the MC estimate $\tilde{Q}_{N_\eta}$ affects $\mathbb{S}_i$ and $\mathbb{T}_i$, *i.e.*, , the parametric sensitivity indices of Q. Then, we propose unbiased estimators for $\mathbb{S}_i$ and $\mathbb{T}_i$ using $\tilde{Q}_{N_\eta}$.

4.5.1 Stochastic solver's effect on sensitivity indices

We begin by considering the first- and total- order SIs of ξ_i on $\tilde{Q}_{N_\eta}$,

$$\mathbb{S}_{i,\tilde{Q}_{N_\eta}} = \frac{\mathbb{V}ar\left[\mathbb{E}\left[\tilde{Q}_{N_\eta} \mid \xi_i\right]\right]}{\mathbb{V}ar\left[\tilde{Q}_{N_\eta}\right]}, \tag{4.17}$$

$$\mathbb{T}_{i,\tilde{Q}_{N_\eta}} = \frac{\mathbb{E}\left[\mathbb{V}ar\left[\tilde{Q}_{N_\eta} \mid \xi_{\sim i}\right]\right]}{\mathbb{V}ar\left[\tilde{Q}_{N_\eta}\right]}. \tag{4.18}$$

From Eq. (4.14), it follows that the numerator of Eq. (4.17) can be expanded as

$$\begin{aligned}\mathbb{V}ar\left[\mathbb{E}\left[\tilde{Q}_{N_\eta} \mid \xi_i\right]\right] &= \mathbb{V}ar_{\xi_i}\left[\mathbb{E}_{\xi_{\sim i},\eta}\left[\tilde{Q}_{N_\eta} \mid \xi_i\right]\right] \\ &= \mathbb{V}ar_{\xi_i}\left[\mathbb{E}_{\xi_{\sim i}}\left[Q \mid \xi_i\right]\right]\end{aligned} \tag{4.19}$$

and that the numerator of Eq. (4.18) can be expanded as

$$\begin{aligned}\mathbb{E}\left[\mathbb{V}ar\left[\tilde{Q}_{N_\eta} \mid \xi_i\right]\right] &= \mathbb{E}_{\xi_i}\left[\mathbb{V}ar_{\xi_{\sim i},\eta}\left[\tilde{Q}_{N_\eta} \mid \xi_i\right]\right] \\ &= \mathbb{E}_{\xi_i}\left[\mathbb{V}ar_{\xi_{\sim i}}\left[Q \mid \xi_i\right] + \frac{1}{N_\eta}\mathbb{E}_{\xi_{\sim i}}\left[\sigma_\eta^2 \mid \xi_i\right]\right] \\ &= \mathbb{E}_{\xi_i}\left[\mathbb{V}ar_{\xi_{\sim i}}\left[Q \mid \xi_i\right]\right] + \frac{1}{N_\eta}\mathbb{E}_{\xi}\left[\sigma_\eta^2\right].\end{aligned} \tag{4.20}$$

We can therefore conclude that the first-order effect of any subset $\boldsymbol{\xi}$ on $\tilde{Q}_{N_\eta}$ is equivalent to the first-order effect of $\boldsymbol{\xi}$ on Q; however, the total-order effect of $\boldsymbol{\xi}$ on $\tilde{Q}_{N_\eta}$ is larger than the total-order effect of $\boldsymbol{\xi}$ on Q. This makes intuitive sense if we consider the meanings of the first- and total-order effects. The first-order effect of $\boldsymbol{\xi}$ on Q is the variance of Q caused exclusively by $\boldsymbol{\xi}$. As $\tilde{Q}_{N_\eta}$ is an unbiased estimator for Q, we would expect $\boldsymbol{\xi}$ to induce that same variance on $\tilde{Q}_{N_\eta}$. The total-order effect of $\boldsymbol{\xi}$ on Q is the variance of Q caused by $\boldsymbol{\xi}$ and its interactions with all remaining variables $\sim \boldsymbol{\xi}$. However, the total-order effect of $\boldsymbol{\xi}$ on $\tilde{Q}_{N_\eta}$ additionally includes the interactions of $\boldsymbol{\xi}$ with solver stochasticity η. An equivalent result was found in [68] by extending the ANOVA decomposition directly to the set of input variables $(\xi_i, \xi_{\sim i}, \eta)$.

We can write the first- and total-order SIs of ξ_i on Q in terms of the first- and total-order effect SIs of ξ_i on $\tilde{Q}_{N_\eta}$ and $R \overset{\text{def}}{=} \frac{\mathbb{E}_\xi\left[\sigma_\eta^2\right]}{\mathbb{V}ar_\xi[Q]}$, the ratio of solver variance to parametric variance:

$$\mathbb{S}_{i,\tilde{Q}_{N_\eta}} = \frac{\mathbb{V}ar_{\xi_i}\left[\mathbb{E}_{\xi_{\sim i}}\left[Q \mid \xi_i\right]\right]}{\mathbb{V}ar_\xi\left[Q\right] + \frac{1}{N_\eta}\mathbb{E}_\xi\left[\sigma_\eta^2\right]}$$

$$\rightarrow \mathbb{S}_i = \mathbb{S}_{i,\tilde{Q}_{N_\eta}}\left(1 + \frac{R}{N_\eta}\right), \tag{4.21}$$

$$\mathbb{T}_{i,\tilde{Q}_{N_\eta}} = \frac{\mathbb{E}_{\xi_{\sim i}}\left[\mathbb{V}ar_{\xi_i}\left[Q \mid \xi_{\sim i}\right]\right] + \frac{1}{N_\eta}\mathbb{E}_\xi\left[\sigma_\eta^2\right]}{\mathbb{V}ar_\xi\left[Q\right] + \frac{1}{N_\eta}\mathbb{E}_\xi\left[\sigma_\eta^2\right]}$$

$$\rightarrow \mathbb{T}_i = \mathbb{T}_{i,\tilde{Q}_{N_\eta}}\left(1 + \frac{R}{N_\eta}\right) - \frac{R}{N_\eta}. \tag{4.22}$$

From Equations (4.21) and (4.22), it is clear that the sets of indices $\left(\mathbb{S}_{i,\tilde{Q}_{N_\eta}}, \mathbb{T}_{i,\tilde{Q}_{N_\eta}}\right)$ and $(\mathbb{S}_i, \mathbb{T}_i)$ are not equivalent. Unlike the relationship among $\mathbb{V}ar\left[\tilde{Q}_{N_\eta}\right]$, $\mathbb{V}ar_\xi\left[Q\right]$, and $\mathbb{E}\left[\sigma_\eta^2\right]$, the relationships between the SIs of $\tilde{Q}_{N_\eta}$ and Q are not simply additive. Because $R \geq 0$, $\mathbb{S}_{i,\tilde{Q}_{N_\eta}}$ will always be *less than* $\mathbb{S}_i$, therefore underestimating the first-order effect of ξ_i. On the other hand, $\mathbb{T}_{i,\tilde{Q}_{N_\eta}}$ will always be *greater than* $\mathbb{T}_i$, therefore overestimating the total-order effect of ξ_i. Substituting $\tilde{Q}_{N_\eta}$ for Q in Equations (4.12) and (4.13) will yield unbiased estimates of $\mathbb{S}_{i,\tilde{Q}_{N_\eta}}$ and $\mathbb{T}_{i,\tilde{Q}_{N_\eta}}$, not of $\mathbb{S}_i$ and $\mathbb{T}_i$, though both $\mathbb{S}_{i,\tilde{Q}_{N_\eta}}$ and $\mathbb{T}_{i,\tilde{Q}_{N_\eta}}$ will approach their parametric counterparts in the limit $N_\eta = \infty$. Because we desire estimates of $\mathbb{S}_i$ and $\mathbb{T}_i$, we extend the variance deconvolution framework to propose unbiased sampling estimators for $\mathbb{S}_i$ and $\mathbb{T}_i$ using $\tilde{Q}_{N_\eta}$ by introducing terms to correct the biases in $\mathbb{S}_{i,\tilde{Q}_{N_\eta}}$ and $\mathbb{T}_{i,\tilde{Q}_{N_\eta}}$.

4.5.2 Unbiased sampling estimators using $\tilde{Q}_{N_\eta}$

For unbiased estimates of $\mathbb{S}_i$ and $\mathbb{T}_i$ from $\tilde{Q}_{N_\eta}$, the denominator of $\mathbb{S}_{i,\tilde{Q}_{N_\eta}}$ in Eq. (4.21) and both the numerator and denominator of $\mathbb{T}_{i,\tilde{Q}_{N_\eta}}$ in Eq. (4.22) require a corrective term. It is possible that this varies from estimator-to-estimator; in short, $\hat{\sigma}_\eta^2$ terms that require

correction arise when $\tilde{Q}_{N_\eta}(\boldsymbol{\xi})$ is squared, but not when two independent realizations of $\tilde{Q}_{N_\eta}$ are multiplied, as in $\tilde{Q}_{N_\eta}(\boldsymbol{B})_v \tilde{Q}_{N_\eta}(\boldsymbol{A}^{(\boldsymbol{i})}_{\boldsymbol{B}})_v$.

To consider the impact of introducing a corrective variance deconvolution term, we introduce two sets of estimators that use $\tilde{Q}_{N_\eta}$: "standard" estimators $\hat{\mathbb{S}}_{i,\tilde{Q}_{N_\eta}}$ and $\hat{\mathbb{T}}_{i,\tilde{Q}_{N_\eta}}$ that do not have corrective $\hat{\sigma}^2_\eta$ terms, and variance deconvolution estimators $\hat{\mathbb{S}}_{i,VD}$ and $\hat{\mathbb{T}}_{i,VD}$ that do.

The standard estimators arise from plugging $\tilde{Q}_{N_\eta}$ directly into the estimators in Section 4.3.1,

$$\hat{\mathbb{S}}_{i,\tilde{Q}_{N_\eta}} \overset{\text{def}}{=} \frac{\frac{1}{N_\xi}\sum_{v=1}^{N_\xi} \tilde{Q}_{N_\eta}(\boldsymbol{B})_v \left[\tilde{Q}_{N_\eta}(\boldsymbol{A}^{(\boldsymbol{i})}_{\boldsymbol{B}})_v - \tilde{Q}_{N_\eta}(\boldsymbol{A})_v\right]}{\frac{1}{2N_\xi}\sum_{v=1}^{N_\xi}\left(\tilde{Q}_{N_\eta}(\boldsymbol{A})_v - \tilde{Q}_{N_\eta}(\boldsymbol{B})_v\right)^2} \overset{\text{def}}{=} \frac{\hat{\mathbb{V}}_{i,\tilde{Q}_{N_\eta}}}{\tilde{S}^2_{(AB)}}, \tag{4.23}$$

where $\left\langle \tilde{Q}_{N_\eta} \right\rangle_{(AB)} = \frac{1}{2N_\xi}\sum_{v=1}^{N_\xi}\left[\tilde{Q}_{N_\eta}(\boldsymbol{A})_v + \tilde{Q}_{N_\eta}(\boldsymbol{B})_v\right]$, and

$$\hat{\mathbb{T}}_{i,\tilde{Q}_{N_\eta}} \overset{\text{def}}{=} \frac{\frac{1}{2N_\xi}\left[\tilde{Q}_{N_\eta}(\boldsymbol{B}^{(\boldsymbol{i})}_{\boldsymbol{A}})_v - \tilde{Q}_{N_\eta}(\boldsymbol{B})_v\right]^2}{\frac{1}{2N_\xi}\sum_{v=1}^{N_\xi}\left(\tilde{Q}_{N_\eta}(\boldsymbol{A})_v - \tilde{Q}_{N_\eta}(\boldsymbol{B})_v\right)^2} \overset{\text{def}}{=} \frac{\hat{\mathbb{E}}^S_{\sim i,\tilde{Q}_{N_\eta}}}{\tilde{S}^2_{(AB)}}. \tag{4.24}$$

The variance deconvolution estimators follow directly from Eqs. (4.21) and (4.22),

$$\mathbb{S}_i \approx \hat{\mathbb{S}}_{i,VD} \overset{\text{def}}{=} \frac{\hat{\mathbb{V}}_{i,\tilde{Q}_{N_\eta}}}{\tilde{S}^2_{(AB)} - \frac{1}{N_\eta}\left\langle \hat{\sigma}^2_\eta \right\rangle_{(AB)}} \quad \text{and} \tag{4.25}$$

$$\mathbb{T}_i \approx \hat{\mathbb{T}}_{i,VD} \overset{\text{def}}{=} \frac{\hat{\mathbb{E}}^S_{\sim i,\tilde{Q}_{N_\eta}} - \frac{1}{N_\eta}\left\langle \hat{\sigma}^2_\eta \right\rangle_{(B^i_A B)}}{\tilde{S}^2_{(AB)} - \frac{1}{N_\eta}\left\langle \hat{\sigma}^2_\eta \right\rangle_{(AB)}}, \tag{4.26}$$

where

$$\left\langle \hat{\sigma}^2_\eta \right\rangle_{(AB)} \overset{\text{def}}{=} \frac{1}{2N_\xi}\sum_{v=1}^{N_\xi}\left[\hat{\sigma}^2_\eta(\boldsymbol{A})_v + \hat{\sigma}^2_\eta(\boldsymbol{B})_v\right]. \tag{4.27}$$

The additional variance deconvolution terms are introduced to correct the noise introduction from the stochastic solver while preserving the behavior of the existing estimators. For example, we estimate $\mathbb{V}ar\left[Q\right]$ consistent with the sampling estimator for $\mathbb{V}ar_\xi\left[Q\right]$ used in

Eqs. (4.12) and (4.13) rather than using a Bessel-corrected estimator as in Eq. (4.16). Other sampling estimators for $\mathbb{V}ar_{\xi}\left[Q\right]$ have been introduced for use with $\mathbb{S}_i$ and $\mathbb{T}_i$, *e.g.*, in [95] and [96]. Importantly, though $\mathbb{T}_i \geq \mathbb{S}_i$ in theory, the set of estimators $\hat{\mathbb{S}}_i$ and $\hat{\mathbb{T}}_i$ do not ensure this [4]; we would expect to see that same behavior with the variance deconvolution versions of these estimators. In the next section, we compare the statistical properties of the standard and variance-deconvolution estimators.

4.5.3 Mean-squared error of the estimators

The performance of an estimator $\hat{\theta}$ for true value θ is characterized by mean-squared error, which captures both its *variance* and *bias*:

$$\begin{aligned} MSE\left[\hat{\theta}\right] &= \mathbb{V}ar\left[\hat{\theta}\right] + \left(\mathbb{E}\left[\hat{\theta}\right] - \theta\right)^2 \\ &= \mathbb{V}ar\left[\hat{\theta}\right] + \mathbb{B}ias^2\left[\hat{\theta}, \theta\right]. \end{aligned}$$

An *unbiased* estimator will on average yield the true values of the Sobol' indices, and an estimator with small variance will on average yield values that remain close to the true values of the Sobol' indices [4]. In 4.8, we establish the variances and biases of the standard and variance-deconvolution estimators under the asymptotic normality assumption [113, 51, 4]. They are, respectively,

$$\mathbb{B}ias^2\left[\hat{\mathbb{S}}_{i,\tilde{Q}_{N_\eta}}, \mathbb{S}_i\right] = \frac{\mathbb{S}_i^2}{{N_\eta}^2} \frac{\mathbb{E}_\xi^2\left[\sigma_\eta^2\right]}{\mathbb{V}ar^2\left[\tilde{Q}_{N_\eta}\right]} \tag{4.28}$$

$$\mathbb{B}ias^2\left[\hat{\mathbb{S}}_{i,VD}, \mathbb{S}_i\right] = 0 \tag{4.29}$$

$$\mathbb{B}ias^2\left[\hat{\mathbb{T}}_{i,\tilde{Q}_{N_\eta}}, \mathbb{T}_i\right] = \frac{\mathbb{T}_i^2}{{N_\eta}^2} \frac{\mathbb{E}_\xi^2\left[\sigma_\eta^2\right] \mathbb{V}_{\sim i}^2}{\mathbb{V}ar^2\left[\tilde{Q}_{N_\eta}\right] \mathbb{E}_{\sim i}^2} \tag{4.30}$$

$$\mathbb{B}ias^2\left[\hat{\mathbb{T}}_{i,VD}, \mathbb{T}_i\right] = 0, \tag{4.31}$$

and,

$$\mathbb{V}ar\left[\hat{\mathbb{S}}_{i,\tilde{Q}_{N_\eta}}\right] = \frac{1}{\mathbb{V}ar^2\left[\tilde{Q}_{N_\eta}\right]}\mathbb{V}ar\Bigg[\tilde{Q}_{N_\eta}(\boldsymbol{B})\left(\tilde{Q}_{N_\eta}(\boldsymbol{A}_{\boldsymbol{B}}^{(\boldsymbol{i})}) - \tilde{Q}_{N_\eta}(\boldsymbol{A})\right) - \mathbb{S}_i\frac{\mathbb{V}ar_\xi\left[Q\right]}{2\mathbb{V}ar\left[\tilde{Q}_{N_\eta}\right]}\left(\tilde{Q}_{N_\eta}(\boldsymbol{A}) - \tilde{Q}_{N_\eta}(\boldsymbol{B})\right)^2\Bigg] \tag{4.32}$$

$$\mathbb{V}ar\left[\hat{\mathbb{S}}_{i,VD}\right] = \frac{1}{\mathbb{V}ar_\xi^2\left[Q\right]}\mathbb{V}ar\Bigg[\tilde{Q}_{N_\eta}(\boldsymbol{B})\left(\tilde{Q}_{N_\eta}(\boldsymbol{A}_{\boldsymbol{B}}^{(\boldsymbol{i})}) - \tilde{Q}_{N_\eta}(\boldsymbol{A})\right) - \mathbb{S}_i\frac{1}{2}\left(\tilde{Q}_{N_\eta}(\boldsymbol{A}) - \tilde{Q}_{N_\eta}(\boldsymbol{B})\right)^2 + \mathbb{S}_i\frac{1}{2N_\eta}\left(\hat{\sigma}_\eta^2(A) + \hat{\sigma}_\eta^2(B)\right)\Bigg] \tag{4.33}$$

$$\mathbb{V}ar\left[\hat{\mathbb{T}}_{i,\tilde{Q}_{N_\eta}}\right] = \frac{1}{\mathbb{V}ar^2\left[\tilde{Q}_{N_\eta}\right]}\mathbb{V}ar\Bigg[\frac{1}{2}\left(\tilde{Q}_{N_\eta}(\boldsymbol{B}_{\boldsymbol{A}}^{(\boldsymbol{i})}) - \tilde{Q}_{N_\eta}(\boldsymbol{B})\right)^2 - \mathbb{T}_i\frac{\mathbb{V}ar_\xi\left[Q\right]\mathbb{E}_{\sim i,\tilde{Q}_{N_\eta}}}{2\mathbb{V}ar\left[\tilde{Q}_{N_\eta}\right]\mathbb{E}_{\sim i}}\left(\tilde{Q}_{N_\eta}(\boldsymbol{A}) - \tilde{Q}_{N_\eta}(\boldsymbol{B})\right)^2\Bigg] \tag{4.34}$$

$$\mathbb{V}ar\left[\hat{\mathbb{T}}_{i,VD}\right] = \frac{1}{\mathbb{V}ar_\xi^2\left[Q\right]}\mathbb{V}ar\Bigg[\frac{1}{2}\left(\tilde{Q}_{N_\eta}(\boldsymbol{B}_{\boldsymbol{A}}^{(\boldsymbol{i})}) - \tilde{Q}_{N_\eta}(\boldsymbol{B})\right)^2 - \frac{1}{2N_\eta}\left(\hat{\sigma}_\eta^2(\boldsymbol{B}_{\boldsymbol{A}}^{\boldsymbol{i}}) + \hat{\sigma}_\eta^2(\boldsymbol{B})\right) - \mathbb{T}_i\left(\frac{1}{2}\left(\tilde{Q}_{N_\eta}(\boldsymbol{A}) - \tilde{Q}_{N_\eta}(\boldsymbol{B})\right)^2 - \frac{1}{2N_\eta}\left(\hat{\sigma}_\eta^2(\boldsymbol{A}) + \hat{\sigma}_\eta^2(\boldsymbol{B})\right)\right)\Bigg]. \tag{4.35}$$

When variance deconvolution is applied to $\mathbb{V}ar\left[\tilde{Q}_{N_\eta}\right]$ to develop the unbiased estimator $\mathbb{V}ar_\xi\left[Q\right] \approx S^2 = \tilde{S}^2 - \frac{1}{N_\eta}\left\langle\hat{\sigma}_\eta^2\right\rangle$, the additive relationship gives rise to a simple bias term $\frac{1}{N_\eta}\left\langle\hat{\sigma}_\eta^2\right\rangle$ and relatively simple variance $\mathbb{V}ar\left[S^2\right] = \mathbb{V}ar\left[\tilde{S}^2\right] + \frac{1}{N_\eta{}^2}\mathbb{V}ar\left[\left\langle\hat{\sigma}_\eta^2\right\rangle\right] - \frac{2}{N_\eta}\mathbb{C}ov\left[\tilde{S}^2, \left\langle\hat{\sigma}_\eta^2\right\rangle\right]$ [16]. Because the SI estimators are ratios, the relationships between $\left(\mathbb{S}_i, \mathbb{S}_{i,\tilde{Q}_{N_\eta}}\right)$ and $\left(\mathbb{T}_i, \mathbb{T}_{i,\tilde{Q}_{N_\eta}}\right)$ are not additive and their biases and variances are less straightforward to compare. The variance deconvolution estimators are unbiased; the biases of the standard estimators do not depend on N_ξ but do depend on N_η, the magnitude of the SIs, and the ratio of the solver noise to the total observed variance.

It is less obvious to draw comparisons between the variances of $\left(\hat{\mathbb{S}}_{i,VD}, \hat{\mathbb{S}}_{i,\tilde{Q}_{N_\eta}}\right)$ and $\left(\hat{\mathbb{T}}_{i,VD}, \hat{\mathbb{T}}_{i,\tilde{Q}_{N_\eta}}\right)$. We can qualitatively compare between the estimators for $\mathbb{S}_i$ and those for $\mathbb{T}_i$: because a correction term is necessary in both the numerator and denominator of $\mathbb{T}_i$, its estimators' biases and variances are more complex than their $\mathbb{S}_i$ counterparts. We investigate the statistics of the estimators in the next section through numerical simulation.

4.6 Numerical results

In this section, we illustrate the performance of the Saltelli SI estimators using stochastic QoIs with and without a variance deconvolution correction. We first discuss results for a test case with an analytic solution and then test the method on a radiation transport example problem.

4.6.1 Ishigami function

To test the accuracy of the derived estimators against analytic solutions, we add a stochastic parameter to the test function from Ishigami and Homma [49]:

$$\begin{gathered} f\left(\xi_1, \xi_2, \xi_3, \eta\right) = \sin\left(\xi_1\right) + a\sin^2\left(\xi_2\right) + b\xi_3^4 \sin\left(\xi_1\right) + c\eta, \\ a = 1, b = 0.1, c = 5, \\ \eta \sim \mathcal{N}\left(0,1\right), \quad \left(\xi_1, \xi_2, \xi_3\right) \sim \mathcal{U}\left(-\pi, +\pi\right), \end{gathered} \tag{4.36}$$

where ξ_1, ξ_2, and ξ_3 are independent input parameters and η represents some intrinsic randomness. Because we have defined η with mean zero and variance 1, the expected value of f is the expected value of the standard Ishigami function and the variance of f is the variance of the standard Ishigami function plus a constant c^2. In Figures 4.1-4.6, we compare the accuracy of the variance deconvolution (Var-D) vs the standard approach (Brute-F) over 200 repetitions for all first- and total-order indices. We use a consistent number of samples $N_\xi = 10^3$ to study the effect of increasing the number of histories per sample N_η. In general, we see that the Var-D estimator is more accurate than the Brute-F estimator, but has a larger variance especially at lower N_η. In some cases this

leads to the Brute-F estimator out-performing the Var-D estimator, in particular when the first-order index is near zero as with $\mathbb{S}_2$ and $\mathbb{S}_3$. With $\mathbb{S}_1$, we can clearly see that the Brute-F approach under-estimates the first-order index. With $\mathbb{T}_2$ and $\mathbb{T}_3$, we see that the Brute-F over-estimates the total-order index.

4.6.2 Radiation transport test problem

We next perform GSA on a test neutron transport problem solved using Monte Carlo radiation transport methods [65]. The problem is based on the steady-state C5G7 benchmark, a nuclear reactor benchmark developed by the OECD/NEA [17]. We simplify the design by reducing to one dimension in space with three materials: uranium dioxide (UO_2) fuel, water moderator, and a control rod. There is a constant source, uniform in energy across all groups, at the spatial halfway point. The neutron energy spectrum is divided into 7 energy groups and we use the cross-sections from the C5G7 benchmark. Parameter uncertainty is introduced in five independent factors: the densities of 1) the fuel, 2) the moderator, and 3) the control rod were allowed to vary uniformly ±70%; 4) the ratio of fuel-width to moderator-width and 5) the control-rod thickness were both allowed to vary uniformly between 0.2 and 0.8. We define two quantities of interest as a function of space: the scalar flux of the first two energy groups, $\phi_F(x)$, and the scalar flux of the remaining five energy groups $\phi_S(x)$.

For reference, using $N_\xi = 5 \times 10^5$ and $N_\eta = 10^5$, Figure 4.7 shows $\phi_F(x)$ and $\phi_S(x)$. Figure 4.8 shows the full set of first- and total- order indices for both QoIs. At such a high N_η, the lines for $\hat{\mathbb{S}}_{i,\tilde{Q}_{N_\eta}}$ and $\hat{\mathbb{T}}_{i,\tilde{Q}_{N_\eta}}$ overlap exactly with those of $\hat{\mathbb{S}}_{i,VD}$ and $\hat{\mathbb{T}}_{i,VD}$, respectively. The faster group flux ϕ_F is most sensitive across space to ξ_2, the density of the moderator, which is understandable as the density of the moderator will greatly impact the number of neutrons and their energies everywhere in the problem. The control rod's density (ξ_3) and thickness (ξ_5) are most impactful for the slower group flux, with both having large inflection points at the nominal moderator–control rod boundary at $x = 1.5$. This is understandable as the control rod is a primarily thermal absorber.

To see the effect of the variance deconvolution correction, we compare the MSE of the standard and corrected estimators. In Figure 4.9, we consider a constant computational

cost $C = \left(N_\xi \times N_\eta\right) = 5 \times 10^5$ in two different combinations of N_ξ and N_η. In the first combination, $\left(N_\xi, N_\eta\right) = \left(5 \times 10^3, 10^2\right)$, we see that the MSE of the standard estimator is clearly lower than that of the var-d estimator for $\mathbb{S}_1$ and $\mathbb{S}_5$. Both of these indices are very close to zero (see Figure 4.8); in this case, the higher variance of the var-d estimator outweighs the bias of the standard estimator. In the second combination, we have increased N_ξ by a factor of 10 and decreased N_η by the same factor to keep C constant. The variance deconvolution estimator benefits from this configuration, with an MSE that is lower than that of the standard estimator at most locations in x.

This pattern is consistent across QoIs: when indices are close to zero the variance of the variance deconvolution estimator can outweigh the bias of the standard estimator, and for a constant C the variance deconvolution estimator generally benefits from increasing the N_ξ at the expense of decreasing N_η. In Figure 4.10, we see this for $\mathbb{S}_i\left[\phi_S\right]$. For estimating $\mathbb{T}_i$, the correction in both the numerator and denominator makes the difference between the standard and variance deconvolution estimators more drastic. In Figures 4.11 and 4.12, we see that the variance deconvolution estimator outperforms the standard across x for both ϕ_F and ϕ_S.

We have shown, in this example and the analytic test case, that when increasing computational cost for more accurate estimates of $\mathbb{S}_i$ and $\mathbb{T}_i$, putting those computational resources towards increasing N_ξ with the variance deconvolution estimator will improve the accuracy of indices that are not near zero.

4.7 Conclusion

In this paper, we extend the variance deconvolution framework introduced in [16] for UQ to global sensitivity analysis (GSA). Sobol' indices are well-suited and widely used for GSA, and there has been abundant work over the past few decades on the most efficient sampling schemes and estimators for SIs. In this work, we analyze the effect on SIs when the underlying solver is stochastic, *i.e.*, , has some underlying inherent variability (*e.g.*, , Monte Carlo radiation transport solvers). We build on a previously-developed variance deconvolution estimator which, rather than computing parametric variance by over-resolving the stochastic solver, explicitly quantifies and removes the solver variance

from the total observed variance. We show in closed-form that in general, using a stochastic solver will always under-estimate the true first-order SIs and over-estimate the true total-order SIs. We find that though the variance-deconvolution version of existing SI estimators has a higher variance than its standard counterpart, the variance deconvolution version is consistently more accurate than the standard version.

Acknowledgements

Sandia National Laboratories is a multimission laboratory managed and operated by National Technology & Engineering Solutions of Sandia, LLC, a wholly owned subsidiary of Honeywell International Inc., for the U.S. Department of Energy's National Nuclear Security Administration under contract DE-NA0003525. This paper describes objective technical results and analysis. Any subjective views or opinions that might be expressed in the paper do not necessarily represent the views of the U.S. Department of Energy or the United States Government. This work was supported by the Center for Exascale Monte-Carlo Neutron Transport (CEMeNT) a PSAAP-III project funded by the Department of Energy, grant number DE-NA003967.

4.8 Mean-squared error from asymptotic limits

The law of large numbers and central limit theorem ensure that the estimators $\hat{\mathbb{S}}_{i,VD}$ and $\hat{\mathbb{T}}_{i,VD}$ converge to $\mathbb{S}_i$ and $\mathbb{T}_i$ almost surely, *i.e.*, $\lim_{N_\xi \to \infty} \hat{\mathbb{S}}_{i,VD} = \mathbb{S}_i$ and $\lim_{N_\xi \to \infty} \hat{\mathbb{T}}_{i,VD} = \mathbb{T}_i$.

The estimators $\hat{\mathbb{S}}_{i,\tilde{Q}_{N_\eta}}$ and $\hat{\mathbb{T}}_{i,\tilde{Q}_{N_\eta}}$ converge almost surely to $\mathbb{S}_{i,\tilde{Q}_{N_\eta}}$ and $\mathbb{T}_{i,\tilde{Q}_{N_\eta}}$ in the limit $N_\xi \to \infty$, and to $\mathbb{S}_i$ and $\mathbb{T}_i$ in the stricter limit $\left(N_\xi, N_\eta\right) \to \infty$.

We assume that the sample estimator $\hat{\mathbb{S}}_{i,VD}$ uses sample sizes N_ξ and N_η for the sensitivity sampling and stochastic solver samples per realization, respectively. In the following, we follow the steps of Janon et al. (2014) [51] and Azzini et al. (2021) [4] to establish that the asymptotic normality of this estimator is,

$$\lim_{N_\xi \to \infty} \sqrt{N_\xi} \left(\hat{\mathbb{S}}_{i,VD} - \mathbb{S}_i \right) \sim \mathcal{N}\left(0, \mathbb{V}ar\left[\alpha - \mathbb{S}_i(\beta - \gamma) \right] \right). \tag{4.37}$$

4.8.1 Proof: First-order Estimators

We define random vector X with mean μ_X, variance Σ_X, and sample mean $\overline{X}_{N_\xi} = N_\xi{}^{-1} \sum_{v=1}^{N_\xi} X_v$, where the statistics of the samples X_v do not depend on v:

$$X = \begin{bmatrix} \tilde{Q}_{N_\eta}(\boldsymbol{B}) \left[\tilde{Q}_{N_\eta}(\boldsymbol{A}^{(i)}_{\boldsymbol{B}}) - \tilde{Q}_{N_\eta}(\boldsymbol{A}) \right] \\ \frac{1}{2} \left(\tilde{Q}_{N_\eta}(\boldsymbol{A}) - \tilde{Q}_{N_\eta}(\boldsymbol{B}) \right)^2 \\ \frac{1}{2N_\eta} \left(\hat{\sigma}^2_\eta(A) + \hat{\sigma}^2_\eta(B) \right) \end{bmatrix} = \begin{bmatrix} \alpha \\ \beta \\ \gamma \end{bmatrix}, \tag{4.38}$$

$$\mu_X = \begin{bmatrix} \mathbb{V}ar\Big[\mathbb{E}\big[Q \mid \xi_i\big]\Big] \\ \mathbb{V}ar\left[\tilde{Q}_{N_\eta}\right] \\ \mathbb{E}\left[\sigma^2_\eta\right] / N_\eta \end{bmatrix} = \begin{bmatrix} \mu_\alpha \\ \mu_\beta \\ \mu_\gamma \end{bmatrix}, \tag{4.39}$$

$$\Sigma_X = \begin{bmatrix} \mathbb{V}ar\left[\alpha\right] & \mathbb{C}ov\left[\alpha, \beta\right] & \mathbb{C}ov\left[\alpha, \gamma\right] \\ \mathbb{C}ov\left[\alpha, \beta\right] & \mathbb{V}ar\left[\beta\right] & \mathbb{C}ov\left[\beta, \gamma\right] \\ \mathbb{C}ov\left[\alpha, \gamma\right] & \mathbb{C}ov\left[\beta, \gamma\right] & \mathbb{V}ar\left[\gamma\right] \end{bmatrix}, \tag{4.40}$$

$$X_v = \begin{bmatrix} \tilde{Q}_{N_\eta}(\boldsymbol{B})_v \left[\tilde{Q}_{N_\eta}(\boldsymbol{A}^{(i)}_{\boldsymbol{B}})_v - \tilde{Q}_{N_\eta}(\boldsymbol{A})_v \right] \\ \frac{1}{2} \left(\tilde{Q}_{N_\eta}(\boldsymbol{A})_v - \tilde{Q}_{N_\eta}(\boldsymbol{B})_v \right)^2 \\ \frac{1}{2N_\eta} \left(\hat{\sigma}^2_\eta(A)_v + \hat{\sigma}^2_\eta(B)_v \right) \end{bmatrix} \overset{\text{i.i.d}}{\sim} F(X). \tag{4.41}$$

From the central limit theorem (CLT), we have $\sqrt{N_\xi} \left(\overline{X}_{N_\xi} - \mu_X \right) \xrightarrow{d} \mathcal{N}_k\left(0, \Sigma_X\right)$. We define a function $g(a, b, c)$ and its gradient ∇g,

$$g(a, b, c) = \frac{a}{b - c}, \qquad \nabla g(a, b, c) = \left[\frac{1}{b - c}, \frac{-a}{(b - c)^2}, \frac{a}{(b - c)^2} \right], \tag{4.42}$$

such that we can write

$$g\left(\mu_X\right) = \frac{\mathbb{V}ar\Big[\mathbb{E}\big[Q \mid \xi_i\big]\Big]}{\mathbb{V}ar\left[\tilde{Q}_{N_\eta}\right] - \frac{1}{N_\eta}\mathbb{E}_\xi\left[\sigma^2_\eta\right]} = \frac{\mathbb{V}ar\Big[\mathbb{E}\big[Q \mid \xi_i\big]\Big]}{\mathbb{V}ar_\xi\left[Q\right]} = \mathbb{S}_i, \tag{4.43}$$

$$g\left(\overline{X}_{N_\xi}\right) = \hat{\mathbb{S}}_{i,VD}. \tag{4.44}$$

From the so-called Delta method [113], given function g with gradient ∇g such that $\nabla g(\mu_X) \stackrel{\text{def}}{=} \nabla_{\mu_X} \neq 0$,

$$\sqrt{N_\xi}\left(g(\overline{X}_{N_\xi}) - g(\mu_X)\right) \xrightarrow{d} \mathcal{N}\left(0, \nabla_{\mu_X} \Sigma_X \nabla_{\mu_X}^T\right).$$

Therefore, we find that the estimator $\hat{\mathbb{S}}_{i,VD}$ is unbiased regardless of stochastic solver sampling size N_η, with variance that depends on both N_ξ and N_η,

$$\mathbb{V}ar\left[\hat{\mathbb{S}}_{i,VD}\right] = \frac{\mathbb{V}ar\left[\alpha - \mathbb{S}_i\left(\beta - \gamma\right)\right]}{\mathbb{V}ar_\xi^2\left[Q\right]}. \tag{4.45}$$

Plugging in α, β, and γ defined in Eq. (4.38) leads to the result in Eq. 4.33.

Analysis of standard estimator $\hat{\mathbb{S}}_{i,\tilde{Q}_{N_\eta}}$ follows by defining vector $Y = [\alpha, \beta, 0]^T$ such that $g(\mu_Y) = \mathbb{S}_{i,\tilde{Q}_{N_\eta}}$ and $g(\overline{Y}_{N_\xi}) = \hat{\mathbb{S}}_{i,\tilde{Q}_{N_\eta}}$. Then,

$$\sqrt{N_\xi}\left(g(\overline{Y}_{N_\xi}) - g(\mu_Y)\right) \xrightarrow{d} \mathcal{N}\left(0, \nabla_{\mu_Y} \Sigma_X \nabla_{\mu_Y}^T\right).$$

Therefore, we find that $\hat{\mathbb{S}}_{i,\tilde{Q}_{N_\eta}}$ is a biased estimator of $\mathbb{S}_i$, where the magnitude of the bias depends on N_η, with variance that depends on both N_ξ and N_η,

$$\mathbb{B}ias^2\left[\hat{\mathbb{S}}_{i,\tilde{Q}_{N_\eta}}, \mathbb{S}_i\right] = \left(\mathbb{E}\left[\hat{\mathbb{S}}_{i,\tilde{Q}_{N_\eta}}\right] - \mathbb{S}_i\right)^2 \tag{4.46}$$

$$= \left(\mathbb{S}_{i,\tilde{Q}_{N_\eta}} - \mathbb{S}_i\right)^2 \tag{4.47}$$

$$= \mathbb{S}_i^2\left(\frac{\mathbb{V}ar_\xi\left[Q\right]}{\mathbb{V}ar\left[\tilde{Q}_{N_\eta}\right]} - 1\right)^2 \tag{4.48}$$

$$= \frac{\mathbb{S}_i^2}{{N_\eta}^2}\frac{\mathbb{E}_\xi^2\left[\sigma_\eta^2\right]}{\mathbb{V}ar^2\left[\tilde{Q}_{N_\eta}\right]} \tag{4.49}$$

$$\mathbb{V}ar\left[\hat{\mathbb{S}}_{i,\tilde{Q}_{N_\eta}}\right] = \frac{\mathbb{V}ar\left[\alpha - \mathbb{S}_{i,\tilde{Q}_{N_\eta}}\beta\right]}{\mathbb{V}ar^2\left[\tilde{Q}_{N_\eta}\right]} \tag{4.50}$$

$$= \frac{1}{\mathbb{V}ar^2\left[\tilde{Q}_{N_\eta}\right]}\mathbb{V}ar\left[\alpha\right] + \frac{\mathbb{V}ar_\xi^2\left[Q\right]}{\mathbb{V}ar\left[\tilde{Q}_{N_\eta}\right]^4}\mathbb{S}_i^2\mathbb{V}ar\left[\beta\right] - 2\frac{\mathbb{V}ar_\xi\left[Q\right]}{\mathbb{V}ar\left[\tilde{Q}^3_{N_\eta}\right]}\mathbb{S}_i\mathbb{C}ov\left[\alpha,\beta\right] \tag{4.51}$$

Plugging in α and β defined in Eq. (4.38) leads to the result in Eq. 4.32.

4.8.2 Proof: Total-order Estimators

To analyze $\hat{\mathbb{T}}_{i,VD}$ and $\hat{\mathbb{T}}_{i,\tilde{Q}_{N_\eta}}$, we follow the same process as for the first-order estimators above. We define random vector X with mean μ_X, variance Σ_X, and sample mean $\overline{X}_{N_\xi} = N_\xi{}^{-1}\sum_{v=1}^{N_\xi} X_v$, where the statistics of the samples X_v do not depend on v:

$$X = \begin{bmatrix} \frac{1}{2}\left(\tilde{Q}_{N_\eta}(\boldsymbol{B}^{(i)}_{\boldsymbol{A}}) - \tilde{Q}_{N_\eta}(\boldsymbol{B})\right)^2 \\ \frac{1}{2}\left(\tilde{Q}_{N_\eta}(\boldsymbol{A}) - \tilde{Q}_{N_\eta}(\boldsymbol{B})\right)^2 \\ \frac{1}{2N_\eta}\left(\hat{\sigma}^2_\eta(\boldsymbol{A}) + \hat{\sigma}^2_\eta(\boldsymbol{B})\right) \\ \frac{1}{2N_\eta}\left(\hat{\sigma}^2_\eta(\boldsymbol{B}^{\boldsymbol{i}}_{\boldsymbol{A}}) + \hat{\sigma}^2_\eta(\boldsymbol{B})\right) \end{bmatrix} = \begin{bmatrix}\alpha\\ \beta\\ \gamma\\ \delta\end{bmatrix}, \tag{4.52}$$

$$\mu_X = \begin{bmatrix} \mathbb{V}ar\Big[\mathbb{E}\big[Q \mid \xi_i\big]\Big] \\ \mathbb{V}ar\left[\tilde{Q}_{N_\eta}\right] \\ \mathbb{E}\left[\sigma^2_\eta\right]/N_\eta \\ \mathbb{E}\left[\sigma^2_\eta\right]/N_\eta \end{bmatrix} = \begin{bmatrix}\mu_\alpha\\ \mu_\beta\\ \mu_\gamma\\ \mu_\delta\end{bmatrix}, \tag{4.53}$$

$$\Sigma_X = \begin{bmatrix} \mathbb{V}ar\left[\alpha\right] & \mathbb{C}ov\left[\alpha,\beta\right] & \mathbb{C}ov\left[\alpha,\gamma\right] & \mathbb{C}ov\left[\alpha,\delta\right] \\ \mathbb{C}ov\left[\alpha,\beta\right] & \mathbb{V}ar\left[\beta\right] & \mathbb{C}ov\left[\beta,\gamma\right] & \mathbb{C}ov\left[\beta,\delta\right] \\ \mathbb{C}ov\left[\alpha,\gamma\right] & \mathbb{C}ov\left[\beta,\gamma\right] & \mathbb{V}ar\left[\gamma\right] & \mathbb{C}ov\left[\gamma,\delta\right] \\ \mathbb{C}ov\left[\alpha,\delta\right] & \mathbb{C}ov\left[\beta,\delta\right] & \mathbb{C}ov\left[\gamma,\delta\right] & \mathbb{V}ar\left[\delta\right] \end{bmatrix}. \tag{4.54}$$

We define a function $g(a, b, c, d)$ and its gradient ∇g,

$$g(a, b, c, d) = \frac{a - d}{b - c} \tag{4.55}$$

$$\nabla g(a, b, c, d) = \left[\frac{1}{b - c}, \frac{-(a - d)}{(b - c)^2}, \frac{(a - d)}{(b - c)^2}, \frac{-1}{b - c}\right], \tag{4.56}$$

such that we can write $g(\mu_X) = \mathbb{T}_i$ and $g(\overline{X}_{N_\xi}) = \hat{\mathbb{T}}_{i,VD}$. Therefore, we find that the estimator $\hat{\mathbb{T}}_{i,VD}$ is unbiased regardless of stochastic solver sampling size N_η, with variance that depends on both N_ξ and N_η,

$$\mathbb{V}ar\left[\hat{\mathbb{T}}_{i,VD}\right] = \frac{\mathbb{V}ar\left[\alpha - \delta - \mathbb{T}_i\left(\beta - \gamma\right)\right]}{\mathbb{V}ar_\xi^2\left[Q\right]}. \tag{4.57}$$

Plugging in α, β, γ, and δ defined in Eq. (4.52) leads to the result in Eq. 4.35.

Analysis of standard estimator $\hat{\mathbb{T}}_{i,\tilde{Q}_{N_\eta}}$ follows by defining vector $Y = [\alpha, \beta, 0, 0]^T$ such that $g(\mu_Y) = \mathbb{T}_{i,\tilde{Q}_{N_\eta}}$ and $g(\overline{Y}_{N_\xi}) = \hat{\mathbb{T}}_{i,\tilde{Q}_{N_\eta}}$. Therefore, we find that $\hat{\mathbb{T}}_{i,\tilde{Q}_{N_\eta}}$ is a biased estimator of $\mathbb{T}_i$, where the magnitude of the bias depends on N_η, with variance that depends on both N_ξ and N_η,

$$\mathbb{B}ias^2\left[\hat{\mathbb{T}}_{i,\tilde{Q}_{N_\eta}}, \mathbb{T}_i\right] = \left(\mathbb{E}\left[\hat{\mathbb{T}}_{i,\tilde{Q}_{N_\eta}}\right] - \mathbb{T}_i\right)^2 \tag{4.58}$$

$$= \left(\mathbb{T}_{i,\tilde{Q}_{N_\eta}} - \mathbb{T}_i\right)^2 \tag{4.59}$$

$$= \mathbb{T}_i^2\left(\frac{\mathbb{V}ar_\xi\left[Q\right]\mathbb{E}_{\sim i,\tilde{Q}_{N_\eta}}}{\mathbb{V}ar\left[\tilde{Q}_{N_\eta}\right]\mathbb{E}_{\sim i}} - 1\right)^2 \tag{4.60}$$

$$= \frac{\mathbb{T}_i^2}{{N_\eta}^2}\frac{\mathbb{E}_\xi^2\left[\sigma_\eta^2\right]\mathbb{V}_{\sim i}^2}{\mathbb{V}ar^2\left[\tilde{Q}_{N_\eta}\right]\mathbb{E}_{\sim i}^2}, \tag{4.61}$$

$$\mathbb{V}ar\left[\hat{\mathbb{T}}_{i,\tilde{Q}_{N_\eta}}\right] = \frac{\mathbb{V}ar\left[\alpha - \mathbb{T}_{i,\tilde{Q}_{N_\eta}}\beta\right]}{\mathbb{V}ar^2\left[\tilde{Q}_{N_\eta}\right]} \tag{4.62}$$

$$= \frac{1}{\mathbb{V}ar^2\left[\tilde{Q}_{N_\eta}\right]}\mathbb{V}ar\left[\alpha\right] + \frac{\mathbb{V}ar_\xi^2\left[Q\right]\mathbb{E}^2_{\sim i,\tilde{Q}_{N_\eta}}}{\mathbb{V}ar\left[\tilde{Q}_{N_\eta}\right]^4\mathbb{E}^2_{\sim i}}\mathbb{T}_i^2\mathbb{V}ar\left[\beta\right] - 2\frac{\mathbb{V}ar_\xi\left[Q\right]\mathbb{E}_{\sim i,\tilde{Q}_{N_\eta}}}{\mathbb{V}ar\left[\tilde{Q}^3_{N_\eta}\right]\mathbb{E}_{\sim i}}\mathbb{T}_i\mathbb{C}ov\left[\alpha,\beta\right]. \tag{4.63}$$

Plugging in α and β defined in Eq. (4.52) leads to the result in Eq. 4.34.

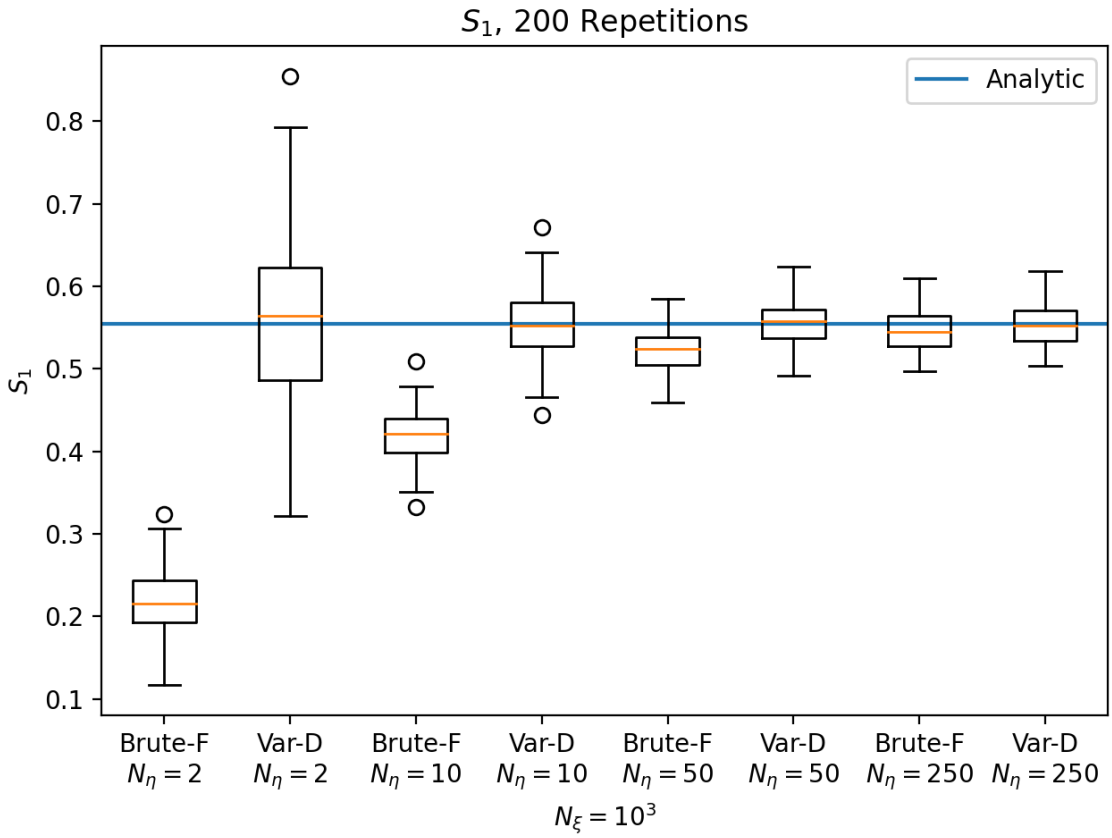

Figure 4.1: For the Ishigami function with added stochasticity, comparing distributions of $\mathbb{S}_1$ calculated using a variance deconvolution (Var-D) vs. a standard approach (Brute-F) with the Saltelli estimator. $N_\xi = 10^3$ in every case, with N_η increasing from left to right within a single plot. Analytic indices reported as solid horizontal line.

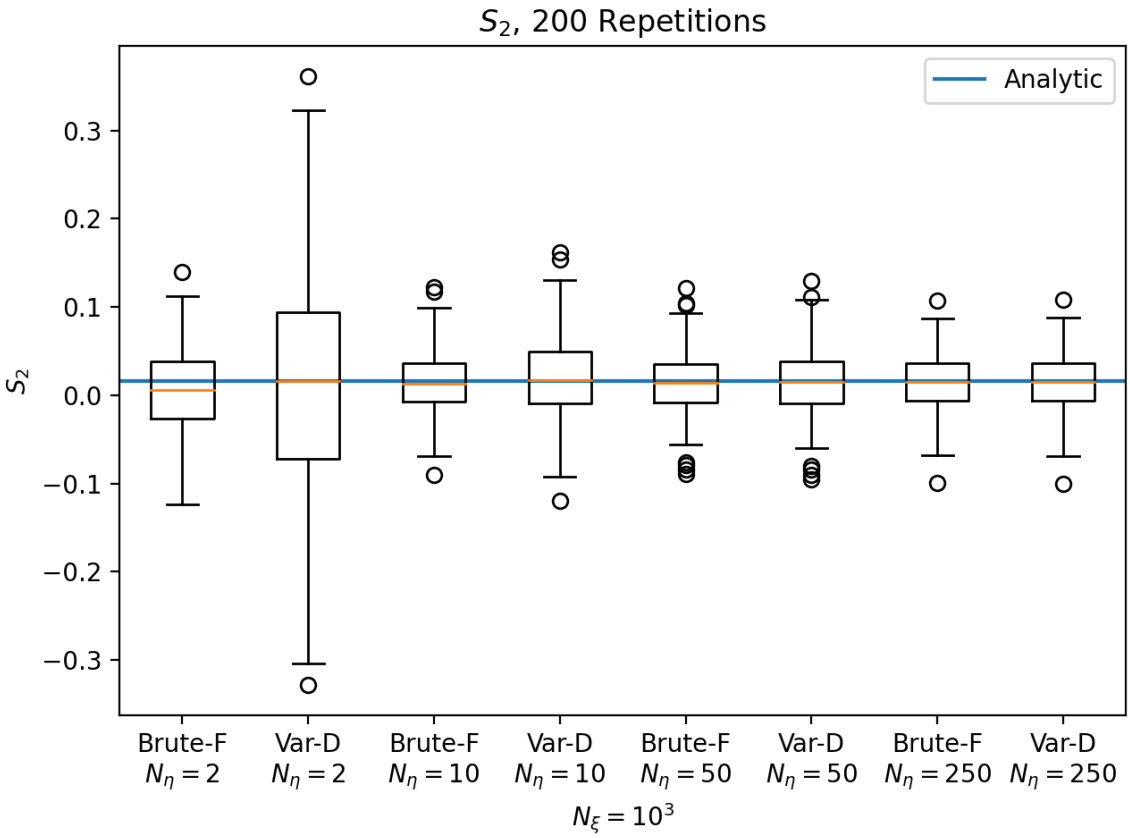

Figure 4.2: For the Ishigami function with added stochasticity, comparing distributions of $\mathbb{S}_2$ calculated using a variance deconvolution (Var-D) vs. a standard approach (Brute-F) with the Saltelli estimator. $N_\xi = 10^3$ in every case, with N_η increasing from left to right within a single plot. Analytic indices reported as solid horizontal line.

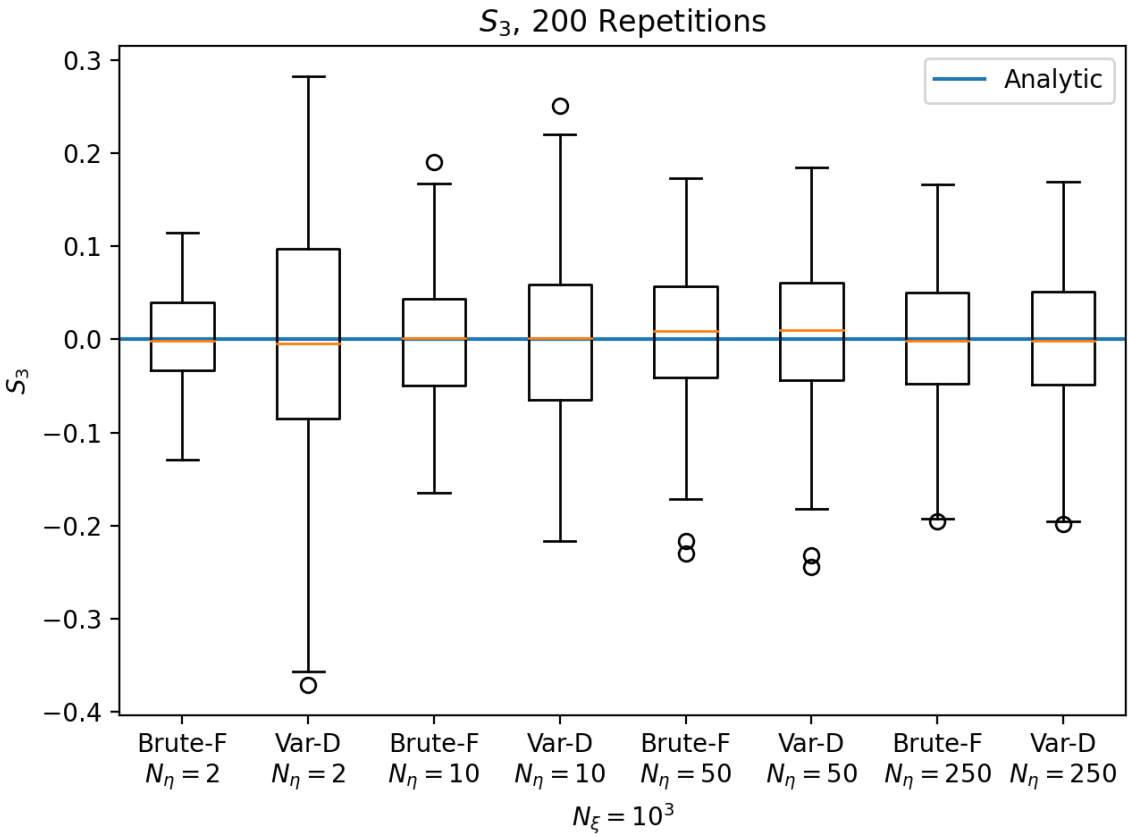

Figure 4.3: For the Ishigami function with added stochasticity, comparing distributions of $\mathbb{S}_3$ calculated using a variance deconvolution (Var-D) vs. a standard approach (Brute-F) with the Saltelli estimator. $N_\xi = 10^3$ in every case, with N_η increasing from left to right within a single plot. Analytic indices reported as solid horizontal line.

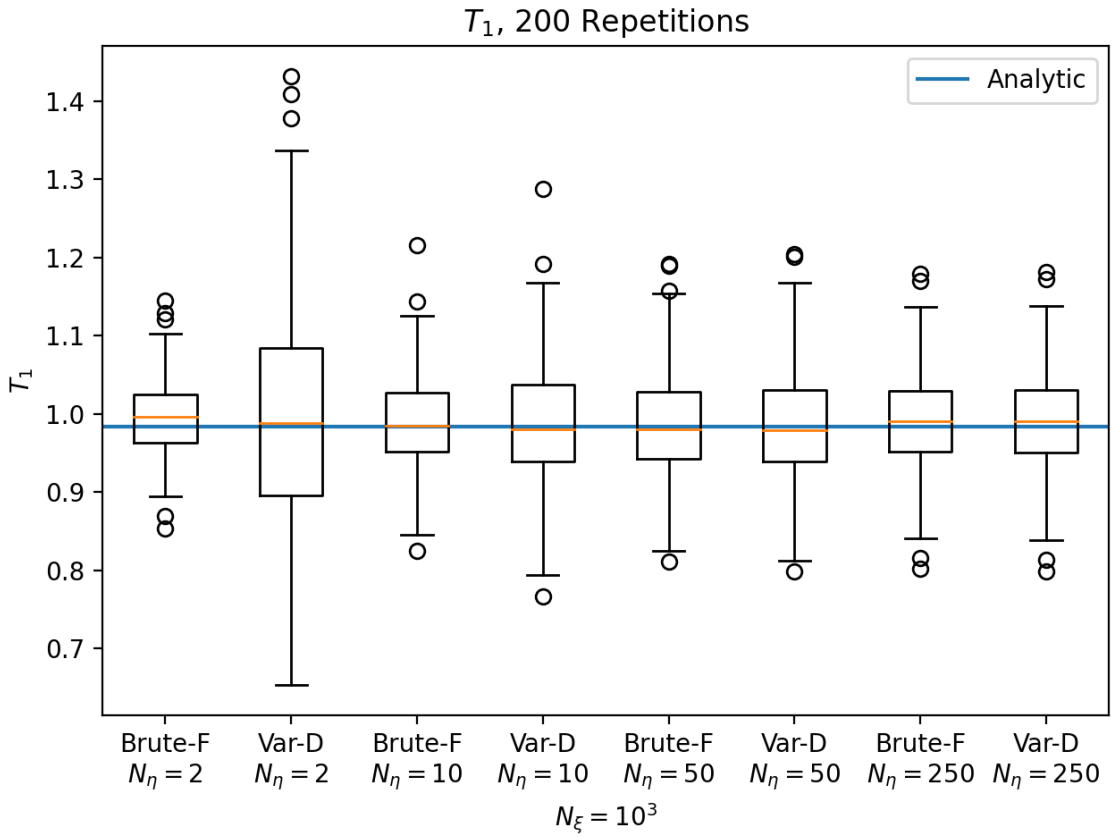

Figure 4.4: For the Ishigami function with added stochasticity, comparing distributions of $\mathbb{T}_1$ calculated using a variance deconvolution (Var-D) vs. a standard approach (Brute-F) with the Saltelli estimator. $N_\xi = 10^3$ in every case, with N_η increasing from left to right within a single plot. Analytic indices reported as solid horizontal line.

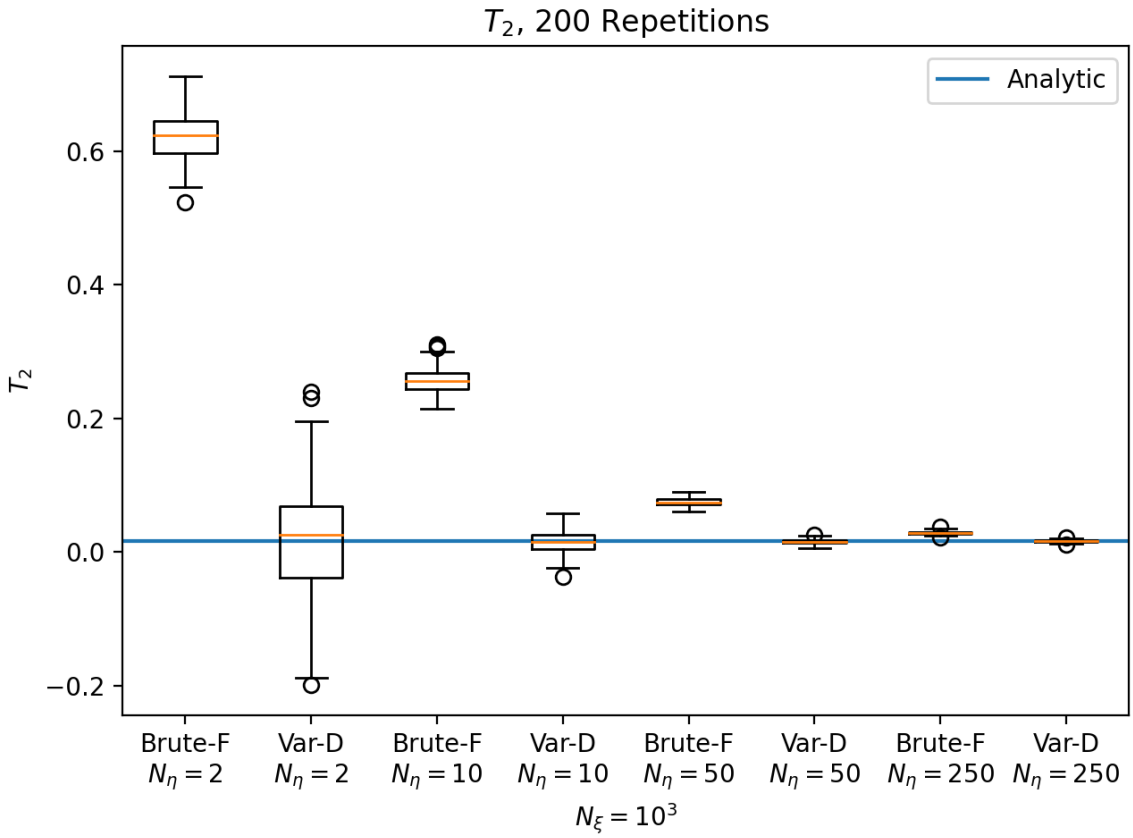

Figure 4.5: For the Ishigami function with added stochasticity, comparing distributions of $\mathbb{T}_2$ calculated using a variance deconvolution (Var-D) vs. a standard approach (Brute-F) with the Saltelli estimator. $N_\xi = 10^3$ in every case, with N_η increasing from left to right within a single plot. Analytic indices reported as solid horizontal line.

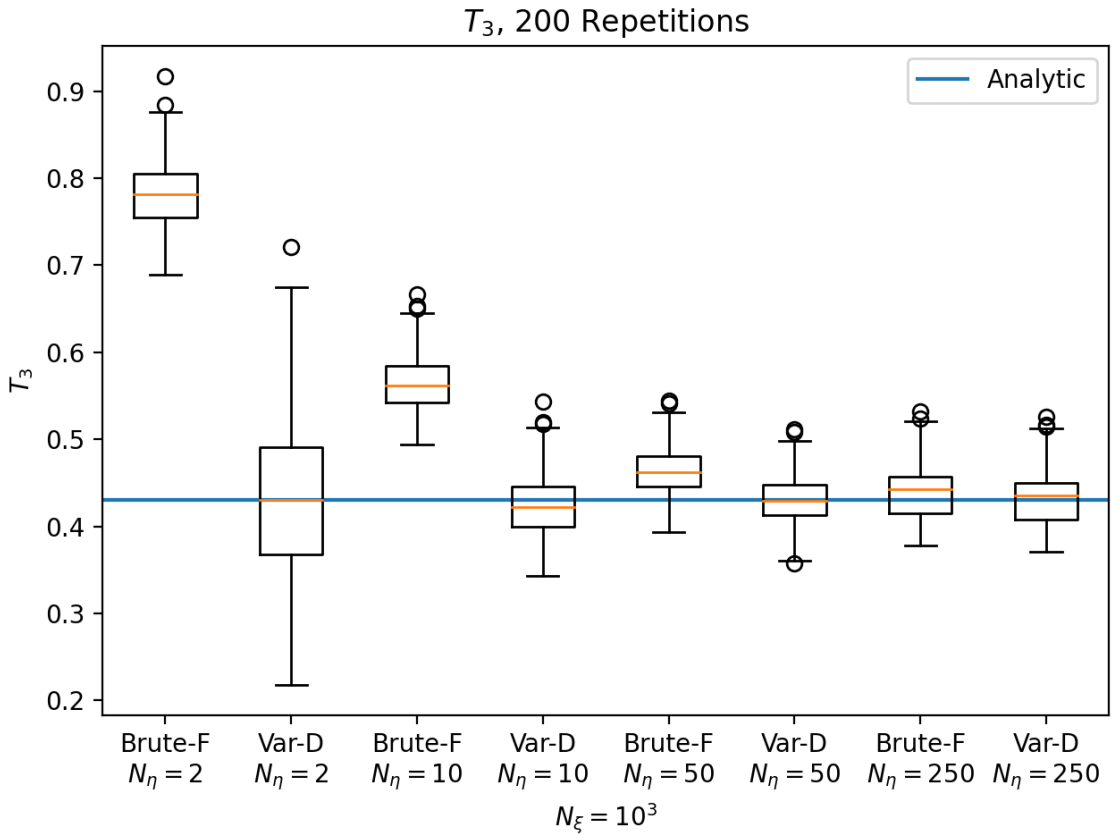

Figure 4.6: For the Ishigami function with added stochasticity, comparing distributions of $\mathbb{T}_3$ calculated using a variance deconvolution (Var-D) vs. a standard approach (Brute-F) with the Saltelli estimator. $N_\xi = 10^3$ in every case, with N_η increasing from left to right within a single plot. Analytic indices reported as solid horizontal line.

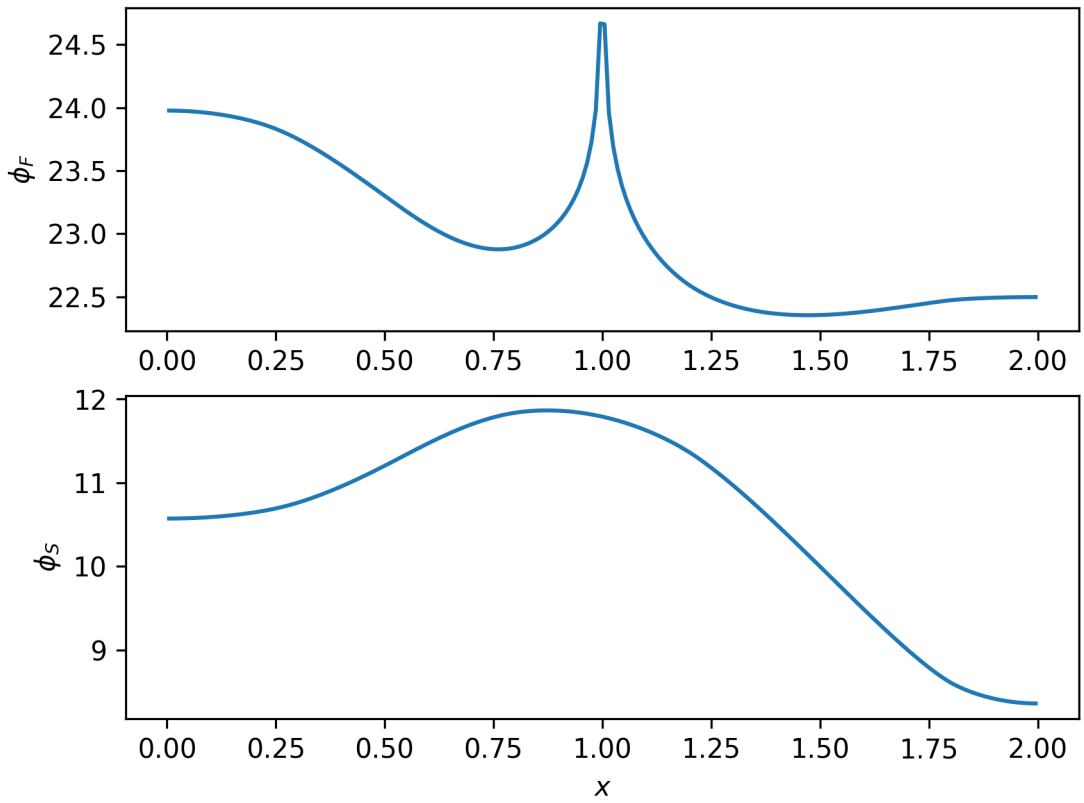

Figure 4.7: Average scalar flux with five uncertain parameters using $N_\xi = 5\times10^5$, $N_\eta = 10^5$.

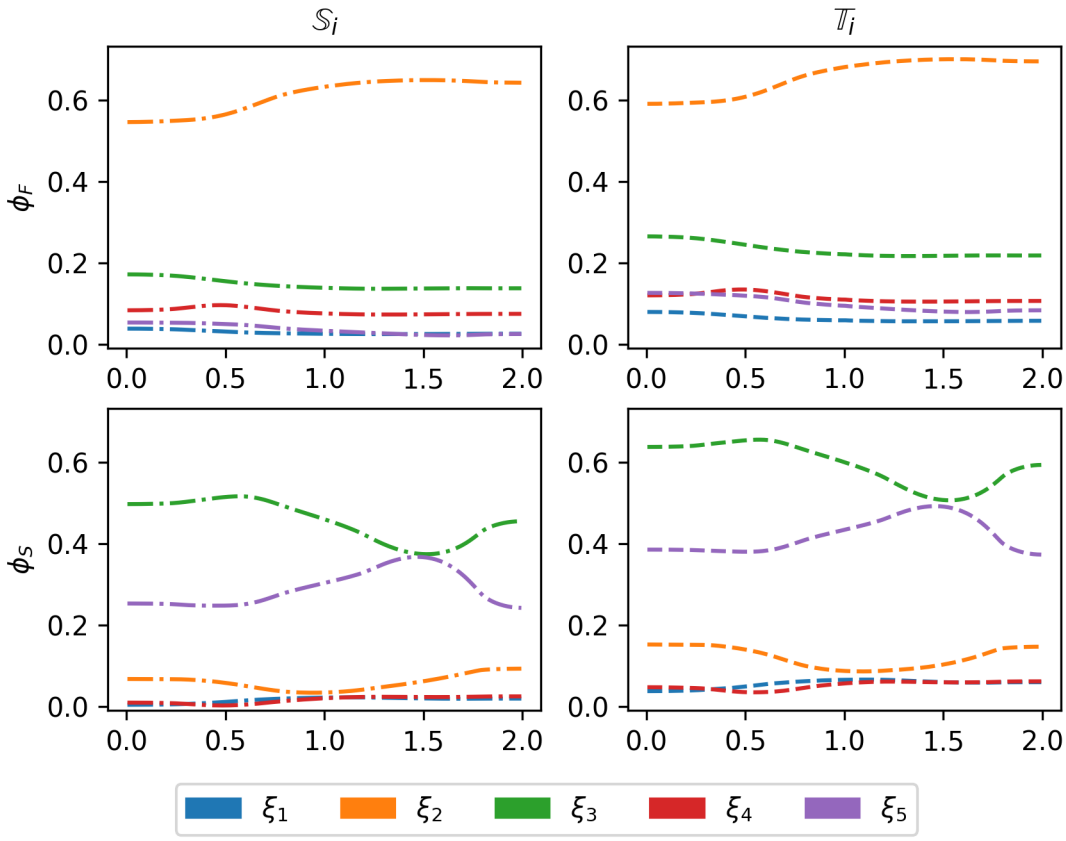

Figure 4.8: Full set of first- and total- order indices of ϕ_F and ϕ_S using $N_\xi = 5 \times 10^5$, $N_\eta = 10^5$. Standard and corrected estimators exactly overlap. Uncertain factors: the densities of 1) the fuel, 2) the moderator, 3) and the control rod were allowed to vary uniformly ±70%; 4) the ratio of fuel-width to moderator-width and 5) the control-rod thickness were both allowed to vary uniformly between 0.2 and 0.8.

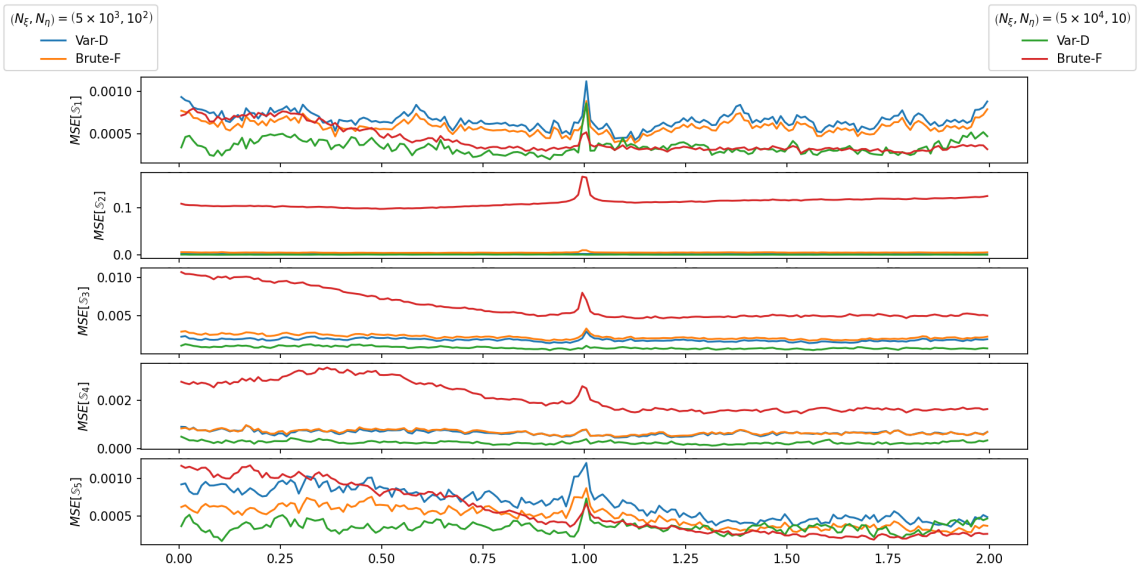

Figure 4.9: $MSE\ [\mathbb{S}_i]$ for ϕ_F, constant computational cost $C = \left(N_\xi \times N_\eta\right) = 5 \times 10^5$.

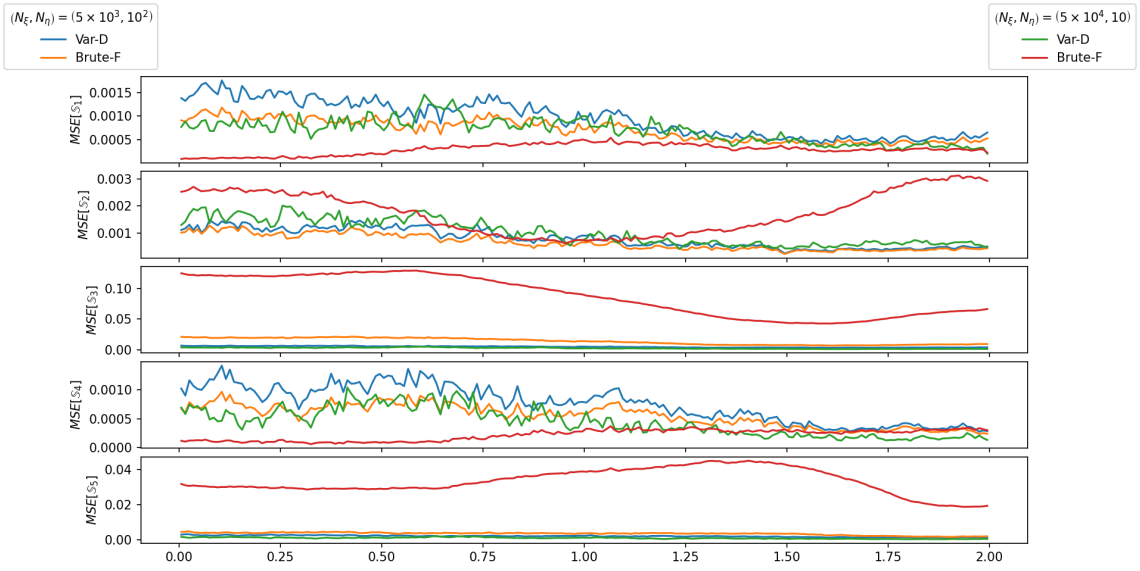

Figure 4.10: $MSE\ [\mathbb{S}_i]$ for ϕ_S, constant computational cost $C = \left(N_\xi \times N_\eta\right) = 5 \times 10^5$.

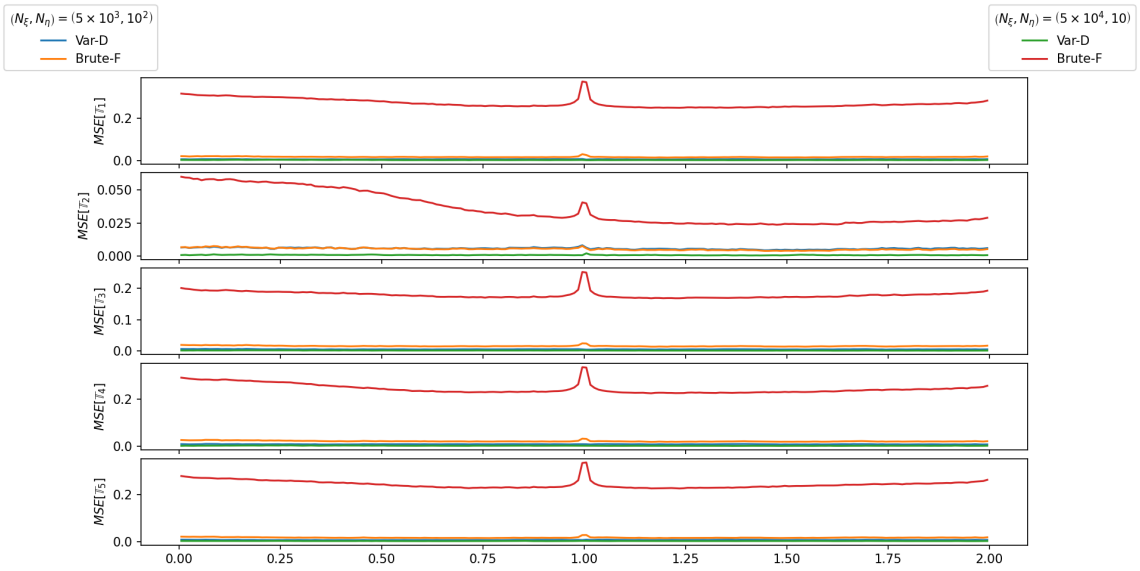

Figure 4.11: $MSE\ [\mathbb{T}_i]$ for ϕ_F, constant computational cost $C = \left(N_\xi \times N_\eta\right) = 5 \times 10^5$.

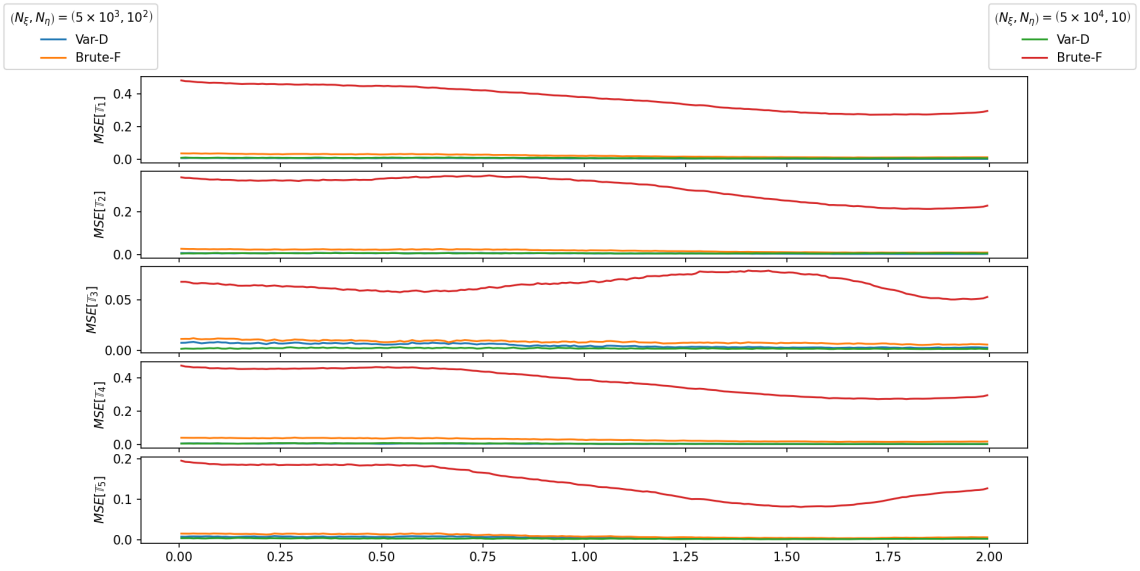

Figure 4.12: $MSE\ [\mathbb{T}_i]$ for ϕ_S, constant computational cost $C = \left(N_\xi \times N_\eta\right) = 5 \times 10^5$.

MONTE CARLO SENSITIVITY ANALYSIS FOR THE C5G7 BENCHMARK

Kayla B. Clements, Todd S. Palmer, Aaron J. Olson, Gianluca Geraci, Ilham Variansyah

Accepted to *The International Conference on Mathematics and Computational Methods Applied to Nuclear Science and Engineering*
Proceedings, Apr 2025.

Chapter 5: Monte Carlo Uncertainty Quantification and Sensitivity Analysis for the C5G7 Benchmark

Abstract

In this study, sampling methods and Monte Carlo (MC) radiation transport (RT) were used to perform uncertainty quantification (UQ) and global sensitivity analysis (GSA) on the 3D C5G7-TD benchmark in its initial unrodded configuration. UQ was performed using variance deconvolution, a recently-developed uncertainty propagation method for stochastic solvers that computes parametric variance by explicitly accounting for the stochastic solver's variance. Additionally, we applied our recent work integrating variance deconvolution with Sobol' sensitivity indices to compute Sobol' indices for eight input parameters – the density and radius of each of the four fuel types in the core. The C5G7 core was modeled using Monte Carlo Dynamic Code (MC/DC), an open-source neutral-particle transport code, and both the core k_{eff} eigenvalue and pinwise core fission rate distribution were considered as quantities of interest. Manufacturing uncertainties of fuel pin radius and density were sampled from a normal distribution of a 5% standard deviation about their respective nominal values. Variation of the densities and radii of the specific pin components such as pellet radius, gap thickness, and clad thickness was limited due to the spatial homogenization of the benchmark cross-sections. Using variance deconvolution allowed for more cost-efficient UQ and GSA with MC RT code than the standard approach of increasing particle count to reduce the solver variance.

5.1 Introduction

It has remained consistently important for nuclear research, industry, safety, and regulation that best-estimate predictions from computational models and simulations be reported with their associated uncertainties. These requirements can be met using uncertainty quantification (UQ, also called uncertainty analysis) and sensitivity analysis, both of which are

important steps in rigorous model validation. To propagate input uncertainties through reactor physics and modeling simulations, both deterministic [26] and statistical sampling methods [94, 5] have been widely proposed and applied for both nuclear data and manufacturing uncertainties. Deterministic approaches, such as approximating first-order sensitivity coefficients by perturbing parameters locally around their nominal values [26], typically require fewer model evaluations than sampling-based approaches and are therefore attractive for computational models for which even one evaluation is computationally expensive. However, these approaches make some assumptions about the linearity of the underlying function and allow for relatively small parameter perturbations. In sampling methods, uncertain parameters are sampled from their probability distributions and propagated through the model, then statistics of the quantity of interest are computed directly using sampling-based estimators [97]. Sampling-based methods are useful because they do not make assumptions about the linearity, smoothness, or regularity of the model response [97]; however, their primary drawback is the potential high computational cost associated with the multiple code evaluations needed to compute the required statistics with satisfactory precision [97], since an independent code evaluation is required for each drawn sample.

Sampling methods can become cost-prohibitive when the underlying solver itself is also stochastic, as is the case with Monte Carlo (MC) radiation transport (RT) solvers. When inputs to a stochastic simulator have some associated uncertainty, the total observed variance of the output is a combination of the variability of the solver itself ("solver variance") and the variability of the input parameters [5, 94]. To estimate variance and sensitivities of the output introduced solely by the uncertain input parameters ("parametric variance" and "parametric sensitivities"), a standard approach to handle the stochasticity of the solver is to increase the number of particle histories such that the solver variance is a relatively small contribution of the total observed variance; the high computational cost of doing so must be paid for each of the multiple code evaluations required for sampling methods.

As an alternative to the standard treatment we have proposed a variance deconvolution approach [16, 74], in which we compute parametric variance by explicitly quantifying and removing the solver variance from the total observed variance, rather than by minimizing the

solver variance. In [16], we rigorously showed that variance deconvolution is accurate and much more cost-effective than the standard approach for computing parametric variance. In recent work [15], we integrated variance deconvolution into sampling estimators for sensitivity indices (SIs, also referred to as Sobol' indices), which is a GSA approach that uses analysis of variance to rank input parameters in order of importance to the output [97]. Exploration of the practical usability and benefit of these capabilities has included analytic functions and simple slab-geometry radiation transport problems with and without stochastic media. However, exploration on more realistic problems has not been performed, leaving questions as to the practical value for large-scale MC RT computations.

In this work, as an example of application to a more realistic MC RT problem, we use variance deconvolution to evaluate the parametric variance and perform sensitivity analysis on the 3D C5G7 criticality benchmark problem [45]. We propagate uncertainties of eight input parameters, namely, the radii and densities of the four fuel types in the core, to compute the k-eigenvalue and fission rate distributions across the core. We perform MC RT simulations with the Monte Carlo Dynamic Code (MC/DC), an open source neutron transport code developed by the PSAAP-III Center for Exascale Monte Carlo Neutron Transport [72].

The remainder of the paper is structured as follows. In Section 5.2, we summarize the variance deconvolution approach and its use for UQ and GSA. In Section 5.3, we briefly describe the C5G7 3D benchmark, then present and discuss the results. A summary and conclusions are provided in Section 5.4.

5.2 Uncertainty and Global Sensitivity Analysis with Variance Deconvolution

In this section, we first summarize and introduce notation for UQ and GSA in a general context, then introduce the case of UQ and GSA for a stochastic solver. For a detailed presentation of variance deconvolution and an algorithmic representation of variance deconvolution for UQ, see [16].

5.2.1 Uncertainty and global sensitivity analysis

We consider a generic scalar quantity of interest (QoI) $Q = Q(\boldsymbol{\xi}), \boldsymbol{\xi} = (\xi_1, \ldots, \xi_k) \in \Xi \subset \mathbb{R}^k$, where $\xi_1, \ldots, \xi_k$ are independent random variables with arbitrary joint distribution function $p(\boldsymbol{\xi})$. To characterize the effect of input uncertainty on Q, we are interested in statistics of Q, like its mean and variance,

$$\mathbb{E}_\xi[Q] = \int_\Xi Q(\boldsymbol{\xi})\, p(\boldsymbol{\xi}) d\boldsymbol{\xi} \qquad \text{and} \qquad \mathbb{V}ar_\xi[Q] = \int_\Xi \Big(Q(\boldsymbol{\xi}) - \mathbb{E}_\xi[Q]\Big)^2 p(\boldsymbol{\xi}) d\boldsymbol{\xi}, \quad (5.1)$$

where a subscript indicates expectation and variance over ξ. We are also interested in computing SIs, which give the ratio of the conditional variance of a parameter or set of parameters to the unconditional parametric variance and are commonly used to rank the parameters in order of importance to the QoI [97]. The importance of parameter ξ_i can be described by its first-order SI $\mathbb{S}_i$ and its total-order SI $\mathbb{T}_i$,

$$\mathbb{S}_i = \frac{\mathbb{V}ar_{\xi_i}\Big[\mathbb{E}_{\xi_{\sim i}}[Q \mid \xi_i]\Big]}{\mathbb{V}ar_\xi[Q]} \qquad \text{and} \qquad \mathbb{T}_i = \frac{\mathbb{E}_{\xi_{\sim i}}\Big[\mathbb{V}ar_{\xi_i}[Q \mid \boldsymbol{\xi}_{\sim i}]\Big]}{\mathbb{V}ar_\xi[Q]} = 1 - \frac{\mathbb{V}ar_{\xi_{\sim i}}\Big[\mathbb{E}_{\xi_i}[Q \mid \boldsymbol{\xi}_{\sim i}]\Big]}{\mathbb{V}ar_\xi[Q]}, \quad (5.2)$$

where $\mathbb{S}_i$ describes the main effect contribution of parameter ξ_i and $\mathbb{T}_i$ describes the effect of parameter ξ_i *and* its interaction with all of the other parameters $\xi_{\sim i}$. By definition, for parameter ξ_i, $0 \le \mathbb{S}_i \le \mathbb{T}_i$, where the difference $\mathbb{T}_i - \mathbb{S}_i$ captures the effect solely of ξ_i's interactions. Additionally by definition, $\sum_{i=1}^k \mathbb{S}_i \le 1$, where the difference $1 - \sum_{i=1}^k \mathbb{S}_i$ provides an idea of how much variance remains to be captured by higher-order effects; refer to [97] for additional details.

The so-called Saltelli method [97] is a sampling-based approach to estimate the full suite of first- and total-order SIs. We outline the general algorithm of this approach below, assuming k uncertain parameters:

1. Define two (N_ξ, k) matrices, $\boldsymbol{A}$ and $\boldsymbol{B}$, which contain independent input samples.

$$\boldsymbol{A} = \begin{bmatrix} \xi_1^{(1)} & \cdots & \xi_i^{(1)} & \cdots & \xi_k^{(1)} \\ \vdots & & \ddots & & \vdots \\ \xi_1^{(N)} & \cdots & \xi_i^{(N_\xi)} & \cdots & \xi_k^{(N_\xi)} \end{bmatrix}, \qquad \boldsymbol{B} = \begin{bmatrix} \xi_{k+1}^{(1)} & \cdots & \xi_{k+i}^{(1)} & \cdots & \xi_{2k}^{(1)} \\ \vdots & & \ddots & & \vdots \\ \xi_{k+1}^{(N_\xi)} & \cdots & \xi_{k+i}^{(N_\xi)} & \cdots & \xi_{2k}^{(N_\xi)} \end{bmatrix}.$$

2. For each i-th input factor, define matrix $\boldsymbol{A}_{\boldsymbol{B}}^{(\boldsymbol{i})}$, which is a copy of $\boldsymbol{A}$ except for the i-th column, which comes from $\boldsymbol{B}$.

$$\boldsymbol{A}_{\boldsymbol{B}}^{(\boldsymbol{i})} = \begin{bmatrix} \xi_1^{(1)} & \cdots & \xi_{k+i}^{(1)} & \cdots & \xi_k^{(1)} \\ \vdots & & \ddots & & \vdots \\ \xi_1^{(N_\xi)} & \cdots & \xi_{k+i}^{(N_\xi)} & \cdots & \xi_k^{(N_\xi)} \end{bmatrix}.$$

3. Compute model output for $\boldsymbol{A}$, $\boldsymbol{B}$, and all $\boldsymbol{A}_{\boldsymbol{B}}^{(\boldsymbol{i})}$ to obtain vectors of model output $Q(\boldsymbol{A})$, $Q(\boldsymbol{B})$, and $Q(\boldsymbol{A}_{\boldsymbol{B}}^{(\boldsymbol{i})})$, all of dimension $(N_\xi, 1)$. Let $Q(\boldsymbol{A})_v$ indicate the v-th element of the vector $Q(\boldsymbol{A})$, i.e., one function evaluation of Q.

4. Approximate the full set of $\mathbb{S}_i$ and $\mathbb{T}_i$ using $Q(\boldsymbol{A})$, $Q(\boldsymbol{B})$ and $Q(\boldsymbol{A}_{\boldsymbol{B}}^{(\boldsymbol{i})})$:

$$\mathbb{S}_i \approx \frac{\frac{1}{N_\xi} \sum_{v=1}^{N_\xi} Q(\boldsymbol{B})_v \left[Q(\boldsymbol{A}_{\boldsymbol{B}}^{(\boldsymbol{i})})_v - Q(\boldsymbol{A})_v \right]}{\frac{1}{2N_\xi} \sum_{v=1}^{N_\xi} \left[Q(\boldsymbol{A})_v - Q(\boldsymbol{B})_v \right]^2} \stackrel{\text{def}}{=} \hat{\mathbb{S}}_i, \tag{5.3}$$

$$\mathbb{T}_i \approx \frac{\frac{1}{2N_\xi} \sum_{v=1}^{N_\xi} \left[Q(\boldsymbol{B}_{\boldsymbol{A}}^{(\boldsymbol{i})})_v - Q(\boldsymbol{B})_v \right]^2}{\frac{1}{2N_\xi} \sum_{v=1}^{N_\xi} \left[Q(\boldsymbol{A})_v - Q(\boldsymbol{B})_v \right]^2} \stackrel{\text{def}}{=} \hat{\mathbb{T}}_i. \tag{5.4}$$

A number of sampling schemes (e.g., quasi-random sequencing, Latin hypercube) can be used to fulfill step 1) of the above algorithm; for simplicity, we use purely random sampling. To approximate $\mathbb{S}_i$ and $\mathbb{T}_i$ in step 4), we have used a sampling estimator for $\mathbb{S}_i$ from [110] and for $\mathbb{T}_i$ from [52], as recommended for general use by [98]. For a broad review of sampling schemes and estimators used with the Saltelli method, see e.g., [87].

In the following, we describe how to compute the statistical quantities introduced above via sampling when the underlying QoI is computed using a stochastic solver.

5.2.2 Variance deconvolution

To enable mathematical treatment of the stochastic solver's variability, we represent it with an additional random variable η and define our QoI Q as the expectation over η of a function $f(\boldsymbol{\xi}, \eta)$: $Q(\boldsymbol{\xi}) = \mathbb{E}\left[f(\boldsymbol{\xi}, \eta) \mid \boldsymbol{\xi}\right] \stackrel{\text{def}}{=} \mathbb{E}_\eta\left[f(\boldsymbol{\xi}, \eta)\right]$. The function $f(\boldsymbol{\xi}, \eta)$ can be directly evaluated as the output from the stochastic solver with input $\boldsymbol{\xi}$, but the expectation $\mathbb{E}_\eta\left[f(\boldsymbol{\xi}, \eta)\right]$ and variance $\mathbb{V}ar_\eta\left[f(\boldsymbol{\xi}, \eta)\right] \stackrel{\text{def}}{=} \sigma_\eta^2(\boldsymbol{\xi})$ are not directly available. Instead, we approximate $Q(\boldsymbol{\xi})$ and $\sigma_\eta^2(\xi)$ as the sample mean and variance of f over N_η independent evaluations:

$$Q\left(\boldsymbol{\xi}\right) \approx \frac{1}{N_\eta}\sum_{j=1}^{N_\eta} f(\boldsymbol{\xi}, \eta^{(j)}) \stackrel{\text{def}}{=} \tilde{Q}_{N_\eta}(\boldsymbol{\xi}) \quad \text{and} \quad \sigma_\eta^2(\boldsymbol{\xi}) \approx \frac{1}{N_\eta - 1}\sum_{j=1}^{N_\eta}\left(f(\boldsymbol{\xi}, \eta^{(j)}) - \tilde{Q}_{N_\eta}(\boldsymbol{\xi})\right)^2 \stackrel{\text{def}}{=} \hat{\sigma}_\eta^2(\boldsymbol{\xi}).$$

In the context of MC RT, $\eta^{(j)}$ corresponds to the internal stream of random numbers comprising a single particle history, $f(\boldsymbol{\xi}, \eta^{(j)})$ corresponds to the result (e.g., tally) of that single particle history, and $\tilde{Q}_{N_\eta}(\boldsymbol{\xi})$ corresponds to the output of a MC RT simulation that used a total of N_η particle histories. Variance deconvolution was introduced [16, 74] to show that the parametric variance of Q, $\mathbb{V}ar_\xi\left[Q\right]$, can be efficiently and accurately estimated from $\tilde{Q}_{N_\eta}$ by explicitly computing and removing the solver variance from the total observed variance. From [16], the total variance of $\tilde{Q}_{N_\eta}$ decomposes into the effect of the uncertain parameters and the effect of the stochastic solver: $\mathbb{V}ar_\xi\left[Q\right] = \mathbb{V}ar\left[\tilde{Q}_{N_\eta}\right] - \frac{1}{N_\eta}\mathbb{E}_\xi\left[\sigma_\eta^2\right]$. Building on [16, 15], we have extended variance deconvolution to examine the first- and

total-order SIs of ξ_i on $\tilde{Q}_{N_\eta}$,

$$\mathbb{S}_{i,\tilde{Q}_{N_\eta}} = \frac{\mathbb{V}ar_{\xi_i}\left[\mathbb{E}_{\xi_{\sim i},\eta}\left[\tilde{Q}_{N_\eta} \mid \xi_i\right]\right]}{\mathbb{V}ar\left[\tilde{Q}_{N_\eta}\right]} = \frac{\mathbb{V}ar_{\xi_i}\left[\mathbb{E}_{\xi_{\sim i}}\left[Q \mid \xi_i\right]\right]}{\mathbb{V}ar_{\xi}\left[Q\right] + \frac{1}{N_\eta}\mathbb{E}_{\xi}\left[\sigma_\eta^2\right]} \quad \text{and} \tag{5.5}$$

$$\mathbb{T}_{i,\tilde{Q}_{N_\eta}} = \frac{\mathbb{E}_{\xi_{\sim i}}\left[\mathbb{V}ar_{\xi,\eta}\left[\tilde{Q}_{N_\eta} \mid \xi_{\sim i}\right]\right]}{\mathbb{V}ar\left[\tilde{Q}_{N_\eta}\right]} = \frac{\mathbb{E}_{\xi_{\sim i}}\left[\mathbb{V}ar_{\xi_i}\left[Q \mid \xi_{\sim i}\right]\right] + \frac{1}{N_\eta}\mathbb{E}_{\xi}\left[\sigma_\eta^2\right]}{\mathbb{V}ar_{\xi}\left[Q\right] + \frac{1}{N_\eta}\mathbb{E}_{\xi}\left[\sigma_\eta^2\right]}. \tag{5.6}$$

Ongoing theoretical work suggests that $\mathbb{S}_{i,\tilde{Q}_{N_\eta}}$ will always be less than $\mathbb{S}_i$, therefore *underestimating* the first-order effect of ξ_i on Q, while $\mathbb{T}_{i,\tilde{Q}_{N_\eta}}$ will always be greater than $\mathbb{T}_i$, therefore *overestimating* the total-order effect of ξ_i on Q. In pursuit of unbiased estimators for $\mathbb{S}_i$ and $\mathbb{T}_i$ using $\tilde{Q}_{N_\eta}$, we introduce bias-correction terms to the numerator of Eq. (5.6) and the denominators of both Equations (5.5) and (5.6).

Steps 1) and 2) of the GSA algorithm in Section 5.2.1 remain the same. When evaluating the model for $\boldsymbol{A}$, $\boldsymbol{B}$, and all $\boldsymbol{A}_{\boldsymbol{B}}^{(\boldsymbol{i})}$ in Step 3), variance deconvolution requires tallying the variance $\hat{\sigma}_\eta^2(\boldsymbol{\xi})$ in addition to the model output $\tilde{Q}_{N_\eta}(\boldsymbol{\xi})$. In practice, every independent code evaluation for $\tilde{Q}_{N_\eta}(\boldsymbol{\xi})$ should also be independent in η, that is, each MC RT code evaluation should use a different initial random number seed. Then, in Step 4), Equations (5.3) and (5.4) are replaced with

$$\mathbb{S}_i \approx \hat{\mathbb{S}}_{i,VD} \overset{\text{def}}{=} \frac{\frac{1}{N_\xi}\sum_{v=1}^{N_\xi} \tilde{Q}_{N_\eta}(\boldsymbol{B})_v\left[\tilde{Q}_{N_\eta}(\boldsymbol{A}_{\boldsymbol{B}}^{(\boldsymbol{i})})_v - \tilde{Q}_{N_\eta}(\boldsymbol{A})_v\right]}{\frac{1}{2N_\xi}\sum_{v=1}^{N_\xi}\left[\tilde{Q}_{N_\eta}(\boldsymbol{A})_v - \tilde{Q}_{N_\eta}(\boldsymbol{B})_v\right]^2 - \frac{1}{N_\eta}\left\langle\hat{\sigma}_\eta^2\right\rangle_{(A,B)}}, \tag{5.7}$$

$$\mathbb{T}_i \approx \hat{\mathbb{T}}_{i,VD} \overset{\text{def}}{=} \frac{\frac{1}{2N_\xi}\sum_{v=1}^{N_\xi}\left[\tilde{Q}_{N_\eta}(\boldsymbol{B}_{\boldsymbol{A}}^{(\boldsymbol{i})})_v - \tilde{Q}_{N_\eta}(\boldsymbol{B})_v\right]^2 - \frac{1}{N_\eta}\left\langle\hat{\sigma}_\eta^2\right\rangle_{(B_A^i,B)}}{\frac{1}{2N_\xi}\sum_{v=1}^{N_\xi}\left[\tilde{Q}_{N_\eta}(\boldsymbol{A})_v - \tilde{Q}_{N_\eta}(\boldsymbol{B})_v\right]^2 - \frac{1}{N_\eta}\left\langle\hat{\sigma}_\eta^2\right\rangle_{(A,B)}}, \tag{5.8}$$

where $\left\langle\hat{\sigma}_\eta^2\right\rangle_{(A,B)} = \dfrac{1}{2N_\xi}\displaystyle\sum_{v=1}^{N_\xi}\left[\hat{\sigma}_\eta^2(\boldsymbol{A})_v + \hat{\sigma}_\eta^2(\boldsymbol{B})_v\right]$.

5.3 Numerical Results

In this section, we first provide a description of the multigroup 3D C5G7 benchmark, on which the k-eigenvalue simulations are based. Then, we present and discuss results of the uncertainty and sensitivity analysis for eight uncertain input parameters: the densities and radii of the four types of fuel in the benchmark.

5.3.1 3D C5G7 Benchmark Description

The C5G7-TD benchmark is a series of space-time neutron kinetics exercises in 2- and 3D [45] based on the well-studied 2-D steady-state neutron transport C5G7 benchmark [17]. We performed a k-eigenvalue simulation of the initial condition of 3D geometry described by the C5G7-TD benchmark, i.e., the unrodded case in which the control rod banks are inserted into the upper axial water reflector.

3D C5G7 is a miniature LWR with sixteen fuel assemblies: eight uranium oxide (UO_2) assemblies and eight mixed oxide (MOX) assemblies, surrounded by a water reflector. There are three different enrichments of MOX fuel: 4.3%, 7.0%, and 8.7%. The quarter-core is radially symmetric in the 2-D plane, and it is assumed that control rods can move continuously across the top water reflector into the active core region. Both the UO2 and MOX assemblies follow a 17 x 17 configuration, consisting of 264 fuel pins, 24 guide tubes for control rods, and one instrument tube for a fission chamber in the center grid cell. The quarter-core with assemblies labeled 1-4 and the fuel-pin configuration are shown in Figure 5.1.

The C5G7 benchmark problems were originally developed to test the capabilities of radiation transport codes that do not utilize spatial homogenization above the fuel pin level. Therefore, the available 7-group macroscopic cross-section data from the original benchmark [17] as well as the kinetics parameters from [45] are spatially homogenized to the fuel pin level. Using all nominal parameter values, the eigenvalue of the unrodded configuration of the 3D C5G7 core was calculated to be $k_{\text{eff}} = 1.16562 \pm 0.02\%$ using MC/DC with a total of 50×10^6 particle histories. Other MC codes [39] found $k_{\text{eff}} = 1.165449 \pm 0.0029\%$ (RMC, 2021) and $k_{\text{eff}} = 1.16532 \pm 0.0034\%$ (OpenMC, 2018).

First, for uncertainty analysis, we consider the parametric variance of k_{eff} and of the

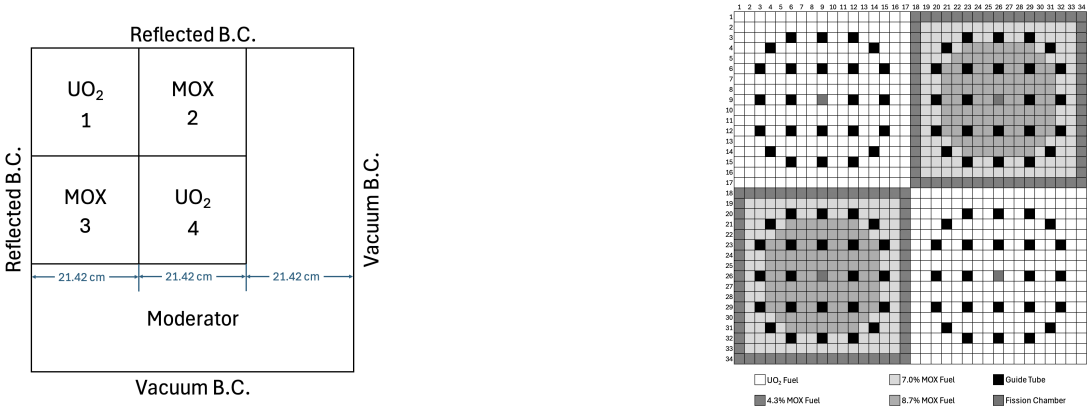

(a) Quarter-core planar section.

(b) Fuel pin configuration.

Figure 5.1: Geometry of the 3D C5G7 benchmark problem, south-east quadrant, reproduced from [45].

pin-wise fission distribution. Then, for sensitivity analysis, we rank the eight parameters in order of importance to k_{eff}.

5.3.2 Uncertainty analysis

We choose manufacturing uncertainties to follow manufacturing uncertainties of the assembly models described in the OECD/NEA UAM benchmark [50]. For each of the four fuel types in C5G7, the density and diameter of the fuel pin are each normally distributed with a standard deviation of 5%.

To study the efficiency of variance deconvolution for a k-eigenvalue simulation, we compare the parametric variance estimate from the variance deconvolution approach with the total observed variance estimate from a standard UQ approach, in which the solver variance is assumed to have been effectively resolved out. First, to establish the problem's solver variance with nominal values, we compute k_{eff} and its standard error σ_k using 50 inactive cycles, 100 active cycles, and 50K histories per cycle for a total of 5M histories. This case is labeled 'Ref.' in Table 5.1, with the total observed standard error of k_{eff} resulting entirely from the solver stochasticity. Then, in Case A, we minimize the solver noise by repeating the reference case 100 times for a total of 500M histories, reducing

$\sigma_{k,\text{MCRT}}/k_{\text{eff}}$ from 0.054% to 0.007%. Next, for the standard UQ approach in Case B, we vary all 8 parameters and perform the simulation 100 times with 50 inactive cycles, 100 active cycles, and 50K histories/cycle for a total of 500M histories. Comparing Cases

Case	**Description**	$\boldsymbol{k}_{\text{eff}}$	$\boldsymbol{\sigma_{k,\text{total}}}$	$\boldsymbol{\sigma_{k,\text{param}}}$	$\boldsymbol{\sigma_{k,\text{MCRT}}}$
Ref.	Nominal parameter values. 5M total histories.	1.16568	0.00064	N/A	0.00064
A	Nominal parameter values. 500M total histories.	1.16562	0.00008	N/A	0.00008
B	Standard UQ. $N_\xi = 100$, 500M total histories.	1.15817	**0.00209**	N/A	N/A
C	Variance deconvolution. $N_\xi = 100$, 10M total histories.	1.15799	0.00214	**0.00208**	0.00048

Table 5.1: Resulting k_{eff} from varying parameters in 3D C5G7 problem. $\sigma_{k,\text{total}}$, $\sigma_{k,\text{param}}$, and $\sigma_{k,\text{MCRT}}$ represent the 1-sigma standard deviation of k_{eff} due to the overall simulation uncertainty, the parameter uncertainty, and the MC RT solver noise, respectively.

A and B, we see that $\sigma_{k,\text{total}}$ in Case A is small compared to that of Case B and we can conclude that almost all the uncertainty in Case B is due to the uncertain parameters. To confirm this, we continue to increase the resolution of the MC RT simulation to observe that $\sigma_{k,\text{total}}$ does not diminish any further. Next, for the variance deconvolution approach in Case C, we reduce to 1K histories/cycle for a total of 10M histories, a 50X reduction in computational cost from Case B. Comparing Cases B and C, we see that variance deconvolution and standard UQ estimate a $\sigma_{k,\text{param}}$ within 0.5% of one another; variance deconvolution does so using 50X fewer histories/cycle, which is directly proportional to a reduction in execution time. In Case C with 10M histories, the standard UQ approach would estimate the parametric σ_k as $\sigma_{k,\text{total}}$, 0.00214.

As an additional QoI, we consider the fission rate distribution calculated in Cases B and C. In Figure 5.2, we compare the variances estimated using the standard approach (Fig. 5.2a) and the variance deconvolution approach (Figs. 5.2b- 5.3b). As in the variance estimates for k_{eff}, the total variance with a standard UQ approach and the parametric variance with the variance deconvolution approach are in agreement. We see that the

parametric variance is peaked in the top left corner of Assembly 1, i.e., at the center of the full-core where it is most active. Using a standard UQ approach with 10M histories, the total variance in Figure 5.3b would be the best available variance estimate. Although the total variance is also the largest in Assembly 1, we can see that it is much less resolved than the sharper relative peaks in Figure 5.2. Comparing Figures 5.3a and 5.3b, we can see the influence that the shape of the solver variance influences the shape of the total variance, and increasing the particle count in Case B provides a clearer image of the impact of the uncertain parameters. Using variance deconvolution, we achieve a comparable resolution for 50X fewer particle histories.

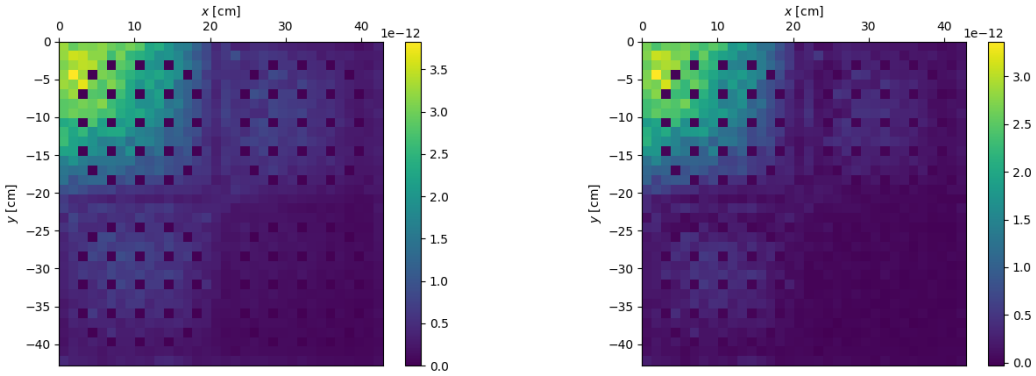

(a) Total variance estimate from Case B, standard UQ, 500M histories.

(b) Parametric variance estimate from Case C, variance deconvolution, 10M histories.

Figure 5.2: Variance estimates using the standard approach (a) and variance deconvolution approach (b). Fuel pin density and diameter each sampled from normal distribution with 5% standard deviation.

5.3.3 Sensitivity analysis

Additionally, we compute the first- and total-order sensitivity indices of the 8 parameters with respect to k_{eff}, comparing the standard and variance deconvolution approaches using Case C. We report all computed indices and rank the parameters in Table 5.2. As seen in the data in Table 5.2, $1 - \sum_{i=1}^{k} \mathbb{S}_i = 0.004$, suggesting that the parametric variance is

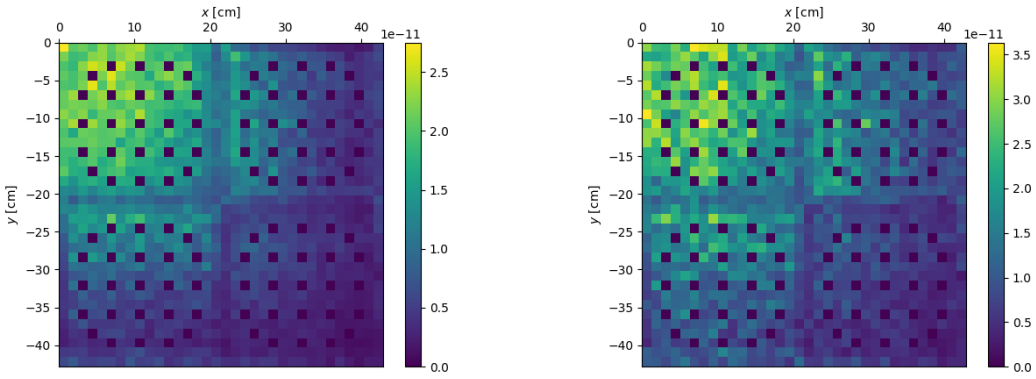

(a) Solver variance estimate from Case C, variance deconvolution, 10M histories.

(b) Total variance estimate from Case C, variance deconvolution, 10M histories.

Figure 5.3: Solver (a) and total (b) variance estimates using the variance deconvolution approach. Fuel pin density and diameter each sampled from normal distribution with 5% standard deviation.

almost entirely comprised of first-order effects. However, $\mathbb{T}_i - \mathbb{S}_i$ ranges between 0.011 and 0.053, suggesting a larger interaction effect than is indicated by the first-order effects alone. We hypothesize that this discrepancy could be due to correlation effects between k_{eff} cycles in a single simulation and that an effective N_η may need to be used rather than taking N_η to be the number of active cycles $\times$ the number of particle histories per cycle. For example, if the solver variance reported by the code were slightly underestimated, it would align with what ongoing theory work suggests that $\mathbb{S}_i$ from variance deconvolution would still be a slight underestimate and $\mathbb{T}_i$ from variance deconvolution would still be a slight overestimate, therefore creating a larger difference between $\mathbb{T}_i$ and $\mathbb{S}_i$. Working through details of this in an orderly way is a topic of ongoing and future work.

In general, we can conclude that the pin radii have a greater impact than the pin densities, which is consistent with the findings of parameter studies that also varied both the fuel radius and the density [5]. Criticality conditions are very sensitive to geometry changes that would necessarily result from changing the radii of the fuel pin. Additionally, unlike the densities, the radii affect the amount of moderator in the problem: the larger the fuel pins, the less space is available around them for the moderator. The radius of the

UO_2 pin is the most important by far; we look to the remaining parameters to highlight the importance of computing the full set of first- *and* total-order indices. One could reasonably set an importance threshold below which parameters are discarded as unimportant, e.g., 0.05 or 0.10. Looking just at the first-order indices, this would qualify most, if not all, of the remaining parameters as unimportant. However, the total-order indices reveal the additional importance contribution of interaction effects. For example, the MOX8. 7% radius nearly doubles from $\mathbb{S}_i = 0.0524$ to $\mathbb{T}_i = 0.1028$. In the same vein, comparing the parametric indices $\mathbb{S}_i$ and $\mathbb{T}_i$ to their total-observed counterparts $\mathbb{S}_{i,\tilde{Q}_{N_\eta}}$ and $\mathbb{T}_{i,\tilde{Q}_{N_\eta}}$, we see that the standard approach could result in misleading conclusions about the importance of a parameter. Although both approaches rank the parameters in the same order, the standard approach *underestimates* $\mathbb{S}_i$ and *overestimates* $\mathbb{T}_i$. For example, all four densities appear more important from $\mathbb{T}_{i,\tilde{Q}_{N_\eta}}$ than they are revealed to be from $\mathbb{T}_i$. This is consistent with the findings discussed in Section 5.2.2.

Parameter	$\mathbb{S}_i$	$\mathbb{T}_i$	$\mathbb{S}_{i,\tilde{Q}_{N_\eta}}$	$\mathbb{T}_{i,\tilde{Q}_{N_\eta}}$
1. UO_2 radius	0.7936	0.8043	0.7497	0.8151
2. MOX7.0% radius	0.0680	0.1178	0.0642	0.1666
3. MOX8.7% radius	0.0524	0.1028	0.0495	0.1524
4. MOX4.5% radius	0.0334	0.0851	0.0316	0.1357
5. UO_2 density	0.0176	0.0699	0.0166	0.1213
6. MOX4.5% density	0.0119	0.0647	0.0112	0.1164
7. MOX7.0% density	0.0106	0.0633	0.0100	0.1151
8. MOX8.7% density	0.0085	0.0614	0.0080	0.1133
Sum over all parameters	0.9960	1.3693	0.9409	1.7359

Table 5.2: First- and total-order sensitivity indices of k_{eff} given fuel pin density and diameter each sampled from normal distribution with 5% standard deviation. UO_2 radius is most important to k_{eff} both on its own and with interaction effects.

5.4 Conclusions

Sampling methods for UQ and GSA are useful because they do not make assumptions about the underlying model; their primary drawback is the potentially-high computational cost of the multiple code evaluations they require. When sampling methods are coupled with

stochastic simulators such as Monte Carlo radiation transport codes, a standard approach to estimate parametric statistics (i.e., statistics due only to parameter uncertainty) is to increase the number of particle histories such that the solver variance is a relatively small part of the total observed variance, exacerbating sampling methods' primary drawback. As an alternative to attempting to minimize solver variance, we have recently proposed variance deconvolution, in which parametric variance is computed by explicitly quantifying and removing the solver variance from the total observed variance. In previous work, we showed that variance deconvolution is accurate and far more cost-effective than the standard approach for computing parametric variance [16] and integrated variance deconvolution into sampling estimators for sensitivity indices [15].

In this study, variance deconvolution was coupled with Monte Carlo radiation transport to perform uncertainty quantification and global sensitivity analysis on the 3D C5G7-TD benchmark in its initial unrodded configuration. The C5G7 core was modeled using Monte Carlo Dynamic Code (MC/DC), a neutral-particle transport code from the PSAAP-III Center for Exascale Monte Carlo Neutron Transport [72]. The manufacturing uncertainties of the radius and density of the fuel pin were sampled from a normal distribution with 5% standard deviation, based on the manufacturing uncertainties from the OECD / NEA benchmarks for Uncertainty Analysis in Modeling of LWRs. The core k_{eff} eigenvalue and pinwise core fission rate distribution were considered as quantities of interest. Using 50 inactive cycles, 100 active cycles, and 100 samples of the uncertain parameters, $\sigma_{k,\text{param}}/k_{\text{eff}}$ was estimated to be 0.18% using the standard approach with 50K histories per cycle and using the variance deconvolution approach with 1K histories per cycle, a 50X reduction in computational cost. Though the exact savings in computation time will vary from code-to-code, reducing particle count consistently reduces code execution time. Both the standard approach and variance deconvolution approach found the fuel-pin radii to be more important than their densities, consistent with findings from similar studies. Indices computed with the standard approach were observed to underestimate first-order and overestimate total-order indices, which is in alignment with what ongoing theory work suggests. Ongoing and future work include presenting the details and theoretical explanation of this behavior and investigating use of effective particle numbers in sensitivity coefficient calculations. Future work also includes extending these methods to correlated input parameters, as

existing variance deconvolution analysis has been based on the assumption that parameters are independently distributed. This extension would allow for application to jointly-distributed parameters such as nuclear data uncertainty, which is highly relevant to the field.

Acknowledgements

This article has been authored by an employee of National Technology & Engineering Solutions of Sandia, LLC under Contract No. DE-NA0003525 with the U.S. Department of Energy (DOE). The employee owns all right, title and interest in and to the article and is solely responsible for its contents. The United States Government retains and the publisher, by accepting the article for publication, acknowledges that the United States Government retains a non-exclusive, paid-up, irrevocable, world-wide license to publish or reproduce the published form of this article or allow others to do so, for United States Government purposes. The DOE will provide public access to these results of federally sponsored research in accordance with the DOE Public Access Plan https://www.energy.gov/downloads/doe-public-access-plan. This work was funded by the Center for Exascale Monte Carlo Neutron Transport (CEMeNT) a PSAAP-III project funded by the Department of Energy, grant number: DE-NA003967.

Chapter 6: Conclusions

The purpose of this research was to analyze the effect of stochastic solvers on UQ and GSA and to develop accurate and efficient estimators for key UQ and GSA statistics. The majority of the large body of work on UQ and GSA methods inherently assumes that the underlying computational model is deterministic; when the underlying computational model is instead stochastic, the statistics computed with UQ and GSA will include the effect of both the input variability and the stochastic solver variability. A standard approach to treating solver uncertainty when using a stochastic computational model with existing UQ and GSA methods is to increase the resolution of the stochastic solver such that the total observed output statistics converge to the parametric statistics. A number of studies have suggested that because of the high computational cost of the standard approach, it would be useful to explicitly compute how much the solver RT variance contributes to the total observed variance when the problem contains uncertain parameters [27, 94, 41, 85, 89]. Over the past decade or so, some approaches to handle the impact of solver stochasticity have suggested fixing the solver's random seed and explicitly treating the covariances of the now-correlated inputs [21, 55]. Specifically for sensitivity indices, many of the proposed methods mitigate the expense of resolving the stochastic solver by instead emulating the stochastic solver with a surrogate model, then calculating Sobol' indices using the constructed surrogate at a reduced computational cost [116].

The objectives of this dissertation research were to asses the effect of stochastic computational models on UQ and GSA theory; to develop accurate, efficient, and broadly applicable estimators for sampling-based UQ and GSA; to analyze the statistical properties of the developed estimators; and to demonstrate the estimator's use on a Monte Carlo radiation transport problem with real-world applicability. The first novel contribution of this dissertation was the development and statistical analysis of a variance deconvolution estimator for UQ, in which the solver variance is explicitly computed during the repeated evaluations of the computational model and is removed from the total observed variance. The variance deconvolution analysis was then extended to sensitivity indices for GSA,

and a novel approach for computing indices was developed by incorporating the variance deconvolution estimator into existing sampling-based estimators for the Saltelli approach. This work is presented in a series of four manuscripts that have been published in or submitted to academic journals and conferences.

In Chapter 2, the law of total variance was applied to present in closed-form how the parametric variance and stochastic solver variance contribute to the total observed variance. The primary outcome was the development of a variance deconvolution estimator to accurately and precisely estimate the parametric variance. Rather than the standard method of over-resolving the stochastic solver variance for each UQ evaluation of the computational model, variance deconvolution explicitly computes the stochastic solver variance and removes it from the total observed variance. We showed both in theory and numerically, with an example neutral-particle radiation transport problem, that the variance deconvolution estimator is unbiased and more efficient than the standard approach for the same computational cost. Statistical analysis of the estimator and numerical results suggest an efficiency trade-off between the number of UQ samples and number of stochastic model samples (e.g., particle histories) for a prescribed computational budget. We used the analytic solution of the example radiation transport problem to find the cost-optimal distribution between UQ samples and stochastic model samples, and ongoing work focuses on constructing a pilot study to numerically estimate the cost-optimal distribution without an analytic solution, for application to more complex and realistic problems. While the presented test problem applied variance deconvolution to Monte Carlo radiation transport methods, the statistical analysis and theoretical conclusions of the variance deconvolution estimator are applicable to sampling-based UQ coupled with any stochastic computational model.

In Chapter 3, the variance deconvolution approach developed in Chapter 2 was incorporated into one estimator for first-order sensitivity index and one estimator for total-order sensitivity index. These variance deconvolution indices were applied to a 1D slab radiation transport problem and compared to a standard approach using the existing SI estimators without variance deconvolution. That work served as a precursor to Chapter 4, in which the theoretical variance deconvolution analysis in Chapter 2 was extended to ANOVA-based sensitivity indices and a full suite of first- and total-order SIs. We show in closed-form that

in general, using a stochastic solver will always under-estimate the parametric first-order SIs and over-estimate the parametric total-order SIs. Though the total observed first- and total-order SIs will still correctly rank the input parameters, the respective under- and over-estimates of the parametric indices could cause an analyst to draw incorrect conclusions about the importance of specific parameters. The accuracy of one first- and one total-order estimator were examined analytically with asymptotic limit analysis. We found that though the variance-deconvolution version of existing SI estimators has a higher variance than its standard-approach counterpart, the variance deconvolution version is consistently more accurate than the standard version. We corroborated these theoretical findings with two numerical test problems: the Ishigami function and a 1-D neutral-particle multi-group radiation transport problem with fission physics.

In Chapter 5, the developed variance deconvolution UQ and GSA methods were coupled with Monte Carlo radiation transport to perform uncertainty quantification and global sensitivity analysis on the 3-D C5G7-TD benchmark in its initial unrodded configuration. The C5G7 core was modeled using Monte Carlo Dynamic Code (MC/DC), a neutral-particle transport code from the PSAAP-III Center for Exascale Monte Carlo Neutron Transport. Manufacturing uncertainties of fuel pin radius and density were sampled from a normal distribution of a 5% standard deviation about their respective nominal values, based on similar manufacturing uncertainties in the OECD/NEA benchmarks for Uncertainty Analysis in Modeling of LWRs. Both the core k_{eff} eigenvalue and pinwise core fission rate distribution were considered as quantities of interest. The standard and variance deconvolution UQ approaches were compared. Using 50 inactive cycles, 100 active cycles, and 100 samples of the uncertain parameters, $\sigma_{k,\text{param}}/k_{\text{eff}}$ was estimated to be 0.18% using 50K histories per cycle for the standard approach and 1K histories per cycle using the variance deconvolution approach, a 50X reduction in computational cost. Though the savings in computation time will vary from code-to-code, code execution time is consistently positively correlated with particle history count. Additionally, variance deconvolution was integrated with existing GSA methods to compute Sobol' sensitivity indices for the density and radii of each of the four fuel types in the core. The ability to vary the densities and radii of the specific pin components such as pellet radius, gap thickness, and clad thickness were limited due to the spatial homogenization of the 7-group

cross sections provided by the benchmark. Nevertheless, the performed sensitivity analysis found that the radii of the fuel pins was largely more influential than their densities, with the radius of UO_2 by far the most important parameter to k_{eff}.

6.1 Future work

There are multiple possible directions for future work with variance deconvolution for UQ and GSA: optimizing the division of computational cost between the number of parameter samples and stochastic solver samples, extending the variance deconvolution for use with correlated input parameters, and continuing to implement the method for large-scale Monte Carlo radiation transport problems.

In Chapter 2, the optimal cost analysis performed for UQ defines the computational cost as the product of the number of parameter samples and the number of stochastic solver samples per realization. Further analysis should go beyond this linear cost definition to consider other contributors to computation time, such as the re-start cost of the stochastic computational model. Additionally, the statistics of the quantity of interest required to find the optimal cost suggested in Chapter 2 are complex, up to the fourth moment of the quantity of interest. Future work could include sensitivity analysis of the estimator itself to the higher-order moments of the quantity of interest in order to simplify the number and complexity of required statistics for optimal-cost analysis. Ideally, an algorithm could be developed for both UQ and GSA that would use a pilot study to compute the statistics necessary for optimal-cost analysis and ascertain the correct balance of parameter samples and stochastic solver samples, akin to a multi-fidelity Monte Carlo study that uses the lower-fidelity simulation to find the proper configuration for the higher-fidelity simulation.

All of the theoretical analysis thus far has assumed that the uncertain input parameters are independently distributed. Much of the uncertainty and sensitivity analysis studies that are performed for nuclear reactor and transport simulations consider nuclear data as the source of input uncertainty. Nuclear data are often jointly distributed and their uncertainties therefore include covariances. Future work could include extending variance deconvolution to the case in which some or all of the input parameters are not independent of one another. This would require a new estimator formulation and additional theoretical

analysis.

In Chapter 5, the 3D-C5G7 nuclear reactor benchmark is used as the stochastic computational model and the core k-eigenvalue is considered as a quantity of interest. We hypothesized that sensitivity indices, with and without variance deconvolution, may be inaccurate due to the effect of correlation between k-eigenvalue cycles. It would be interesting to continue to explore this space by looking for the same effect in other cases where correlation might arise, like in a time-dependent problem where the solution at a given time depends on the solutions at the previous times. Additionally, future work could investigate whether it would be necessary or useful to substitute the actual number of stochastic solver samples used with an effective number of stochastic solver that takes into account the correlated cycles.

Bibliography

[1] G. Archer, A. Saltelli, and I. Sobol'. Sensitivity measure, anova-like techniques and the use of bootstrap. *Journal of Statistical Computation and Simulation*, 58:99–120, 1997.

[2] S. Azzi, B. Sudret, and J. Wiart. Sensitivity analysis for stochastic simulators using differential entropy. *International Journal for Uncertainty Quantification*, 2020.

[3] I. Azzini, T. Mara, and R. Rosati. Monte carlo estimators of first- and total-orders sobol' indices, 2020. This is on arXiv and the pdf says it's an Elsevier preprint. However, I can't find a published version.

[4] I. Azzini, T.A. Mara, and R. Rosati. Comparison of two sets of monte carlo estimators of sobol' indices. *Environmental Modelling and Software*, 144:105167, 2021.

[5] Forrest Brown, Jeremy Sweezy, and Robert Hayes. Monte carlo parameter studies and uncertainty analysis with MCNP5. In *Proceedings of PHYSOR 2004*, Chicago, Illinois, USA, 2004. PHYSOR.

[6] T. Browne, L. Le Gratiet, J. Lonchampt, and E. Remy. Stochastic simulators based optimization by gaussian process metamodels – application to maintenance investments planning issues. *International Journal of Quality and Reliability Engineering*, 32(6):2067–2080, 2016.

[7] O. Buss, A. Hoefer, J. C. Neuber, and M. Schmid. Hierarchical Monte-Carlo approach to bias estimation for criticality safety calculations. *Proceedings of PHYSOR 2010-Advances in Reactor Physics to Power the Nuclear Renaissance*, 2010.

[8] D. Cacuci and M. Ionescu-Bujor. A comparative review of sensitivity and uncertainty analysis of large-scale systems-ii: Statistical methods. *Nuclear Science and Engineering*, 147(3):204–217, 2004.

[9] Eungchun Cho and Moon Jung Cho. Variance of sample variance. *Proceedings of the Survey Research Methods Section*, pages 1291–1293, 2008.

[10] Eungchun Cho and Moon Jung Cho. Variance of sample variance. *Proceedings of the Survey Research Methods Section*, pages 1291–1293, 2008.

[11] K. Clements, G. Geraci, and A. Olson. A variance deconvolution approach to sampling uncertainty quantification for Monte Carlo radiation transport solvers. In *Computer Science Research Institute Summer Proceedings 2021*, pages 293–307, 2021. Technical Report SAND2022-0653R, https://www.sandia.gov/ccr/csri-summer-programs/2021-proceedings/.

[12] K Clements, G. Geraci, and A. J. Olson. A variance deconvolution approach to sampling uncertainty quantification for monte carlo radiation transport solvers. In *Computer Science Research Institute Summer Proceedings 2021*, number Technical Report SAND2022-0653R, pages 293–307, 2021. https://cs.sandia.gov/summerproceedings/CCR2021.html.

[13] K. B. Clements, G. Geraci, and A. J. Olson. Numerical investigation on the performance of a variance deconvolution estimator. *Trans. Am. Nucl. Soc.*, 126:344–347, 2022.

[14] Kayla Clements, Gianluca Geraci, and Aaron J Olson. Numerical investigation on the performance of a variance deconvolution estimator. *Transactions of the American Nuclear Society*, 126(1):344–347, 2022.

[15] Kayla Clements, Gianluca Geraci, Aaron J Olson, and Todd S Palmer. Global sensitivity analysis in monte carlo radiation transport. In *Proceedings of the M&C 2023*, Niagara Falls, Canada, 2023. American Nuclear Society.

[16] K.B. Clements, G. Geraci, A.J. Olson, and T.S. Palmer. A variance deconvolution estimator for efficient uncertainty quantification in monte carlo radiation transport applications. *Journal of Quantitative Spectroscopy and Radiative Transfer*, 319, 2024.

[17] Nuclear Science Committee. Benchmark on deterministic transport calculations without spatial homogenization. Technical report, Organization for Economic Cooperation and Development Nuclear Energy Agency (OECD/NEA), 2005.

[18] National Research Council. *Assessing the Reliability of Complex Models: Mathematical and Statistical Foundations of Verification, Validation, and Uncertainty Quantification*. The National Academies Press, Washington, DC, 2012.

[19] T. Crestaux, O. L. Maitre, and J-M. Martinez. Polynomial chaos expansion for sensitivity analysis. *Reliability Engineering & System Safety*, 94(7):1161–1172, 2009.

[20] J. Crussell, T.M. Kroeger, A. Brown, and C. Phillips. Virtually the same: Comparing physical and virtual testbeds. In *2019 International Conference on Computing, Networking and Communications (ICNC)*. IEEE, 2019.

[21] S. Da Veiga, F. Wahl, and F. Gamboa. Local polynomial estimation for sensitivity analysis on models with correlated inputs. *Technometrics*, 51:452–463, 2009.

[22] Erin Davis and Anil Prinja. The stochastic collocation method for radiation transport in random media. *Journal of Quantitative Spectroscopy and Radiative Transfer*, 112, 2011.

[23] Andrew W Decker. Verification and validation report for the radiation protection factor methodology using Monte-Carlo N-Particle Code, version 6. Technical report, Research and Development Directorate, Nuclear Science and Engineering Research Center, 2018.

[24] Kevin Dowding. Overview of asme v&v 20-2009 standard for verification and validation in computational fluid mechanics and heat transfer. Technical report, V&V, UQ, and Credibility Processes Department, Sandia National Laboratories, 2016.

[25] James J. Duderstadt and Louis J. Hamilton. *Nuclear Reactor Analysis*. John Wiley & Sons, 1976.

[26] M. essee and D. Dehart. Generalized perturbation theory capability within the scale code package. In *Proceedings of M&C 2009*, Saratoga Springs, New York, USA, 2009. American Nuclear Society.

[27] A Fierro, E. Barnat, M. Hopkins, et al. Challenges and opportunities in verification and validation of low temperature plasma simulations and experiments. *The European Physical Journal D*, 75, 2021.

[28] G. Geraci, K. Clements, and A. J. Olson. A polynomial chaos approach for uncertainty quantification of monte carlo transport codes. In *Proceedings of ANS M&C*, August 2023.

[29] G. Geraci, K. Clements, and A.J. Olson. A polynomial chaos approach for uncertainty quantification of monte carlo transport codes. In *Proceedings of the American Nuclear Society M&C 2023*, 2023.

[30] G. Geraci, P.M. Congedo, R. Abgrall, and G. Iaccarino. High-order statistics in global sensitivity analysis: Decomposition and model reduction. *Computer Methods in Applied Mechanics and Engineering*, 301:80–115, 2016.

[31] G. Geraci and A. J. Olson. Impact of sampling strategies in the polynomial chaos surrogate construction for monte carlo transport applications. In *Proceedings of ANS M&C*, pages 76–86, October 2021.

[32] G. Geraci, L.P. Swiler, and B.J. Debusschere. Multifidelity uq sampling for stochastic simulations. *16th U.S. National Congress on Computational Mechanics*, 2021.

[33] Gianluca Geraci and Aaron Olson. Impact of sampling strategies in the polynomial chaos surrogate construction for monte carlo transport applications. *Proceedings of the International Conference on Mathematics and Computational Methods Applied to Nuclear Science and Engineering*, pages 76–86, 2021.

[34] Roger Ghanem, David Higdon, and Houman Owhadi. *Handbook of Uncertainty Quantification*. Springer International Publishing, Switzerland, 2017.

[35] Michael B Giles. Multilevel Monte Carlo path simulation. *Operations Research*, 56(3):607–617, 2008.

[36] G. Glen and K. Isaacs. Estimating sobol' sensitivity indices using correlations. *Environmental Modelling and Software*, 37:157–166, 2012.

[37] A. Gorodetsky, G. Geraci, M.S. Eldred, and J.D. Jakeman. A generalized approximate control variate framework for multifidelity uncertainty quantification. *Journal of Computational Physics*, 408, 2020.

[38] Loic Le Gratiet and Josselin Garnier. Recursive co-kriging model for design of experiments with multiple levels of fidelity. *International Journal for Uncertainty Quantification*, 4(5):365–386, 2014.

[39] X. Guo et al. Kinetic methods in monte carlo code rmc and its implementation to c5g7-td benchmark. *Annals of Nuclear Energy*, 2021.

[40] J.L. Hart, A. Alexanderian, and P.A. Gremaud. Efficient computation of sobol' indices for stochastic models. *SIAM Journal on Scientific Computing*, 39(4):A1514–A1530, 2017.

[41] Shintaro Hashimoto and Tatsuhiko Sato. Estimation method of systemic uncertainties in Monte Carlo particle transport simulation based on analysis of variance. *Journal of Nuclear Science and Technology*, 56, 2019.

[42] J.C. Helton. Uncertainty and sensitivity analysis for models of complex systems. In Frank Graziani, editor, *Computational Methods in Transport: Verification and Validation*, pages 207–228. Springer, Berlin, 2008.

[43] T. Homma and A. Saltelli. Importance measures in global sensitivity analysis of model output. *Reliability Engineering System Safety*, 52(1):1–17, 1996.

[44] S. Hora and R. Iman. A comparison of maximum/bounding and bayesian/monte carlo for fault tree uncertianty analysis (no. sand85-2839). Technical report, Sandia National Laboratories, 1986.

[45] Jason Hou, Kostadin Ivanov, Victor Boyarinov, and Peter Fomichenko. Oecd/nea benchmark for time-dependent neutron transport calculations without spatial homogenization. *Nuclear Engineering and Design*, 317:177–189, 2017.

[46] R. Iman and S. Hora. A robust measure of uncertainty importance for use in fault tree system analysis. *Risk Analysis*, 10(3):401–403, 1990.

[47] M. Ionescu-Bujor and D. Cacuci. A comparative review of sensitivity and uncertainty analysis of large-scale systems-i: Deterministic methods. *Nuclear Science and Engineering*, 147(3):189–203, 2004.

[48] B. Iooss and M. Ribatet. Global sensitivity analysis of computer models with functional inputs. *Reliability engineering and system safety*, 94:1194–1204, 2009.

[49] T. Ishigami and T. Homma. An importance quantification technique in uncertainty analysis for computer models. In *Proceedings of the ISUMA'90, First International Symposium on Uncertainty Modelling and Analysis*, University of Maryland, 1990.

[50] K. Ivanov, M. Avramova, and S. Kamerow. Benchmarks for uncertainty analysis in modeling (uam) for the design, operation and safety analysis of lwrs. Technical Report NEA/NSC/DOC(2013)7, OECD Nuclear Energy Agency, 2013.

[51] A. Janon, T. Klein, A. Lagnoux, M. Nodet, and C. Prieur. Asymptotic normality and efficiency of two sobol' index estimators. *ESAIM: Probability and Statistics*, 18(3):342–364, 2014.

[52] M. Jansen. Analysis of variance designs for model output. *Computer Physics Communications*, 117(1-2):35–43, 1999.

[53] M. Jimenez, O.P. Le Maitre, and O.M. Knio. Nonintrusive polynomial chaos expansions for sensitivity analysis in stochastic differential equations. *SIAM Journal on Uncertainty Quantification*, 5(1), 2017.

[54] A.J. Koning and D. Rochman. Towards sustainable nuclear energy: Putting nuclear physics to work. *Annals of Nuclear Energy*, 2008.

[55] A.J. Koning and D. Rochman. Modern nuclear data evaluation with the talys code system. *Nuclear Data Sheets*, 113(12):2841–2934, 2012.

[56] K. Kontolati, D. Loukrezis, D.G. Giovanis, L. Vandanapu, and M.D. Shields. A survey of unsupervised learning methods for high-dimensional uncertainty quantification in black-box-type problems. *Journal of Computational Physics*, 464, 2022.

[57] S. Kucherenko, D. Albrecht, and A. Saltelli. Exploring multi-dimensional spaces: a comparison of latin hypercube and quasi Monte Carlo sampling techniques. *arXiv - University of Cornall (USA)*, 2015.

[58] Joel Aaron Kulesza, Terry R. Adams, Jerawan Chudoung Armstrong, Simon R. Bolding, Forrest Brooks Brown, et al. MCNP code version 6.3.0 theory & user manual. Technical Report LA-UR-22-30006, Rev. 1, Los Alamos National Laboratory, 2022.

[59] R. Larsen and M.L. Marx. *An Introduction to Mathematical Statistics and Its Applications*. Pearson Education, Boston: Prentice Hall, 5 edition, 2012.

[60] Richard Larsen and Morris L. Marx. *An Introduction to Mathematical Statistics and Its Applications*. Pearson Education, Boston: Prentice Hall, 5 edition, 2012.

[61] A.M. Lattanzi and S. Subramaniam. *Modeling Approaches and Computational Methods for Particle-Laden Turbulent Flows*, chapter 10 - Stochastic models. Academic Press, 2023.

[62] E.E. Lewis and W.F. Miller. *Computational Methods of Neutron Transport*. American Nuclear Society, La Grange, Illinois, 1993.

[63] L. Lilburne and S. Tarantola. Sensitivity analysis of spatial models. *International Journal of Geographic Informational Systems*, 2009.

[64] Los Alamos National Laboratory. *MCNP - A General Monte Carlo N-Particle Transport Code, Version 5*, 2008.

[65] I. Lux and L. Koblinger. *Monte Carlo Particle Transport Methods: Neutron and Photon Calculations*. CRC Press, 1991.

[66] Olivier Le Maitre and Omar Knio. *Spectral methods for uncertainty quantification: With applications to computational fluid dynamics*. Springer Netherlands, 2010.

[67] T.A. Mara and O.R. Joseph. Comparison of some efficient methods to evaluate the main effect of compute model factors. *Journal of Statistical and Computational Simulations*, 2008.

[68] A. Marrel, B. Iooss, S. Da Veiga, and M. Ribatet. Global sensitivity analysis of stochastic computer models with joint metamodels. *Statist Comput*, 22:833–847, 2012.

[69] M.D. McKay. Evaluating prediction uncertainty (no. nureg/cr-6311). Technical report, Nuclear Regulatory Commission, 1995.

[70] M.D. McKay, R.J. Beckman, and W.J. Conover. Comparison of three methods for selecting values of input variables in the analysis of output from a computer code. *Technometrics*, 21(2):239–245, 1979.

[71] H. Monod, C. Naud, and D. Makowski. *Uncertainty and Sensitivity Analysis for Crop Models*, pages 35–100. Elsevier Science, 1 edition, 2006. eBook ISBN: 9780080461939.

[72] Joanna Piper Morgan, Ilham Variansyah, Samuel L. Pasmann, Kayla B. Clements, Braxton Cuneo, Alexander Mote, Charles Goodman, Caleb Shaw, Jordan Northrop, Rohan Pankaj, Ethan Lame, Benjamin Whewell, Ryan G. McClarren, Todd S. Palmer, Lizhong Chen, Dmitriy Y. Anistratov, C. T. Kelley, Camille J. Palmer, and Kyle E. Niemeyer. Monte Carlo / Dynamic Code (MC/DC): An accelerated Python package for fully transient neutron transport and rapid methods development. *Journal of Open Source Software*, 9:6415, 2024.

[73] W.L. Oberkampf and C.J. Roy. *Verification and Validation in Scientific Computing*. Cambridge University Press, Cambridge, 2010.

[74] A. J. Olson. Calculation of parametric variance using variance deconvolution. In *Transactions of the American Nuclear Society*, volume 120, 2019.

[75] A. J. Olson, K. Clements, and James Petticrew. A sampling-based approach to solve sobol' indices using variance deconvolution for arbitrary uncertainty distributions. *Trans. Am. Nucl. Soc.*, 127:450–453, 2022.

[76] A. J. Olson, A. K. Prinja, and B. C. Franke. Error convergence characterization for stochastic transport methods. In *Transactions of the American Nuclear Society*, volume 116, 2017.

[77] Aaron J. Olson, Kayla B. Clements, and James M. Petticrew. A sampling-based approach to solve Sobol' indices using variance deconvolution for arbitrary uncertainty distributions. *Transactions of the American Nuclear Society*, 127:450–453, 2022.

[78] A.B. Owen. Better estimation of small sobol' sensitivity indices. *ACM Transactions on modeling and computer simulation (TOMACS)*, 2013.

[79] Art B. Owen. Monte carlo theory, methods and examples, 2013.

[80] Art B. Owen, Josef Dick, and Su Chen. Higher order Sobol' indices. *Information and Inference: A Journal of the IMA*, 3(1):59–81, 03 2014.

[81] Benjamin Peherstorfer, Karen Willcox, and Max Gunzburger. Optimal model management for multifidelity Monte Carlo estimation. *SIAM Journal on Scientific Computing*, 38(5):A3163–A3194, 2016.

[82] P. Perdikaris, M. Raissi, A. Damianou, N. D. Lawrence, and G. E. Karniadakis. Nonlinear information fusion algorithms for data-efficient multi-fidelity modelling. *Proceedings of the Royal Society A: Mathematical, Physical and Engineering Sciences*, 473(2198):20160751, 2017.

[83] S. Lo Piano, F. Ferretti, A. Puy, D. Albrecht, and A. Saltelli. Variance-based sensitivity analysis: The quest for better estimators and designs between explorativity and economy. *Reliability Engineering and System Safety*, 206, 2021.

[84] E. Plischke, E. Borgonovo, and C.L. Smith. Global sensitivity measures from given data. *European Journal of Operational Research*, 2013.

[85] Dean Price, Andrew Maile, Joshua Peterson-Droogh, and Derreck Blight. A methodology for uncertainty quantification and sensitivity analysis for responses subject to Monte Carlo uncertainty with application to fuel plate characteristics in the ATRC. *Nuclear Engineering and Technology*, 54, 2022.

[86] A. Puy, W. Becker, S. Lo Piano, and A. Saltelli. A comprehensive comparison of total-order estimators for global sensitivity analysis. *International Journal for Uncertainty Quantification*, 2:1–18, 2022.

[87] A. Puy, S. Lo Piano, A. Saltelli, and S. Levin. Sensobol: An r package to compute variance-based sensitivity indices. *Journal of Statistical Software*, 102, 2022.

[88] G. Kroisandt R. Korn, E. Korn. *Monte Carlo Methods and Models in Finance and Insurance*. CRC Press, 2010.

[89] Greg A Radtke et al. Robust verification of stochastic simulation codes. *Journal of Computational Physics*, 451, 2022.

[90] T. Rainforth, R. Cornish, H. Yang, A. Warrington, and F. Wood. On nesting monte carlo estimators. *Proceedings of the 35th International Conference on Machine Learning*, 80:4264–4273, 2018.

[91] M. Ratto, A. Pagano, and P. Young. State dependent parameter metamodelling and sensitivity analysis. *Computational Physics Communications*, 2007.

[92] S. Razavi and H.V. Gupta. A new framework for comprehensive, robust, and efficient global sensitivity analysis: 1. theory. *Water Resources Research*, 52(1):423–439, 2016.

[93] S. Razavi and H.V. Gupta. A new framework for comprehensive, robust, and efficient global sensitivity analysis: 2. application. *Water Resources Research*, 52(1):440–455, 2016.

[94] D. Rochman, W. Zwermann, S. C. van der Marck, A. J. Koning, H. Sjöstrand, P. Helgesson, and B. Krzykacz-Hausmann. Efficient use of monte carlo: Uncertainty propagation. *Nuclear Science and Engineering*, 177, 2014.

[95] A. Saltelli. Making best use of model evaluations to compute sensitivity indices. *Computer Physics Communications*, 145:280–297, 2002.

[96] A. Saltelli, P. Annoni, I. Azzini, F. Campolongo, M. Ratto, and S. Tarantola. Variance based sensitivity analysis of model output. design and estimator for the total sensitivity index. *Computer Physics Communications*, 181:259–270, 2010.

[97] A. Saltelli et al. *Global Sensitivity Analysis: The Primer*. John Wiley & Sons, United Kingdom, 2008.

[98] A. Saltelli, M. Ratto, S. Tarantola, and F. Campolongo. Update 1 of: sensitivity analysis for chemical models. *Journal of Chemistry*, 112(5):PR1–PR21, 2012.

[99] A. Saltelli and I.M. Sobol'. About the use of rank transformation in sensitivity analysis of model output. *Reliability Engineering and System Safety*, 50:225–239, 1995.

[100] A Saltelli and S Tarantola. On the relative importance of input factors in mathematical models: safety assessment for nuclear waste disposal. *Journal of the American Statistical Association*, 97:702–709, 2002.

[101] Andrea Saltelli et al. *Global Sensitivity Analysis: The Primer*. John Wiley & Sons, Inc., United Kingdom, 2008.

[102] Andrea Saltelli et al. *Global Sensitivity Analysis: The primer*. John Wiley & Sons, 2008.

[103] Andrea Saltelli et al. Variance based sensitivity analysis of model output. design and estimator for the total sensitivity index. *Computer Physics Communications*, 181:259–270, 2010.

[104] J. Kenneth Shultis and Richard E. Faw. *Interactions of Radiation with Matter*. American Nuclear Society, La Grange Park, Illinois USA, 2000.

[105] A.V. Skarbeli and F. Álvarez Velarde. Sparse polynomial chaos expansion for advanced nuclear fuel cycle sensitivity analysis. *Annals of Nuclear Energy*, 142, 2020.

[106] I. Sobol'. On the distribution of points in a cube and the approximate evaluation of integrals. *USSR Computational Mathematics and Mathematical Physics*, 7(4):86–112, 1967.

[107] I. Sobol'. Uniformly distributed sequences with an additional uniform property. *USSR Computational mathematics and mathematical physics*, 16(5):236–242, 1976.

[108] I. Sobol'. Sensitivity estimates for nonlinear mathematical models. *Mathematical Modeling and Computational Experiment*, 1(4):407–414, 1993.

[109] I.M. Sobol'. Global sensitivity indices for nonlinear mathematical models and their monte carlo estimates. *Mathematics and Computers in Simulation*, 55(1-3):271–280, 2001.

[110] I.M. Sobol', S. Tarantola, D. Gatelli, S. Kucherenko, and W. Mauntz. Estimating the approximation error when fixing unessential factors in global sensitivity analysis. *Reliability Engineering and System Safety*, 97(7):957–960, 2007.

[111] T.J. Sullivan. *Introduction to Uncertainty Quantification*. Springer, 2015.

[112] B.K. Tripathy, M. Parimala, and G.T. Reddy. *Data Analytics in Biomedical Engineering and Healthcare*, chapter 11 - Innovative classification, regression model for predicting various diseases. Academic Press, 2020.

[113] A.W. Van der Vaart. *Asymptotic Statistics*. Cambridge University Press, 2000.

[114] Markus Widorski, Davide Bozzato, Robert Froeschl, and Vasiliki Kouskoura. FLUKAVAL - a validation framework for the FLUKA radiation transport Monte Carlo code. *EPJ Web of Conf.*, 284, 2023.

[115] ML Williams et al. A statistical sampling method for uncertainty analysis with SCALE and XSUSA. *Nuclear Technology*, 183, 2013.

[116] X. Zhu and B. Sudret. Global sensitivity analysis for stochastic simulators based on generalized lambda surrogate models. *Reliability Engineering and System Safety*, 214, 2021.